Order Number 9020814

Three-dimensional reconstruction of the arterial lumen

Suardíaz, Manuel, Ph.D.

City University of New York, 1990

U·M·I
300 N. Zeeb Rd.
Ann Arbor, MI 48106

THREE-DIMENSIONAL RECONSTRUCTION

OF THE ARTERIAL LUMEN

by

MANUEL SUARDÍAZ

A dissertation submitted to the Graduate Faculty in Engineering in partial fulfillment of the requirements for the degree of Doctor of Philosophy, The City University of New York.

1990

This manuscript has been read and accepted for the Graduate Faculty in Engineering in satisfaction of the dissertation requirement for the degree of Doctor of Philosophy.

1/26/90
Date

Ralph Barker
Chair of Examining Committee

1/26/90
Date

Jacques E. Benveniste
Executive Officer

Professor Joseph Barba

Professor Sanghamitra Basu

Professor Nenad M. Marinovic

Supervisory Committee

The City University of New York

ABSTRACT

THREE-DIMENSIONAL RECONSTRUCTION OF THE ARTERIAL LUMEN

by

Manuel Suardíaz

Adviser: Professor Joseph Barba

An accurate method for the three-dimensional (3-D) reconstruction of the arterial lumen from two orthogonal digitally subtracted X-ray angiograms was developed. 3-D reconstruction was obtained by multiple two-dimensional (2-D) reconstructions of vessel cross-sections at a sequence of transverse cuts across the vessel main axis. The arterial lumen cross-section was reconstructed using an iterative probabilistic algorithm which introduces multiple constraints to reduce the ambiguity in the reconstruction. Also, two algorithms for the automatic determination of arterial center line position in 3-D space were developed. While the first 3-D positioning algorithm is suitable for center lines with single-valued projections, the second one can work with both single and multi-valued projected center lines. These 3-D positioning algorithms use cubic spline interpolation (CSI) techniques to obtain a piecewise functional representation of the projected center line on each of the two orthogonal views. Cross-sectional reconstructions of computer simulated stenotic arterial segments with crescentic lumen shapes are presented. The accuracy of the

cross-sectional reconstruction algorithm when applied to computer simulated density profiles in the presence of additive Gaussian noise of different magnitudes was investigated. The sensitivity of this method to boundary constraint error was also evaluated. Moreover, the cross-sectional reconstruction error of the algorithm when applied to actual X-ray images of a physical model with a crescent-shaped lumen is presented. The accuracy of the 3-D positional algorithms when reconstructing different computer simulated center line shapes was also examined. In addition, 3-D positional accuracy in the presence of both input data error and a stenosed segment of increasing magnitude was also studied. Application of these algorithms to biplane images of coronary arteries may permit increased understanding of three-dimensional arterial lumen shape and consequent hemodynamic significance of atherosclerotic lesions.

To Sharon

ACKNOWLEDGEMENTS

I wish to express my deep gratitude to my mother, Oilda, and my father, Manolo, whose continuous and unselfish support made this Ph.D. dissertation possible. I also owe a significant debt of gratitude to my research mentor, Professor Joseph Barba, for his very valuable advice, criticism, and support which significantly improved the quality of my dissertation. In addition, I want to acknowledge my indebtedness to all my good friends, who are too many to mention all of their names here, for their constant encouragement and endless help during my years in the Ph.D. program. Lastly, I would like to thank The Frances L. & Edwin L. Cummings Memorial Fund for generously supporting this research with grants RF-775-707 and RF-775-819.

Table of Contents

Table of Figures

1 INTRODUCTION

Coronary Heart Disease (CHD) is the main cause of death in the Western World. In the United States alone it is responsible for more than half a million deaths each year and it also affects millions of other persons with less severe effects.[1] The main cause of Coronary Heart Disease is atherosclerosis, a process by which plaques of fatty deposits form in the inner layer of large and medium-sized arteries forming a lesion which eventually obstructs the flow of blood through the affected blood vessels.

Due to the devastating effects of this disease, the medical and scientific community have made great efforts to better understand[2] and cure[3] cardiovascular diseases. One of the focuses of these efforts has been on the development of more advanced imaging methods to enable physicians to locate the arterial lesions and determine their severity, as well as to monitor the progress of the disease or a particular treatment.

There are a number of computerized imaging techniques which physicians have started to use to peer inside the human body in the recent years. The major ones are Magnetic Resonance Imaging (MRI), Positron Emission Tomography (PET), Computerized Axial Tomography (CAT), Sonography (SONO), and Digital Subtraction Angiography (DSA).[4] DSA is the imaging modality of choice to visualize the blood vessels because it produces clear, sharp images of these structures due to its high spatial and temporal resolution qualities.[5]

Angiography, a technique in wide use now, was perfected in 1953[6] by Seldinger.[7] It allows the visualization of arteries and veins in a radiographic examination. In conventional

radiography it is not possible to differentiate these structures from their surroundings. However, by injection of a radiopaque substance into the vessel lumen (typically a water-soluble substance containing iodine), angiography allows blood vessels to be distinguished from the surrounding tissues and organs. This is reflected on the radiograph by having the structures containing the contrast substances (arteries or veins) casting denser shadows than the tissues without the iodine based solution. Angiography permits the imaging not only of the arteries, but also of the organs to which they supply blood.

At present, most cardiac catheterization laboratories still use conventional angiography for the radiological examination of their patients. In conventional angiography the medical images are recorded on photographic film. The most widely used technique is based on detection of the X-ray photons using an image intensifier device. The output of the image intensifier (a transducer and amplifier device) is coupled to a TV camera or a cine camera using a beam splitter device. During the injection of the contrast substance, the output of the X-ray tube is synchronized with the cine camera, typically at around 30 frames per second, and the flow of the mixture of blood and contrast material through the heart and nearby blood vessels is recorded on a high quality film. This technique is known as cine-angiography. It provides radiologists with a valuable amount of anatomical and dynamical information about the cardiovascular structures being imaged.

Over the past two decades, the development and acceptance of computerized cardiac imaging techniques have introduced into this medical field the power, flexibility and speed of computers, and brought about digital fluorographic systems.[8-11] In these systems, the X-ray photons are also detected with an image intensifier, but then the optical output of the image intensifier is captured by a TV camera and converted into an electrical signal. After

this stage, there is an analog-to-digital (A/D) converter which samples and digitizes the signal which is subsequently stored into a digital electronic memory ready to be processed by a computer. A very important advantage of this technique is the elimination of film from the recording process and the cost and waiting time associated with its developing. Also, digital fluorography allows the use of more powerful and sophisticated display devices such as high resolution, color video stations with dedicated controls for multiple useful operations like zooming. Finally, this kind of systems permit the use of digital image processing techniques for picture enhancement, feature extraction and image interpretation.

The main application of digital fluorography is digital subtraction angiography (DSA) which, according to Riederer[12], was introduced by Kruger and Ovitt in 1979. DSA allows the acquisition of high quality images of the coronary arteries. It can also be used in many other medical applications such as ventriculography, pulmonary arteriography, interventional radiology, renal arteriography and the imaging of the carotid and peripheral arteries.

In general, digital subtraction groups several different subtractive methods. These methods are temporal subtraction, energy subtraction and hybrid subtraction (combination of the first two). Temporal subtraction is the earliest, most effective and most widely used method of subtraction and because of that, is generally referred to as digital subtraction angiography. In DSA an image, generally called the mask, is acquired and stored prior to the injection of the contrast material. After the injection of the radiopaque substance, a second image (the contrast image) is acquired and subtracted pixel by pixel from the mask image. If subtraction is done appropriately, the only non-zero signal on the difference image will correspond to the distribution of contrast material. Thus, this technique permits the display of the chosen vascular structures without the bones and tissues which are behind

and in front of them.

Typically digital arteriograms have less spatial resolution than the images taken on film, however they do achieve greater density resolution due to the elimination of the areas without contrast medium. Digital arteriography allows physicians to perform very useful and powerful manipulations on the image data such as picture enhancement, immediate review and quantitative measurements on coronary stenosis.

However, even with all the progress witnessed in this area over the past few years, the imaging techniques which assist physicians in the treatment of CHD still need improvement and innovation. For instance, the accuracy and reliability problems of the standard methods of angiographic analysis are well documented.[13-20] These studies have shown that significant errors are made in the determination of the location and severity of coronary atherosclerosis. In addition, there is a growing need for better and new, innovative methods and equipment capable of extracting more clinically useful information from angiograms than what it is possible now.[21,22]

One such new technique, which could prove extremely powerful, is the three-dimensional reconstruction of the coronary arterial lumen. This type of reconstruction would provide to cardiologists new, important clinical information, such as stenosis length and lumen shape, which may contribute to a more effective diagnosis and therapy of coronary atherosclerosis. Therefore, due to the importance of this problem, we want to propose the development of the methods to obtain the 3-D reconstruction of the coronary arterial lumen.

1.1 General Goal of the Research

The aim of this research is the development of clinically applicable methods to obtain the three-dimensional reconstruction of arterial lumen using only two orthogonal X-ray angiograms. We propose to develop a technique which permits maximum utilization of imaging equipment presently available in hospitals to guarantee a low cost for the 3-D arterial reconstructions obtained with these methods. Consequently, we have decided to use the two orthogonal images provided by the biplane X-ray systems already present in the radiology and cardiology laboratories of many hospitals. In addition, we are going to use digitally subtracted arteriograms because of their capacity to provide vascular images that are free of bone structures and surrounding tissues which are irrelevant to our problem.

Computerized Axial Tomography, in principle, can be used for the 3-D reconstruction of the arterial lumen. However, this imaging technique would encounter the following limitations and drawbacks if it were to be used for the 3-D reconstruction of the arteries:

1. Relatively low longitudinal resolution (thick reconstructed slices).

2. Multiple injections of radiopaque contrast substance since only one or two slices can be reconstructed at one time (injection of radiopaque substance is required to bring image contrast to clinically useful levels).

3. Relatively high radiation dose due to the use of multiple radiographs at different angles.

4. Expensive specialized equipment: Custom-made, costly, ultra-fast CT systems have been proposed and/or developed for the imaging of the coronary arteries and for the use of high rate tomography.[23-25] In addition, these systems also suffer from some of the problems stated above.

5. A CT based method would still require additional expensive tests since both a CT and an angiographic examination would be needed for a complete clinical study of a patient.

In contrast, our proposed methods use only two, preferably digitally subtracted, orthogonal radiographs, which guarantees the use of accepted safe radiation exposures. In addition, these two images are acquired at the same time, instead of sequentially, thereby requiring only a single injection of the iodine solution. The use of two simultaneous orthogonal views also offer the additional advantage of eliminating any problems associated with possible temporal changes in vessel shape, position and/or orientation during the heart cycle. Furthermore, the biplane angiographic equipment required for acquisition of the image data is already available, with or without digital processing capabilities, in many standard catheterization laboratories. Institutions lacking biplane equipment would also have guaranteed considerable savings, because instead of having to buy some new kind of expensive and specialized equipment, they would just have to purchase a digital biplane X-ray system. This kind of system has been available in the market from various manufacturers for quite some time already, therefore its cost would be much lower.

1.2 Significance of the Research

At present, the parameter most widely used to clinically assess the severity of coronary atherosclerosis is Percent Stenosis; a relative measurement, visually made by radiologists or cardiologists on coronary artery X-ray images, representing lumen percent diameter or area reduction relative to a "normal" nearby lumen.

It is known that the Percent Stenosis standard, which provides most of the basis for deciding the medical and surgical therapy of this disease, have a number of major deficiencies. First, many studies have shown that this visual estimate is subject to substantial intra- and inter-observer measurement errors in assessing both the location and degree of abnormality of coronary stenosis.[13-20] Second, the visualization of arterial lesions is very sensitive to the viewing angle since the cross-sectional shape of stenosed lumena is in many cases irregular and eccentric. Third, the denominator of the expression for Percent Stenosis is the diameter of a nearby "normal" section. However, this nearby "normal" cross-section is seldom normal since it is impossible to exactly determine what the healthy, normal vessel of a patient might have looked like in the past. Nearby arterial portions may be dilated by the aging process or post-stenotic turbulence, or narrowed by some diffusion of the atherosclerotic plaque. Finally, even with the more accurate videodensitometric approach for determining cross-sectional narrowing from computer-based digital images of coronary arteries[26], Percent Stenosis is still not the best parameter to predict the effect of arterial stenoses on blood flow since it only provides relative cross-sectional area information. Blood flow rate through atherosclerotic coronary arteries, however, is not only influenced by stenosis cross-section area narrowing, but also by the arterial-venous pressure gradient, stenosis length, and stenosis cross-sectional shape.[27-30] Therefore, to fully assess the

hemodynamic consequences of a coronary stenosis, it is necessary to estimate the pressure drop flow profile through the stenosed region, which requires obtaining the 3-D reconstruction of the arterial lumen along the entire vessel segment, from the undiseased proximal region of the vessel, through the stenosis, to the distal region of the lesion.

All this additional information may lead to a more effective medical therapy of coronary atherosclerosis, specially for cases of moderate stenoses (approximately between 40% to 70% diameter reduction). Cases with severe degree of stenosis, typically associated with angina or myocardial infarction, will probably continue to be treated surgically in most instances. Additionally, this 3-D information may give clues about the prognostic significance of stenoses, particularly how the effect of both shape and length on flow turbulence[31] and blood shear stresses[32,33] may potentiate the progression of vessel occlusion.

It is clear that there is a need for accurate three-dimensional reconstructions of the coronary arterial lumen. This may be accomplished by extracting additional existing information in biplane angiograms. Three-dimensional reconstruction would facilitate absolute measurements, as opposed to the customary relative Percent Stenosis one, and would permit a more effective characterization of coronary stenoses. As a cardiologist from the University of Iowa said, the traditional Percent Stenosis measurements are "quick, dirty and wrong".[34]

2 REVIEW OF PRIOR WORK

2.1 Cross-sectional Reconstruction from Two Views

The problem of reconstructing an image from two views (or projections) has attracted very little attention in the past. This could perhaps be attributed to the fact that in general this problem does not have a unique solution. It has been shown that even the reconstruction of binary images (those which can be represented by matrices whose elements are 0's and 1's only) is an "ambiguous problem" because there may exist no, one, or more than one solution matrix satisfying a given pair of orthogonal projections.[35,36,37] However, there are certain cases when the cross-sectional shape may be reconstructed unambiguously. For example, objects that are convex, symmetric with respect to the two orthogonal axes, and have a piecewise linear boundary can be reconstructed correctly (see Section 2.1.1). Furthermore, if sufficient a priori information is incorporated into an algorithm specially developed to solve a very specific problem, concave and asymmetric shapes could be, at least, approximately reconstructed too, because the additional information could be used to eliminate incorrect possible solutions or to produce one.

Several researchers have tackled the problem of cross-sectionally reconstructing bodies using either two or a small number of views in the past. Most have used their techniques to solve problems in the areas of medical diagnostic radiology and industrial inspection. Others have just presented general algorithms which have never been used for solving any specific problem. In the area of medical diagnostic radiology reconstruction

techniques have been used to obtain the cross-sectional shape of both the heart ventricles and blood vessels, whereas for the industrial inspection area an application was developed to examine the fuel rods inside nuclear reactors. Below we present an overview of all the studies found which are relevant to this research.

2.1.1 Applications of cross-sectional reconstruction for determining ventricular shape

The ambiguity in the cross-sectional reconstruction of an arbitrary body from two orthogonal projections can be eliminated if certain assumptions are made about the shape of this body. For example, Chang et al.[38,39] have developed the techniques for reconstructing objects that are convex, symmetric with respect to the two orthogonal axes, and have a piecewise linear boundary. These algorithms were applied to the binary reconstruction of the chambers of the heart. Data from X-ray images of a clay model and of a dog's heart was used to obtain 2-D and 3-D images of these objects. However, no quantitative measure of the quality of these results was presented; nor it is explained how the correspondence between the profiles of the two views was obtained. Although the algorithm described by these researchers is limited because there are cases in which the object to be reconstructed does not have convex symmetric cross-sections (for example, some typical arterial stenosis shapes), this paper is important because that it shows that the ambiguities in this type of reconstruction can be resolved by introducing a priori knowledge.

Onnasch and Heintzen[40,41] have reported a non-iterative probabilistic algorithm called BASE (Binary Phase Shape Estimation) which also uses a priori known information of the

problem. This algorithm was developed for obtaining the three-dimensional reconstruction of the right or left ventricle at each of the phases of the heart cycle from biplane angiocardiographic recordings. Using a tomographic approach and the two orthogonal X-ray shadowgraphs associated with each cardiac phase, each ventricular shape is reconstructed slice by slice. The final 3-D reconstruction is obtained by stacking the slices previously reconstructed with the BASE algorithm. To eliminate the ambiguities expected when performing this type of reconstruction, this method exploits the similarities existing in time and space with the slice being reconstructed. In other words, to avoid the possible incorrect solutions which may arise when reconstructing each ventricular cut, this algorithm uses the likeness that both the binary pattern representing the same slice in the previous contraction phase, as well as the binary pattern spatially adjacent, have with the slice being reconstructed. The BASE algorithm performs the reconstruction of binary arrays by assuming homogeneous mixing of the contrast agent. This algorithm works by first calculating a fundamental probability $F(i,k)$ derived from the normalized multiplication of the two orthogonal projections $KDX(i)$ and $KDY(k)$ as represented by the equation below:

$$F(i,k) = KDX(i) \times KDY(k) \qquad (2.1.1\text{-}1)$$

Where $\times$ denotes multiplication.

Subsequently, a probability array $W(i,k)$ is obtained from the multiplication of the fundamental probability $F(i,k)$, the 2-D probability distribution function $S(i,k)$ derived from the adjacent slice (similarity in space), and the 2-D probability distribution function $T(i,k)$ derived from the same slice in the previous contraction phase (similarity in time) as shown below:

$$W(i,k) = F(i,k) \times S(i,k) \times T(i,k) \qquad (2.1.1\text{-}2)$$

The elements of the binary pattern are filled then using this probability array $W(i,k)$, starting with the most likely ones, from center to periphery, and column-wise.

This algorithm was tested with ideal data obtained from more than three hundred left and right ventricular human casts, which were cut into parallel slices. These slices were digitized and stored on magnetic tape by following their borders with a pencil follower. Subsequently, pairs of orthogonal projections were generated from the digitized slices and the BASE algorithm was applied to them. This is not the best way to test this algorithm, because this type of data eliminates the most basic problems, such as incomplete mixing of the radiopaque medium and picture deterioration by factors such as pincushion distortion and various types of noise, normally encountered in any X-ray image. Therefore, they have not shown conclusively whether the homogeneous mixing assumption is valid for the reconstruction of the heart ventricles. Their results show that the accuracy in the reconstructions of left ventricle cast cross-sections was 80.8% when using no model and 94.0% when using the information of the reconstructed adjacent slice. They show no results for the case when the algorithm uses both the similarities in time and space.

One of the drawbacks of this method is that it is prone to propagate the unavoidable reconstruction errors of one slice into other slices. In addition, the use of the similarity between adjacent slices assumes continuity of the body walls, which may result in errors when reconstructing sections with abrupt discontinuities of the wall contours. Similarly, the use of the similarity of the same slice in the previous contraction phase may introduce reconstruction errors too, because it ignores likely temporal shape changes. Also, due

perhaps to the characteristics of the ideal data used by these researchers, the important problem of determining the corresponding profiles in each of the two views associated with each plane to be reconstructed has not been addressed. The non-trivial problem of determining corresponding points in the two views must be properly resolved if the technique is to be successful in a clinical environment. The accuracy of the reconstructions will depend on how well corresponding profiles are matched. Additionally, it is desirable for this matching process to be carried out in an automatic fashion, or else the method will be impractical. Finally, this method was used to reconstruct cross-sections of the cardiac chambers; the cardiac chambers having shapes which are approximately convex, specially during end-diastole, may be better suited for binary cross-sectional reconstruction.[38]

Onnasch et al.[42] have also published a good analysis of the problems associated with the reconstruction of the heart ventricles from two orthogonal angiocardiograms when using the BASE algorithm. This paper focuses on the factors which distort the absolute absorption level of the processed density image (geometrical and intensity distortions) obtained with biplane systems. Specific analyzed sources of distortions are X-ray beam divergence, scattering, veiling glare, and magnification factors. It also shows how these researchers corrected the errors caused by these problems. This is a paper of interest to us because it offers solutions to typical problems of varying degree of importance, such as pincushion and X-ray beam hardening distortions, which we are also going to encounter, sooner or later, as we attempt to reconstruct the coronary arteries with our algorithms.

A different technique for the reconstruction of cross-sections of the heart chambers has been proposed by Alliney and Sgallari[43] which uses the morphological information present in each angiographic view. This algorithm was developed to obtain approximate

ventricular cross-sectional reconstructions from estimations of the curvature radii of the ventricular walls in each projection. Each reconstructed cross-section is approximately obtained by joining the four arcs of a circle which optimally match, in the least squared error sense, the four points determined by the intersection of the projections of the ventricular walls with the reconstruction plane. To obtain a numerical solution an iterative scheme based on a descent algorithm is used. The usefulness of the method is still not clear, since these researchers did not performed an objective and thorough analysis of the accuracy of the results.

In addition, it is not difficult to see that this approach cannot be used to find the solution of our problem, since it assumes that the object to be reconstructed has concave projections, and this is obviously not true for images of the arteries.

2.1.2 Applications of cross-sectional reconstruction for determining blood vessel lumen shape

The first study that we found on computer reconstruction of cross-sectional views of arteries from radiographic images was the one published by Spears et al.[44]. Using a maximum entropy algorithm called MENT[45,46], these researchers obtained cross-sectional reconstructions of cylindrical phantoms representing stenosed arteries.

The MENT algorithm, which obtains the solution using a constraint optimization approach, defines the entropy $\eta(f)$ of an unknown, continuous, source function $f(x, y) \geq 0$ with compact support D as

$$\eta(f) = -\int dx \int_D dy f(x,y) \ln[f(x,y)A] \qquad (2.1.2\text{-}1)$$

Where A is the area of D.

When the number of available views is small, this iterative algebraic reconstruction technique gives better results than other techniques such as Fourier space inversion and convolutional projection, particularly if the data are noisy. The reason for this is that the MENT algorithm yields the image with the lowest information content consistent with the existing data, thereby avoiding the introduction of extraneous information or artificial structures. This is evidenced by the results presented by these researchers, which show reconstructions without the streaking artifacts associated with other kinds of algorithms.

Because of the above property of the MENT approach, and others such as the convergence rate and its stability against noise errors in the data, this and other maximum entropy algorithms are receiving increasing attention in the field of image processing. For example, the MENT algorithm has also been used in an industrial application for reconstructing the cross-section of the simulated fuel core bundle of a nuclear reactor and in which the amount of X-ray radiation used is not a primary concern (see Section 2.1.3). Another example is the maximum entropy algorithm for restoring degraded images reported by Daniel et al.[47].

Spears et al. tested the MENT algorithm with X-ray data obtained from an in vitro model lumena. This model was constructed using tubes, approximately the size of human arteries (2 to 5 mm), filled with contrast medium (Renographin-76) which simulated four well defined lumen shapes: a circular, an elliptical, a crescent-shaped, and a double lumen.

This model was only rotated around its longitudinal axis and X-rays were always taken perpendicular to this axis. The algorithm, however, was not tested with clinical cineangiographic data.

The results presented in this study showed that the quality of the reconstructed images depended on the number of views used as input data and on the concentration of the contrast medium. Their images showed good results when using five views. However, for more practical number of views, namely three, the reconstructed shapes show very noticeable artifacts and the lumen borders are poorly defined. No results are offered for two views, which is the case of interest to us.

The MENT algorithm is a multiple view method which conveniently does not require the use of any a priori information about the body being reconstructed. The application of this algorithm to cardiology applications, however, is difficult because the maximum number of images that can be simultaneously acquired in standard catheterization laboratories is two. Therefore, any method using more than two views would be subject to the errors caused by the temporal changes in shape, position and orientation normally present in non-simultaneous images of the coronary arteries. In addition, using more than two views is unpractical because it increases the total radiation dose to the patient.

Another method for the 3-D reconstruction of the arterial lumen using a tomographic approach and a priori known information has been published by Reiber et al.[48,49]. To reconstruct each cross-section, these investigators used a slightly modified version of a minimum cost capacitated network flow algorithm referred to as the Slump reconstruction method. The Slump method was originally developed to reconstruct the chambers of the heart and was tested by reconstructing cross-sections of a dog's left ventricle.[50] This

technique reconstructs each cross-section by finding the binary matrix which satisfies the two orthogonal projections and has the maximum resemblance with the spatially adjacent or temporally corresponding slice. To introduce the resemblance criterion in the formulation of the problem, a cost function which assigns to each element $x_{ij} \in \{0,1\}$ of the $m \times n$ matrix M under reconstruction the coefficient c_{ij} representing the penalty of making x_{ij} equal to unity.

Minimization of the total cost C_t defined as

$$C_t = \sum_{i=1}^{m} \sum_{j=1}^{n} c_{ij} x_{ij} \tag{2.1.2-2}$$

under the constraints

$$\sum_{j=1}^{n} x_{ij} = XP_i \qquad i = 1,\ldots,m \tag{2.1.2-3}$$

$$\sum_{i=1}^{m} x_{ij} = YP_j, \qquad j = 1,\ldots,n \tag{2.1.2-4}$$

where $XP_i, i = 1,\ldots,m$ and $YP_j, j = 1,\ldots,n$ are the X and Y X-ray density profiles respectively, leads to reconstructed slices with a high similarity with the previously reconstructed one. This optimization problem can be related to the so-called Hitchcock or transportation problem and solved efficiently with the maximal flow algorithm developed by Ford and Fulkerson.[51]

The Slump algorithm was tested by reconstructing slices of both a perspex model with circular cross-sections and a stenosed artery with more or less convex lumenal cross-sectional shapes. A second more complex version of the algorithm called "noisy" Slump was also tested producing similar results. In addition, the same data used to test the Slump's method was also utilized to test a modified version of the BASE algorithm developed by Onnasch et al.[40,41] to reconstruct the chambers of the heart. A tabulated comparison of both algorithms was presented. The accuracy of both algorithms when reconstructing 290 slices of the perspex model was measured by the relative mean error $\overline{R}$ defined as

$$\overline{R} \equiv \frac{\sum_{i=1}^{m}\sum_{j=1}^{n} |x_{ij} - o_{ij}|}{\sum_{i=1}^{m}\sum_{j=1}^{n} o_{ij}} \qquad (2.1.2\text{-}5)$$

Where

o_{ij} ≡ Elements of the original binary matrix.

x_{ij} ≡ Elements of the reconstructed matrix.

Since the actual cross-sectional shape of the arterial segment was not known, another criterion was used to measure the results of both algorithms when reconstructing 155 slices from true arterial data. This resulted in a new parameter $\overline{S}$ called the mean model dependency. This parameter measures the model dependency of the algorithms by calculating the average difference between the results obtained when the reconstruction process starts from the proximal part of the segment and when it starts from the distal part. This parameter $\overline{S}$ was defined as

$$\overline{S} \equiv \frac{\sum_{i=1}^{m}\sum_{j=1}^{n} |x1_{ij} - x2_{ij}|}{\sum_{i=1}^{m}\sum_{j=1}^{n} \frac{x1_{ij}+x2_{ij}}{2}} \qquad (2.1.2\text{-}6)$$

Where

$x1_{ij}$ ≡ Elements reconstructed when the process starts from proximal part.

$x2_{ij}$ ≡ Elements reconstructed when the process starts from distal part.

Unfortunately, this is not the best way to measure the quality of the reconstructions because $\overline{S}$, rather than giving a sense of the accuracy, it gives a certain measure of the inaccuracy of these algorithms.

For both kinds of data the BASE algorithm yielded better results than the Slump algorithm ($\overline{R} = 13.2\%$ and $\overline{S} = 9.9\%$ vs. $\overline{R} = 18.5\%$ and $\overline{S} = 13.1\%$ respectively). This seems to indicate that probabilistic algorithms will reconstruct better the arteries than minimum cost capacitated network flow algorithms. In addition, the computational cost of the BASE algorithm is also much less because it does not need to compute the minimum cost matrices which requires involved algorithms.

These researchers did not address the problem of the partially filled pixels encountered on the periphery of the vessel. In addition, the matching of the two corresponding orthogonal profiles required for reconstructing each slice was performed manually. This is a major drawback because manual processing is tedious and impractical for a clinical environment. Another problem is that this algorithm uses the similarities of the previously reconstructed

slice to eliminate the ambiguity in the solution of the next cross-section. This approach can intrinsically introduce errors for two different reasons: first, because the unavoidable errors of each reconstructed slice can propagate to the next ones; and second, because when there are abrupt discontinuities of the vessel walls, the spatial similarity assumption does not hold well. Finally, this work does not investigate the reconstruction of concave, asymmetric cross-sectional shapes.

2.1.3 Application of cross-sectional reconstruction to nuclear reactor fuel pin diagnostics

The maximum entropy algorithm (MENT) developed by Minerbo[45,46] and already discussed above (see Section 2.1.2) has also been used in an industrial inspection application for reconstructing the simulated thirty seven pin fuel core of a nuclear reactor.[52] This algorithm has produced better reconstruction results than other techniques, particularly when the number of views is small. Using MENT, reconstructions a test model were obtained using three, six and eighteen views. The presented results show accurate reconstructions when using six views for the configuration tested. This paper offers a good example where the MENT algorithm performs well because this is a case in which more than two views can be easily obtainable, and the use of very small amounts of radiation is not a primary requirement.

2.1.4 Other cross-sectional reconstruction algorithms

We have found in the published scientific literature several iterative algorithms, primarily developed for pattern recognition or data compression applications, which can also be used for cross-sectional binary reconstruction.[53,54] These algorithms have never been tested with any kind of ventricular or arterial data. They attempt to obtain an approximate cross-section for cases with ambiguous solution by using a selection function which gives values to each pixel based on the projections. Using an assignment rule which selects the highest given values, the pixels in the binary array **M** are then filled. However, since no additional information is used, when ambiguities are present, the cross-section **M** is solved to within the four-point switching components present in it. A four-point switching component of the binary pattern **M** is defined as a 2×2 submatrix of **M** of the form

$$\begin{pmatrix} 0 & 1 \\ 1 & 0 \end{pmatrix} \quad \text{or} \quad \begin{pmatrix} 1 & 0 \\ 0 & 1 \end{pmatrix}$$

When a binary pattern **M** at least contains one of these four-point switching components, its reconstruction is ambiguous.

An excellent introduction to the study of image reconstruction from a few projections is offered in a paper published by Herman[55], which describes a reconstruction algorithm, BART, which was not specifically developed for solving any individual problem. This algorithm is basically a particular case of a previously developed more general CAT type algorithm applied to the reconstruction of binary images from two orthogonal views only. This is probably the weakest point of this method. We think that because the amount of

existing information when using only two views is very small, better results can be obtained by utilizing an algorithm specifically designed for the problem at hand that, in addition, uses all the available a priori information.

Since the patterns used to test the BART algorithm contained noise with a very small standard deviation ($\sigma_n = 0.03$ and $\sigma_n = 0.1$ pixel), and the resulting reconstructions were not compared to the original patterns, but to their digitized versions, the results presented here may be misleading. Finally, three other algorithms were also tested with the same data patterns mentioned before for comparison purposes. The results showed a slightly larger reconstruction error when using these algorithms than when using BART.

The "reconstruction by block projection" algorithm developed by Wong and Yue[56] uses another approach to eliminate the ambiguities which arise in the reconstruction of binary patterns from two orthogonal projections. This technique, which was conceived for the efficient storage and further recovery of these patterns, can solve to a large extent the ambiguity problem provided that the "block projections" of sub-matrices formed by partitioning the original pattern can be obtained. In addition, the initial binary algorithm is extended to general patterns too. Although the approach reported by these investigators can useful for certain applications, it is certainly not suitable for the reconstruction of the arteries, since in this problem there is no control on how the projections are formed.

Similarly, Kuba[57] has presented another reconstruction algorithm which obtains the solution under a necessary directional connectivity property of the original pattern which in general does not apply to arterial cross-sections.

2.2 Three-dimensional Positional Reconstruction from Two Views

The goal of 3-D positional reconstruction is the precise localization of points in their 3-D object space from measurements of their projection coordinates onto 2 orthogonal planes.

In general, the solution to this problem requires the following:

1. Knowledge about the geometry and the location of the X-ray equipment during the image recording process.

2. To be able to identify the corresponding projections of each image point in the two orthogonal views.

We have found in our literature survey of prior related work that 3-D positional reconstruction has mostly been used in the past to solve problems arising in several related areas of Cardiology. We have also found a general application which can be used for making measurements in any X-ray photograph. We have classified all these prior applications of 3-D positional reconstruction according to the following areas: ventricular volume measurements, X-ray stereo photogrammetry, heart wall motion analysis, 3-D display of the arterial tree, and the tracking of the arterial tree. What follows is a review of all the found relevant work.

2.2.1 Applications of 3-D positional reconstruction for ventricular volume measurements

The early use in Cardiology of 3-D positional reconstruction was connected to the measurement of the left ventricular (LV) volume of the heart.[58,59,60] The calculation of LV volume from angiocardiograms have generally been obtained by means of many geometric models. These analytic models assume that the ventricular shape can be represented by one or more analytic ellipsoidal bodies whose sizes can be determined from measurements performed on the X-ray pictures. However, since the X-ray beams are non-parallel for the typical tube-to-film distance of less than 6 feet, they cause a magnification effect on the shadows cast onto the input screens. This effect needs to be rectified in order to arrive to correct volumetric dimensions. By finding the true 3-D coordinates of the points on the heart which determine the dimensions of the assumed geometric model, cardiologists are able to obtain accurate LV volume values (We have also found that a similar idea has been proposed for measuring the true length of airways within the lung using stereoscopic broncograms[61]).

In these studies, corresponding projections of the points onto the two views were always selected manually by a skilled operator. This is a drawback since it makes the method very slow and prone to subjective errors. In addition, none of these early investigations have presented an analysis of the errors which can be caused by problems such as:

a. Possible non-perpendicularity between the two views.

b. Possible non-perpendicularity between imaging planes and their corresponding central X-ray beams.

c. Measurement errors in the distances between the input screens and their corresponding X-ray sources.

d. Measurement errors in the coordinates of the projected points.

Error propagation analysis is important, especially when working with minute anatomical structures such as arteries. In the actual practice, the ideal conditions under which the formulas for the 3-D coordinates of a point in space are derived rarely hold. Therefore, the positional information obtained from these expressions will always contain a certain amount of error which can be acceptable or not depending on the application.

2.2.1.1 Pincushion distortion problems

Another area that the above mentioned studies have not addressed is pincushion distortion. This type of distortion also introduces errors in the calculation of the 3-D coordinates of points in object space. Pincushion distortion is produced by the curvature of the image intensifier input screen. This kind of distortion affects all images recorded with the same image intensifier in the same way. Therefore, this distortion can be measured and a rule for its correction can be obtained. Once that the amount of correction is determined for an image intensifier, this information can be used to correct the pincushion distortion on any image acquired with this device.

Pincushion distortion correction can be applied either to only specific points of interest on an image or it can be applied on the coordinates of every single pixel on an image. The advantage of the first approach is speed since the process only works on a small number of pixels. The second approach, on the other hand, requires much more computational power

but it has the advantage that after the correction has been applied, the user can have different programs working on any region of the image without having to consider the pincushion distortion again.

Several methods to correct for pincushion distortion have been reported in the literature (see Reference 72). Some assume the distortion to be radially symmetric. The better ones however, assume it to have a more complex behavior and use for correction the image of a rectangular metallic grid of known dimensions which is placed parallel to the image intensifier. Accurate methods for the determination of the 3-D coordinates of points in object space should therefore also include a good technique for pincushion distortion correction.

Later research in the area of 3-D positional reconstruction has attempted to circumvent the errors which occur when the ideal conditions usually assumed in stereoscopic radiography are not met.

2.2.2 General application of 3-D positional reconstruction to X-ray stereo photogrammetry

In stereoscopic radiography, the X-ray shadowgraphs are produced by two X-ray tubes which are mounted on a known configuration (producing perpendicular or non-perpendicular images) and at known distances from each other. The distances from the focal points of the X-ray tubes to their respective image intensifiers or film planes are also known. Alternatively, a single X-ray tube can be used, given that after the first exposure it is moved by a fixed distance to provide the second exposure. Both methods above require

accurate measurement of the image intensifier to focal point distances, that the image intensifier plane is perpendicular to its central X-ray beam, and in the case of orthogonal pictures, that the views are perpendicular to each other. These ideal conditions are difficult to achieve in practice and this is why, sometimes, these methods are referred to as approximate solution methods.

Adams[62] has reported a method for analytically locating the precise 3-D position of points using ideas from the field of projective geometry which avoids the approximate solution methods. This method, which has also earlier been used by Sayre (see Section 2.2.4), does not require any measurements of the distances between the elements of the X-ray system nor does it assumes any specific configuration of the X-ray system components. Furthermore, it does not require a modification of the X-ray apparatus. This technique, hereafter called the perspective transformation method, is accurate but it is somewhat mathematically complex. It describes and relates the 3-D coordinates of points in space and their 2-D projection coordinates using a homogeneous coordinates representation and perspective transformations.

2.2.2.1 Perspective transformation method

The central projection is the basic geometrical property of X-ray photographs in which all rays pass through a perspective center. In Radiology the perspective center is the focus of the X-ray tube which is not really a mathematical point but a small surface which varies from one device to another. This surface's size is very small, however, and it can generally

be approximated to a point without introducing significant errors. An X-ray picture represents the projection of a 3-D space onto a 2-D recording plane. This suggests that it is possible to use projective geometry and in particular, the mathematics of projective transformations[63] to describe the coordinates of the points being imaged in an X-ray system.

In general, the relationship between a 3-D point located at coordinates (x, y, z) and its perspective projection located at point (y', z') can be described by the following relation:

$$(x \quad y \quad z \quad 1)\begin{pmatrix} p_{11} & p_{12} & p_{13} \\ p_{21} & p_{22} & p_{23} \\ p_{31} & p_{32} & p_{33} \\ p_{41} & p_{42} & p_{43} \end{pmatrix} = \kappa(u \quad v \quad 1) \qquad (2.2.2.1\text{-}1)$$

Where

$(x \quad y \quad z \quad 1)$: homogeneous coordinates representation of the source point in 3-D space.

$(y' \quad z' \quad 1)$: Homogeneous coordinates representation of the source point projection.

κ : scaling factor.

$$\mathbf{P} \equiv \begin{pmatrix} p_{11} & p_{12} & p_{13} \\ p_{21} & p_{22} & p_{23} \\ p_{31} & p_{32} & p_{33} \\ p_{41} & p_{42} & p_{43} \end{pmatrix} : 4 \times 3 \text{ perspective transformation matrix.}$$

The matrix **P** defines the mapping between a point in 3-D space and its projection onto a plane. This matrix describes any arbitrary linear transformation in 3-D space, therefore it can be used to obtain the perspective projection of points in 3-D space using any arbitrary positioning of the X-ray tube and the image intensifier. This method, however, will not correct for the non-linear distortion introduced by the curvature of the image intensifier known as pincushion distortion. Pincushion distortion is a problem which needs to be solved separately (see Section 2.2.1.1).

Equation (2.2.2.1-1) represents a set of three linear equations which can be reduced to

$$(p_{11}-p_{13}y')x+(p_{21}-p_{23}y')y+(p_{31}-p_{33}y')z+(p_{41}-p_{43}y')=0 \qquad (2.2.2.1\text{-}2)$$

$$(p_{12}-p_{13}z')x+(p_{22}-p_{23}z')y+(p_{32}-p_{33}z')z+(p_{42}-p_{43}z')=0 \qquad (2.2.2.1\text{-}3)$$

by solving for the scaling factor κ in the third equation of the set represented by Equation (2.2.2.1-1) and substituting the obtained value in the other two equations.

If one measures the projections (y', z') of points in a calibration object with known (x, y, z) 3-D coordinates, it is possible to find the values of the unknown elements of **P** in Equations (2.2.2.1-2) and (2.2.2.1-3) provided that enough points are used.

Letting p_{43} be an overall scale term equal to 1, the above set of two equations gets reduced to 11 unknowns. Therefore, the unknown transformation matrix can be found by

imaging a calibration object with a minimum of 6 points. This is an overdetermined system with 11 unknowns and 12 equations whose optimal solution in the least squared sense can be obtained by using a generalized inverse.

To calculate the projective transformation parameters in his experiment, Adams used 15 reference points provided by means of a surrounding control framework. The control framework employed was a cage-like metal structure with two separate 5 cm parallel grid planes which had to surround the object to be X-ray photographed. In addition, the positions of these control points met the following condition: if using a minimum of 6 control points, no more than four should be coplanar and no more than three of their images should be colinear.

Adams tested the accuracy of his approach using a series of small radiopaque balls whose positions inside of an irregularly shaped polyurethane head model was known very accurately. He showed that his technique is very accurate. He calculated that using this method the 3-D coordinates of points in space can be determined with an accuracy of ± 0.4 mm on the average.

The advantages of this method over previous ones are its accuracy and the fact it is not necessary to assume any specific arrangement of the X-ray equipment or to make any distance measurements between its elements. Unfortunately, the method proposed by Adams has some serious disadvantages; it requires the use of a control framework, which not only must be built to very accurate dimensions, but also must surround the object to be X-ray photographed. These requirements make this method very unpractical to be used on any regular clinical application. In addition, this technique requires that the free net control framework and the object must move as a rigid unit. When taking X-ray images of patients

sometimes is virtually impossible to avoid certain amount of movement. Finally, it should be pointed out that in this study the identification of corresponding projections of each reference point in the two views and also the position of the projections of the radiopaque test balls was done manually by a trained operator. This makes this method slow and subject to intra- and inter-observer variability.

2.2.3 Applications of 3-D Positional Reconstruction for heart wall motion analysis

Following cardiologists' great interest on observing the ability of the heart to pump blood, many researchers began to develop methods for quantifying heart wall motion starting at the beginning of this decade.

The quantification of the movement of the heart walls requires the identification of many points and the tracking of their movement in 3-D space over several heart cycles. Many radiological techniques such as LV angiography and ultrasound have been used, but they do not really provide enough information, since they produce two-dimensional projected images or two-dimensional slices of the heart.

MacKay et al.[64] have developed a technique to track over time and in three-dimensions bifurcation points of coronary arteries or surgically implanted markers by tracking their projections onto biplane coronary cineangiograms. This method uses again the perspective transformation method and the homogeneous coordinate representation explained in Section 2.2.2.1 because it permits any arbitrary geometry and position of the X-ray tubes and image intensifiers. This method uses a plexiglass cube with lead pellets placed at accurately known

locations as a calibration object. This cube needs to be imaged immediately after the patient is examined and before the X-ray equipment is moved. The projections of the lead pellets of the calibration cube are used to generate the perspective transformation matrix that mathematically describe the mapping between the 3-D object space and the 2-D input screen.

2.2.3.1 Introduction of the auxiliary line technique

One the most powerful ideas introduced by this paper is the utilization of the so-called auxiliary line technique for identifying corresponding projections of points in the two views (see also Section 3.6.3). This technique uses the fact that the true position of a point must lie along the line determined by its projection in one view and the X-ray focal spot. Using the appropriate perspective transformation, the equation of this line in 3-D space and its projection onto the other view can be calculated. Since it is known that the projection of the point in question must lie on this auxiliary line, particularly, at its intersection with the blood vessel, this technique provides a method for the identification of corresponding projections in each view of any point in space.

The selection by an operator of corresponding projections onto two different views has always been a slow and confusing task. For example, bifurcation points can often be on edges or obscured in one or the other view, and corresponding projections of implanted markers are hard to identify since there isn't any arterial connectivity to guide the task. The auxiliary line technique is therefore a very powerful tool for solving all the of above identification problems and other ones as well.

These investigators have used a metal grid with known spacing to correct for the non-linear geometric distortion introduced by the curvature of the image intensifier input screen (see Section 2.2.1.1). They have used a cubic polynomial method to find the relation between measured distorted image coordinates and known undistorted coordinates of points on the reference grid. The coefficients of this polynomial are chosen to minimize the squared distance between the polynomial estimate of the undistorted position and the actual position.

The accuracy with which this method can locate the original position of points in 3-D space. The 3-D positioning accuracy was tested using one of the spatial calibration cubes to take advantage of the precise knowledge of the 3-D position of the lead pellets embedded in the plexiglass cube. The average error between the distance measured directly between 15 points on the cube and the ones calculated using the results of the 3-D positioning program was less than 0.03 cm.

This method, although very accurate and elegant, presents one big disadvantage. It requires the imaging on the spatial calibration cube immediately after the patient examination and before the position of the X-ray equipment is changed. This is a condition which is very hard to achieve in the day-to-day clinical environment because usually for each patient study images are taken from various different angles. Also, often, after the last image has been acquired, the setting of the X-ray equipment has to be changed to make room to move the patient out of the examination table.

After this work, several other studies have been published which exploit the elegance and accuracy of the perspective transformation method and the power of the auxiliary line technique.

Potel et al.[65,66] have used this technique to evaluate the three-dimensional motion of left ventricular epicardial points by tracking coronary artery bifurcations using three different coordinate systems. Liu et al.[67] have also applied the same methods to the study of the motion of the left ventricular wall by tracking surgically implanted metallic markers throughout the cardiac cycle on several animals.

Some preliminary work has also been reported about an analysis system developed for generating moving three-dimensional images of the heart and coronary arteries.[68] This system also uses both the perspective transformations and the auxiliary line methods. The first step of this method is to manually identify corresponding coronary artery bifurcation points for the first frame of a cardiac cycle aided by the auxiliary line. These bifurcation points are then automatically identified on each view for the subsequent frames of the cardiac cycle utilizing a technique based on statistical correlation methods used for image registration.[69] Initially, a 64×64 reference image $R(x,y)$ from the first frame and centered on bifurcation point (x_1, y_1) is determined. This reference image is then correlated with a 128×128 search image $S(i,j)$ centered on point (x_1, y_1) from the next consecutive frame. Each correlation coefficient $C(i,j)$ is computed using the following equation:

$$C(i,j) = \frac{\sum_{x=0}^{63}\sum_{y=0}^{63} R(x,y)S(i+x-31, j+y-31)}{\sqrt{\left[\sum_{x=0}^{63}\sum_{y=0}^{63} R^2(x,y)\right]\left[\sum_{x=0}^{63}\sum_{y=0}^{63} S^2(i+x-31, j+y-31)\right]}} \qquad (2.2.3.1\text{-}1)$$

Due to the enormous computational complexity of this operation, this part of the analysis was implemented in the Fourier domain using an array processor. The output data generated by this stage of the process is for the analysis of epicardial wall movement and for the establishment of the start and end point of each vessel branch.

The next step is to automatically track each defined vessel segment along its center line on each frame of the cycle. After the generated center lines are smoothed the diameters of the vessel segments are computed using the second derivative of the intensity profiles at every second pixel along each of the center lines. By carrying out this process for each vessel section in each view, the center line can be positioned in the true 3-D space. In addition, these researchers report that by utilizing the information obtained about the diameters of the different vessel segments, they can obtain a three-dimensional solid-model representation of the arteries using the technique reported by Mol et al.[72,73,74]. However, no results of any kind are shown for this part. The fundamental problem of this method is, again, that it requires an enormous amount of operator intervention, which makes the process unpractical for the clinical environment and subject to human errors.

2.2.4 Applications of 3-D positional reconstruction for the display of the arterial tree

The first attempt at obtaining computerized 3-D displays of the coronary arterial tree which we have found in the scientific literature was published in 1976 by Smith and Starmer.[70] It was connected to the desire of investigating the relationship between the geometrical shape of this vascular structure and coronary artery disease. Using two orthogonal views, these investigators developed algorithms which approximate the arterial tree as a simple 3-D structure formed by a number of connected straight lines. The correspondence between points in the two views is simplified by assuming equal magnification for the two projections. The final 3-D coordinates of each point was determined by using the expressions developed by Dodge et al.[58] already mentioned in Section 2.2.1. Unfortunately, this first method for

displaying the arteries in three dimensions present a number of major problems: First, the representation of each arterial segment as a straight line is a rather crude approximation; second, normally the magnification for each orthogonal view is different and not equal as it was assumed here; and third, an enormous amount of operator interaction is required, which makes this approach very slow, tedious, and subject to human errors. In addition, there is no information about the accuracy of this method since no error analysis was presented.

Perspective transformations, on the other hand, seem to have been used for the first time for obtaining the exact 3-D position of points from measurements of their projections onto pairs of X-ray shadowgraphs by Sayre et al.[71] in 1979. This perspective transformation approach is convenient and accurate because it does not require to make any assumption about the geometrical arrangement of the system components or any measurement of the positions of the X-ray tubes and image intensifiers (see Section 2.2.2.1 for a detailed explanation of this method). However, this approach requires the imaging of a calibration object immediately after the patient study is completed but before changing the position of the elements of the system. This is necessary for inferring the elements of the perspective transformation matrices. Unfortunately, as we pointed out before, for most typical clinical environments this requirement becomes a problem, since usually for each patient X-ray images are obtained from several different angles. Also, often, at the end of the study, the position of the X-ray equipment has to be changed in order to make room to move the patient out of the examination table.

The purpose of this work was to create 3-D angiograms which could be superimposed on CAT scan images in order to show the position of vessels which normally cannot be seen

in the scan. This method was tested with angiographic images of the cerebral arteries and CAT scan images of the head. Arteries were approximated by a series of interconnected straight line segments.

A very serious problem with this method is that it requires the manual tracing of all the vessels to be superimposed on the scan (these investigators used approximately 300 points per angiogram). This makes the process time-consuming and inaccurate. Furthermore, no analysis on the accuracy of the results was presented in this report.

Later research has again used the perspective transformation method to obtain a more realistic 3-D display of the arteries. Mol et al.[72,73,74] have obtained 3-D solid representations of blood vessels from biplane images which included the aortic root and major arteries leading up to the head and arms. They have also applied their 3-D reconstruction technique to cerebral arterio-venous malformations.

Using very sophisticated software and hardware, these researchers have developed a method which performs automatic measurement of vessel width at regular intervals. The reconstructed vessels were modelled as a series of cylinders with diameters equal to that of the measured vessel segments which are connected with spheres to smooth the transitions. The auxiliary line technique was used in conjunction with perspective transformations to identify corresponding stretches of the vessels on the two views. Prior to any measurements, the image pincushion distortion was corrected using a "rubbersheeting" transformation which doesn't assume the distortion to be radially symmetric and which is applied to all images. This type of correction decreases the error in the positioning of specific points in

3-D space from 0.4 mm to 0.2 mm. These accuracy results were obtained using images of the same plexiglass cube used for the spatial calibration which contains steel markers whose positions are known very accurately.

Major drawbacks of this work are the need for a tremendous amount of computational power (e.g., the computations required just for the displaying of one single image was reported to take up to ten minutes), and the considerable amount of time required by an operator to identify the various landmarks on the two views. These problems preclude the use of these techniques as they are in an automated imaging system for routine clinical use.

A different approach for the identification of corresponding projections of a point onto two orthogonal planes has been used for the 3-D reconstruction of cerebral arteries in both a dog experiment and a clinical study.[75] The correspondence of projections in this work is obtained by using the fact that the dye density at the leading edge of the moving substance shows the same changing patterns in the two projected views. The detection of the moving dye-edge is accomplished by means of a dye-edge tracking algorithm. This algorithm uses a cross-correlating matching method to determine the dye-edge displacement on consecutive frames. For each digitally subtracted orthogonal X-ray density profiles of consecutive frame pairs $D_i(n)$ and $D_{i-1}(n)$, the cross-correlation coefficients $\rho_i(k)$ for different values of the pixel shift variable k as

$$\rho_i(k) = \frac{\sum_{n=1}^{N-k} [D_{i-1}^{k}(n) - \overline{D}_{i-1}]\,[D_i(n) - \overline{D}_i]}{\sqrt{\sum_{n=1}^{N-k} [D_{i-1}^{k}(n) - \overline{D}_{i-1}]^2 \sum_{n=1}^{N-k} [D_i(n) - \overline{D}_i]^2}} \qquad (2.2.4\text{-}1)$$

with

$$\overline{D}_i = \frac{1}{N-k}\sum_{n=1}^{N-k} D_i(n) \qquad (2.2.4\text{-}2)$$

Where

i : Sequence number of present image frame.

n : Pixel position number in the center line for each frame.

N : Total # of pixels of the center line of one frame.

$D_i(n)$: Contrast density at the n^{th} pixel position in the i^{th} frame.

The peak point of each cross-correlation operation provides an estimated value of the displacement of the dye-edge, which is positioned along a manually traced vessel center line. In this way, the position of projection of the dye-edge along the vessel center line can be specified simultaneously in both views for each frame.

To obtain the 3-D coordinates of these points, the perspective transformation method is used. These researchers report that they have developed a new simplified algorithm for obtaining the perspective transformation matrices which describe the projected image. For working with small size vessels, for which the accuracy of the cross-correlation method is low, the auxiliary line technique has been incorporated to the reconstruction algorithm as a complementary tool. To demonstrate the validity of the results, images of the original recorded cerebral vessels and of the reconstructed ones are shown. Although the visual comparison of the images is quite good, one can conclude that the accuracy of the results still needs to be improved and more quantitative means of measuring the reconstruction

error should be found. In addition, unless the processes for both the generation of the center lines and the identification of corresponding points for the case of small vessels gets automated, this approach will continue to be unpractical for the clinical environment.

Sometimes it may be desirable to know the exact position of the cerebral blood vessels for planning or guiding brain surgery. Due to this interest, Suetens et al.[76] studied the feasibility of three-dimensionally reconstructing these vessels using a lateral and a frontal angiogram (orthogonal views). Using a tomographic approach, they attempted to obtain binary reconstructions with and without a priori knowledge about the problem. They demonstrated that it is impossible to reconstruct the cerebral blood vessels without the use of a priori knowledge. Since these investigators also felt that using some a priori knowledge, would not enable them to satisfactorily solve this particular problem, they decided to develop a second different approach. The goal of this second method is to reconstruct the skeleton of cerebral blood vessels using stereoscopic pairs of DSA images.[77] This skeleton is represented by string of micropatterns characterized by their orientation, width and intensity in each view. Subsequently, corresponding micropatterns in each view are identified using an algorithm for automatic segment matching based on concepts from human stereoscopic depth perception. Finally, the 3-D position of these points are determined using the following classical expressions of the field of stereometry:

$$x = \frac{z x_l}{f} \tag{2.2.4-3}$$

$$y = \frac{z y_l}{f} \tag{2.2.4-4}$$

$$z = \frac{fd}{x_l - x_r} \qquad (2.2.4\text{-}5)$$

Where

f : Focus-detector distance.

d : Distance between focal points of X-ray tubes 1 and 2.

The above formulas give the 3-D position (x, y, z) of a point p imaged with a stereoscopic X-ray system with its origin at the focus of the left X-ray tube. The l and r subscripts denote measurements associated with the left and right views respectively.

These algorithms were tested with both clinical data and data generated from a model of the cerebral arteries built with a human skull and copper wires representing the blood vessels. From these results these researchers concluded that this "algorithm is not completely reliable." In addition, these methods requires a large amount of computational power. Lastly, these investigators pointed out a problem which should be expected with stereoscopic systems and which has to do with the accuracy of measurements in the Z direction. Their conclusion regarding this aspect was that the accuracy of the values obtained for the z component was poor, and that an error in z due to a measurement error in the X direction is almost ten times larger than the measurement error itself.

2.2.5 Applications of 3-D positional reconstruction for the tracking of the arterial tree

Although this research project is not concerned with developing methods for the tracking of the arterial tree, we have decided to include here a section reviewing prior work on this area because of three reasons: First, because some of the techniques used in these tracking algorithms that we have found are relevant to our 3-D positional reconstruction problem; second, because of the importance that automated or semi-automated methods for the analysis of angiocardiograms are gaining at present; a goal which seems the next logical step in computerized processing of X-rays images of the arteries; and third, because we have designed our reconstruction algorithms modularly so that in the future they can be easily combined with some automatic tracking algorithm in order to be able to produce automatic 3-D reconstructions of the whole coronary arterial tree.

Several research groups have attempted to automate the computerized quantitative analysis of digitized angiograms in the recent past. So far, most proposed approaches require a great deal of operator interaction, which makes this type of analysis on clinical images a very time consuming process.

Hoffmann et al. have reported a very successful method for to the automatic tracking of human vasculature[78] which uses a previously developed, computationally efficient, double-square-box region-of-search algorithm.[79] This method can automatically track single-view cranial images and stereoscopic pairs of cerebral angiograms after they have been digitally subtracted. These investigators have also shown that this algorithm may be capable of automatically tracking non-processed, unsubtracted images. Another feature of

this tracking method is that it automatically computes and saves the vessel width, contrast and center line position at each tracked point on the blood vessel. The information obtained from automatically tracked pairs of stereoscopic angiograms can later be used to generate 3-D representations of the vascular tree. Once this is accomplished, it is also possible to generate 2-D projected images of the same vasculature from any viewpoint for observation.

To identify the corresponding projections of a point onto the two different views, these investigators have taken advantage of the high spatial correlation which characterizes stereoscopic pairs of images (see Section 3.6.3). In stereoscopic imaging the X-ray sources are separated from each other only by a small shift. Consequently, the projected images exhibit a large degree of similarity. To map each tracked point on one image to the corresponding one on the other image, a density profile perpendicular to the direction of tracking was obtained. This density profile was then compared to a set of profiles obtained on both sides of the stereoscopic image shift line also perpendicular to the tracking direction. The center point of the profile from the second view which yields the smallest RMS difference is the one which gets correlated to the point being tracked on the first image. By repeating this step at each tracked point after the calculation of the vessel contrast, width and 3D center line position, the 3D representation of the vascular tree was generated.

The tracking algorithm used in this work processes each image of the stereoscopic pair independently. The coronary arterial tree, however, has a geometrically complex 3-D structure. In addition, depending on the imaging angle this complexity can increase on the recorded image. When this fact gets combined with the noise, artifacts, overlapping structures and background level variations typically present in this type of images, cases arise in which automatic tracking algorithms make identification errors. Because of this

problem, we think that an algorithm simultaneously using both views to track the arterial is likely to be more accurate when performing this difficult task, since it has more information available to predict the course of the artery. In addition, the accuracy of the obtained computer reproductions of the arteries was not analyzed in any way other than visual. Moreover, the arteries were assumed to have cylindrical cross-sections, which may not be a very realistic assumption.

Parker et al.[80] have developed a semi-automated method for the 3-D reconstruction of the moving arterial tree from two X-ray images. This method requires the intervention of an operator for the identification of all the bifurcation points of the vascular bed for each of the frames of a sequence of images in one view. The identified nodes in one view are corresponded to the other view using perspective transformations and the auxiliary line technique. Subsequently, edge detection is performed automatically in order to determine the edges of the vessel and the center line.

To obtain the 3-D representation of the outlined vessels, these investigators have introduced a technique incorporating dynamic programming and least squares techniques which produce the most likely 3-D arterial tree from the 2-D trees obtained from each view.

The approach presented in this paper presents the following problems:

a. It assumes that the arterial cross-section is circularly shaped, which is unrealistic specially in regions where there are stenoses present.

b. The method requires a considerable amount of operator intervention, which makes the results subject to errors and the processing slow and tedious.

c. An objective analysis on the accuracy of the results has not been presented.

Nguyen and Sklansky[81] have developed a completely automatic, computationally efficient, and accurate method for tracking the skeleton of the coronary arterial tree in two dimensions. The detection of the skeleton is obtained without having to determine the boundaries of the arteries. Instead, they developed a technique to track the ridge pattern present in the intensity profiles of each scan line. Using this approach, these investigators can automatically separate the arteries from the background and measure their medically significant features (boundaries, orientation, and others).

Other researchers have taken a different approach to automatically generate the arterial tree. This other approach uses expert systems for the analysis of the blood vessels. One of the advantages of using this type of systems is that they may help to reduce the large intra- and inter-observer variability that it is known to occur with past techniques for angiogram analysis. Stanfield[82] has proposed a rule-based expert system developed for obtaining the automatic segmentation of coronary arteries and a 2-D representation of the obtained tree using monoplane DSA images. This system uses about 50 production rules which use basic image segmentation concepts and also cardiac anatomy and physiology knowledge. Some results were shown and solutions being studied for solving persisting problems were presented.

Suetens et al.[83] have reported the development of an expert system for the segmentation of blood vessels. The objective of this system is to automatically find and quantify lesions in the blood vessels and also to automatically generate 2-D representations of the arterial tree. Using a bottom-up problem solving approach, this knowledge based system processes the blood vessels in three major steps:

1. The first step uses only geometrical knowledge of line patterns.

2. The second step uses general knowledge about the blood vessels.

3. The third step uses domain specific knowledge about the kind of arteriogram, the patient, the disease, etc.

This paper also describes the development and test of about 30 production rules which only deal with the first step of the knowledge based analysis. Examples of some of these rules are discussed. The results presented were obtained by only making use of low-level geometrical knowledge of line patterns. They evidence the need for considerable improvement of the technique. No accuracy analysis was reported.

More recent research has proposed a three step method to automatically obtain the skeleton of coronary arteries using two orthogonal X-ray images.[84] These three steps are the following:

1. Segmentation: Identifies all the segments composing the tree in each view.

2. Correspondency: Matches corresponding segments in the two views.

3. Reconstruction: Obtains the 3-D coordinates of the points in each original segment.

This method modeled the arteries as a series of connected thin segments, and there was no attempt at all in reconstructing the cross-sectional shape of the arterial lumen. In addition, they assumed a system in which there is no magnification effect present and they used this fact to easily obtain the correspondance of points in the two views, as well as the 3-D coordinates of the vessel center line. This is an impossible situation in any real biplane

X-ray system in which typically there exists a different amount of magnification for each view. In such real systems it would not be possible to reconstruct the position of points using this simplified approach.

Finally, these researchers used images acquired by a TV camera of a tree-like simple structure to test their algorithms. Resulting images are provided for visual evaluation, but no objective analysis of their results was presented.

3 THEORY OF THE RECONSTRUCTION METHODS

In this chapter we will explain in detail the theory associated with the different areas into which the research conducted for this dissertation can be grouped, and in the following chapters we will present the obtained results, discuss them, and suggest future related work.

The purpose of this research was to develop a clinically practical, inexpensive, and accurate method to obtain the 3-D representation of the arterial lumen from two orthogonal digitally subtracted X-ray angiograms by stacking 2-D reconstructions of arterial cross-sections at a sequence of adjacent cuts across the vessel main axis. Using this tomographic approach, the problem of the 3-D reconstruction of arteries can then be subdivided into two smaller basic problems. The first is that of finding the arterial cross-sectional shape for each of a number of selected transverse cuts, and the second one that of obtaining the 3-D position of the reconstructed slices from the position of their projections on the two orthogonal views.

It may be of interest to the reader to know that the tomographic approach to 3-D reconstruction of bodies (i.e., reconstruction of slices) is not always possible.[85] There are cases, such as in some practical applications of electron microscopy, in which it is not possible to define an axis of rotation and for which direct 3-D reconstructions techniques have been formulated.

To solve the two basic problems mentioned above independently a cross-sectional reconstruction algorithm and a 3-D positional reconstruction algorithm were developed. In addition, to progressively improve and to test the accuracy of the algorithms mentioned above, the following work was also completed:

1. Development of a computer-simulated 3-D solid model of a cylindrical arterial segment containing a stenosed region that can be projected onto two orthogonal planes to simulate biplane X-ray shadowgraphs of arteries. The cross-section of the stenosed portion can simulate stenosis shapes and sizes similar to those typically encountered in patients suffering from atherosclerosis. This allows us to simulate cross-sections with varying degree of reconstruction difficulty. This model also has the capability of rotating and translating the arterial segment in order to permit the generation of simulated X-ray views of the vessel from many possible angles.

2. Development of a computer-simulated model of the center line of an arterial segment and its projection onto two orthogonal planes. This model can simulate various arterial center-line shapes as well as the presence of a stenotic lesion (optional).

3. Addition of noise to the computer simulations mentioned in Steps 1 and 2.

4. Acquisition of digitally subtracted X-ray images of a plexiglass model of an arterial segment built to a 1:1 scale to test the cross-sectional reconstruction algorithm.

5. Development of the programs for the adequate display of the generated data and reconstructions.

A great deal of effort was spent on the testing of these algorithms with computer and plexiglass vessel models under many different conditions, since the usefulness of the developed methods depends to a large extent on the accuracy of the two different reconstruction algorithms. Computer simulation permitted us to concentrate on each possible problem independently and solve it. It also allowed us to perform a careful error analysis. Afterwards, the algorithms were confirmed with X-ray images of the plexiglass vessel model (whose dimensions were also known), and improved when necessary. Notice that it is impossible to check the degree of reconstruction error when using patient X-ray data.

In the following sections, topics pertinent to this research are discussed in detail.

3.1 Computer-simulated X-ray Shadowgraphs of Stenosed Vessel Model

A computer program to simulate X-ray shadowgraphs of mathematically defined vessel segments of cylindrical shape and variable size containing one stenosed section was developed. The stenosed vessel model is graphically represented on Figure 3.1-1. This computer model permits the generation of ideal X-ray density profiles that are used as input data to test the cross-sectional reconstruction algorithm.

This data generation program can simulate various lumenal cross-sectional shapes for the stenosis section by defining there different regions over a geometrical arrangement of one or more circles. To simulate the various dissimilar tissues, typically found in X-ray images of the arteries, the model cross-sections are divided into several regions, each associated with a different value of the parameter D representing the X-ray absorption

density coefficient. Figure 3.1-2a shows a half-circle-shaped stenosed cross-section and Figures 3.1-2b and 3.1-2c two different types of crescent-shaped cross-sections. Crescent shape II was created to resemble the crescent shape simulated with the plexiglass model. The variable radii of the circumferences permit the simulation of different values of Percent Stenosis. $D1, D2$ and $D3$ represent the X-ray absorption densities of the different regions. $D1$ is the density of the region that represents the unobstructed part of the arterial cross-section, containing the mix of blood and contrast substance, which we intend to reconstruct. This area was assigned a density value equal to k units per pixel. By varying the value of k we were able to vary the sensitivity of the detector unit of the system (number of gray levels of absorption per pixel). The remaining regions, which do not contain blood, were always assigned density values of 0 unit per pixel. This model also simulates the effect of the partially filled pixels on the periphery of the vessel (see Section 3.1.3).

3.1.1 Variation of the spatial orientation of the simulated vessel segment

In order to simulate X-ray density profiles taken from different angles, the vessel segment can be arbitrarily translated and rotated with respect to the origin.

By defining

$(x, y, z) \equiv$ original coordinates of a point.

$(x_t, y_t, z_t) \equiv$ coordinates of the point after translation.

$(x_r, y_r, z_r) \equiv$ coordinates of the point after any rotation.

$(x_{rt}, y_{rt}, z_{rt}) \equiv$ coordinates of the point after any rotation plus translation.

$\Delta x, \Delta y, \Delta z \equiv$ displacements in the x, y, and z direction respectively.

$\theta_x, \theta_y, \theta_z \equiv$ angles of rotation about the x, y, and z axis respectively.

$$\mathbf{p} \equiv \begin{pmatrix} x \\ y \\ z \\ 1 \end{pmatrix}$$

$$\mathbf{p}_r \equiv \begin{pmatrix} x_r \\ y_r \\ z_r \\ 1 \end{pmatrix}$$

$$\mathbf{p}_t \equiv \begin{pmatrix} x_t \\ y_t \\ z_t \\ 1 \end{pmatrix}$$

$$\mathbf{p}_{rt} \equiv \begin{pmatrix} x_{rt} \\ y_{rt} \\ z_{rt} \\ 1 \end{pmatrix}$$

and a coordinate system like the following

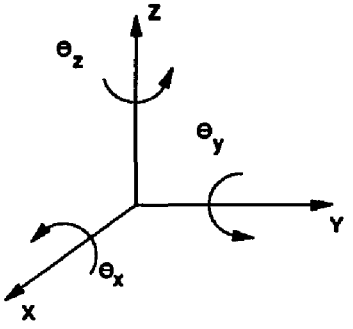

the above mentioned translation can be accomplished using transformation

$$\mathbf{p}_t \equiv \mathbf{T}_t \mathbf{p} \tag{3.1.1-1}$$

$$\mathbf{T}_t \equiv \begin{pmatrix} 1 & 0 & 0 & \Delta x \\ 0 & 1 & 0 & \Delta y \\ 0 & 0 & 1 & \Delta z \\ 0 & 0 & 0 & 1 \end{pmatrix} \tag{3.1.1-2}$$

and any rotation can be obtained using combinations of the following transformations:

a. For rotation with respect to the X axis:

$$\mathbf{p}_r \equiv \mathbf{T}_x \mathbf{p} \tag{3.1.1-3}$$

$$\mathbf{T}_x \equiv \begin{pmatrix} 1 & 0 & 0 & 0 \\ 0 & \cos\theta_x & -\sin\theta_x & 0 \\ 0 & \sin\theta_x & \cos\theta_x & 0 \\ 0 & 0 & 0 & 1 \end{pmatrix} \tag{3.1.1-4}$$

b. For rotation with respect to the Y axis:

$$\mathbf{p}_r \equiv \mathbf{T}_y \mathbf{p} \tag{3.1.1-5}$$

$$\mathbf{T}_y \equiv \begin{pmatrix} \cos\theta_y & 0 & \sin\theta_y & 0 \\ 0 & 1 & 0 & 0 \\ -\sin\theta_y & 0 & \cos\theta_y & 0 \\ 0 & 0 & 0 & 1 \end{pmatrix} \tag{3.1.1-6}$$

c. For rotation with respect to the Z axis:

$$\mathbf{p}_r \equiv \mathbf{T}_z \mathbf{p} \tag{3.1.1-7}$$

$$\mathbf{T}_z \equiv \begin{pmatrix} \cos\theta_z & -\sin\theta_z & 0 & 0 \\ \sin\theta_z & \cos\theta_z & 0 & 0 \\ 0 & 0 & 1 & 0 \\ 0 & 0 & 0 & 1 \end{pmatrix} \tag{3.1.1-8}$$

Finally, the combined results of the translation and rotations can be combined into a single transformation matrix $\mathbf{T}_{rt}$ resulting in

$$\mathbf{T}_{rt} \equiv \mathbf{T}_x \mathbf{T}_y \mathbf{T}_z \mathbf{T}_t \tag{3.1.1-9}$$

which allows to compute the final position of each point as

$$\mathbf{p}_{rt} \equiv \mathbf{T}_{rt} \mathbf{p} \tag{3.1.1-10}$$

3.1.2 Generation of the two orthogonal X-ray images

To simulate X-ray shadowgraphs of the simplified stenosed arterial segment described above, we have assumed a parallel geometry, i. e., the transmitted X-ray energy travelling in straight lines to the detector from an X-ray source at infinity.

The rotated body simulated by the computer model can be represented by the three-dimensional function $f(x,y,z)$. This function can only take values equal to $D1, D2$, or $D3$ depending on the region. Then, an X-ray projection of this object can be obtained by creating a two-dimensional image formed with the values of the line integrals of this function along assumed parallel X-ray paths.

Let the two orthogonal projections onto the XZ and the YZ planes, corresponding to the biplane X-ray views, be initially denoted as f_{xz} and f_{yz} respectively. Then, these projections can be obtained from the following expressions:

$$f_{xz} = \int f(x,y,z)dy \tag{3.1.2-11}$$

$$f_{yz} = \int f(x,y,z)dx \tag{3.1.2-12}$$

Since the model is created using digital techniques, the continuous function $f(x,y,z)$ can be approximated by the discrete three-dimensional function $F_{xyz}(i,j,k)$ which satisfies the equation

$$F_{xyz}(i,j,k) = \int_{\Delta V} f(x,y,z)dV \qquad \forall \quad i,j,k \tag{3.1.2-13}$$

where ΔV is the volume *dxdydz* centered about (i,j,k).

Then, the two orthogonal projections F_{xz} and F_{yz}, corresponding to the biplane X-ray views can be generated as

$$F_{xz} = \sum_{\text{all } j} F_{xyz}(i,j,k) \tag{3.1.2-14}$$

$$F_{yz} = \sum_{\text{all } i} F_{xyz}(i,j,k) \tag{3.1.2-15}$$

3.1.3 Treatment of the model surface

In most real cases, the periphery of vessel cross-sections does not occupy entirely the rectangular areas associated with each border pixel and this affects, accordingly, the intensity of digitized X-ray shadowgraphs.

To introduce the effect of incomplete pixel filling, the data generation program includes the optional simulation of partially filled pixels around the border of the vessel lumen. This is done by approximating the value of the X-ray absorption density of the volume of size 1^3 pixel-spacing, centered about each rotated border pixel, by the average of the densities of the 64 smaller equal volumes which subdivide each original 1^3 pixel-spacing volume.

3.1.4 Simulation of image noise

In order to simulate the noise present in X-ray images, the program developed for the generation of arterial cross-sectional profiles has the optional capability of adding noise to

the generated ideal X-ray density profiles.

The noise added had zero Mean, various Variance values and followed a Gaussian probability density function. Usually, it was created in sets of 512 values. A large quantity of sets of pseudo-random numbers was always generated (usually 100), but we only picked those sets whose mean (always zero) and variance values were very close, or equal, to the desired ones. The noise was added, pixel by pixel, to the density profiles associated with the cut that was to be reconstructed. Therefore, for each cross-sectional reconstruction two different noise sets were used; one for the XZ density profile and the other for the YZ one.

The Gaussian noise was generated a priori, and using a look-up table technique. Two hundred numbers following a Gaussian probability density function were stored in a program and selected at random using a pseudo-random number generator having a uniform probability density function. This pseudo-random number generator was created as a subroutine using a multiplicative algorithm. After appropriate transformations, to obtain the mean and the variance requested by the user, the generated noise values were stored in a file. Later, during the data generation process, those files containing the noise sets with mean and variance values closest to the desired ones were selected, and their contents added to the signal.

3.2 Computer Model of Arterial Center Line with Stenosis

This computer model was created with the purpose of generating input data for the 3-D positional reconstruction algorithm. The data provided by this program was used for both the development and the final accuracy evaluation of the 3-D positional reconstruction

algorithm.

The positional reconstruction algorithm, which automatically interpolates the center line on each of the two arterial projections and computes the true coordinates of this center line in the original 3-D space, accepts as input data two sets of non-corresponding arterial center points (one set per view), previously determined by a center-finding algorithm (we have used a very accurate method develop by Barba et al.[86,87]).

The two sets of input center points were obtained using the biplane X-ray system geometry shown in Figure 3.2-1. Mathematically defined, three-dimensional curves, simulating the known center line of a vessel, were regularly sampled. These samples were then projected from two different point sources, representing the X-ray tubes focal spots, onto two perpendicular planes, representing the image intensifier input screens. Using Equations (3.1.1-1) through (3.1.1-10), different combinations of rotations and translations of the 3-D curves were possible. This resulted on biplane projections of vessel center points following a variety of center line shapes on the View 1 and View 2 planes.

3.2.1 Simulation of a stenosed region

The presence of an arterial stenosis will generally show on an angiogram as a region where the width or the opacity of the blood and contrast mixture decreases proportionally to the degree of narrowing, or even as a discontinuous lumen in the case of a sub-total stenosis. In these cases, the centering algorithm will generally yield incorrect vessel midpoints through the stenosed region, which in turn will produce an erroneous vessel center line in that area. Therefore, it is preferred to interpolate the center line through the diseased

portion using some of the center points determined immediately before and after the stenosis.

For this reason, the data generation program described before has the option of introducing a stenosed segment in any portion of the simulated center line by the truncation of some of the projected arterial center lines samples in each view. In this manner, a stenosed segment of variable length and position along the vessel can be introduced in the data generated by this computer program. In addition, the 3-D coordinates of the center line samples corresponding to the truncated region were saved, along with the rest of the data samples, for future comparison with the results generated by the positional reconstruction algorithm.

3.2.2 Simulation of errors in input data

Any center-finding method always introduces some amount of error in the computation of the vessel center points which should be taken into account in the simulation. The presence of errors in the input data of the 3-D positional algorithm was simulated by adding previously generated Gaussian noise to the coordinates of the projected center line samples. The standard deviation of the added noise was made equal to the desired mean centering error (MCE). The values of noise standard deviation used included the range of typical errors produced by the centering algorithm described by Barba et al.[86,87] (MCE = 0.1 - 0.4 pixel).

3.3 Plexiglass Vessel Model

This model was utilized for the generation of actual X-ray shadowgraphs that were used for performing cross-sectional reconstructions. These results and the ones obtained

from similar computer-simulated data are shown in Section 4.

The vessel model was developed and built by Dr. Edmund M. Herrold, a researcher at the Division of Cardiology of The New York Hospital-Cornell Medical Center and a member of our Medical Imaging Research Team. The model is made of plexiglass and shown on Figure 3.3-1. It is divided into three plexiglass slabs which are held together, in perfect alignment, by two metal screws. The stenosis portion is simulated with the middle slab. A number of these slabs are available for representing various asymmetric shapes and sizes of stenosed lumena. The model is built to a 1:1 scale. The reference section is always three mm and since the typical diameter of coronary arteries is approximately between three to five mm, this model simulates the relatively more difficult to reconstruct arteries.

The X-ray images of this model were acquired at the Catheterization Laboratory of the Department of Cardiology of The New York Hospital-Cornell Medical Center.

3.4 General Methodology of the 3-D Reconstruction Technique

The 3-D reconstruction technique requires the use of a digital biplane X-ray system to generate two orthogonal digitally subtracted images of the coronary arteries. On each of these two images, a radiologist or cardiologist should select a number of approximate center points along the arterial branch to be reconstructed. The selected points must progress along the artery in one direction and should be close enough so that the straight line segments joining them approximate the vessel center line. If a stenosed region is present, instead of specifying approximate center points along this portion of the vessel, the operator is required to mark the beginning and end of this region.

The 3-D reconstruction process proceeds to:

1. On each view, estimate the exact position of the vessel center points at the operator selected locations and at intermediate intervals. Each vessel center is found with a very accurate cross-correlation method (sub-pixel accuracy) for center and diameter finding developed by Barba et al.[86,87].

2. Automatically determine the center line of the whole vessel (including along stenosed region(s) with a local interpolation) on each of the views, using the 3-D positional reconstruction algorithm.

3. Using the 3-D positional reconstruction algorithm, automatically find corresponding projected center points on each view and their original 3-D coordinates at a series of regularly spaced intervals along the complete estimated arterial center line on View 2.

4. Estimate the vessel projected diameters, using the method of Step 1, at the above selected points on each view.

5. Determine the shape of the arterial lumen at horizontal cuts made at each of the points selected in Step 3, using the cross-sectional reconstruction algorithm and vessel diameters obtained in Step 4.

6. Obtain the 3-D reconstruction of the artery by stacking the reconstructed cross-sections using the positional information computed in Step 3.

3.5 Arterial Cross-sectional Reconstruction Algorithm

The cross-sectional reconstruction algorithm was developed to obtain the shape of coronary artery lumen cross-sections at various selected transverse cuts along the vessel. For each slice to be reconstructed, the algorithm uses as input data a pair of X-ray photon density profiles obtained from two orthogonal, logarithmically amplified, digitally subtracted coronary angiograms. Based on the law of Lambert and Beer[88,89,90], these X-ray photon density profiles are linearly proportional to contrast concentration and depth. Assuming uniform contrast mixing, the X-ray photon density then becomes linearly proportional to lumen depth only.

The reconstructed cross-sections were represented as binary matrices. These are matrices whose elements are zeros where the mix of blood and contrast material is absent (outside the vessel), and ones where this mix is present (inside the vessel).

This algorithm assumes that the X-ray sources are placed at infinity, and therefore, that the transmitted X-ray photons (i.e., those which are not absorbed or scattered by the imaged object) travel in straight lines towards the detector. A restriction of this algorithm is that it also assumes that the artery segment to be reconstructed forms small angles with the imaging planes. However, this limitation can be overcome by reading the X-ray density profile data along the X direction if the vessel inclination angle is larger than 45^0, or along the Y direction if the vessel inclination angle is less than 45^0. The vessel inclination angle can be easily determined with our 3-D positional reconstruction algorithm.

3.5.1 Statement of the problem

First, let the artery to be reconstructed be defined by the three-dimensional discrete function $F_{xyz}(i,j,k)$, and also let the two-dimensional discrete functions $F_{xz}(i,k)$ and $F_{yz}(j,k)$ be the two orthogonal digitally subtracted X-ray images of this artery.

Then, the cross-sectional cut, or slice, determined by the plane z equal to a constant ($z = C$), which is to be reconstructed, can be represented by the matrix **M** which contains the values of the function $F_{xyz}(i,j,k)$ which are intersected by the plane $z = C$. This cross-section is always associated with two image scan lines, one for each orthogonal X-ray image, denoted by $F_{xz}(i,C)$ and $F_{yz}(j,C)$ and usually called the X and Y X-ray density profiles respectively. The signal in the X/Y density profile represents the line integrals or projections along Y/X direction on the plane $z = C$ slicing the body represented by the function $F_{xyz}(i,j,k)$.

The cross-sectional reconstruction problem can now be generally stated as that of determining the elements c_{ij} of the matrix **M**, representing the cross-section, which best matches the two orthogonal projections $F_{xz}(i,C)$ and $F_{yz}(j,C)$.

3.5.2 Use of constraints to obtain solution

In general, this problem does not have a unique solution. Even for the case when **M** is a matrix of binary elements, it has been shown[35-37] that two orthogonal projections are not sufficient to uniquely characterize any given shape since it is possible that, in some instances, several different shapes can yield the same two orthogonal projections.

Our approach to solve this problem is to use a constrained, iterative, probabilistic algorithm which uses a priori known information to reduce the ambiguities which are known to exist. The constraints used by this method are the following:

1. Binarization of the pixel values to be reconstructed. If one assumes homogeneous mixing of the blood and radiopaque substance, then one constant value of the X-ray absorption density can be assigned to each of the pixels inside of the blood-filled lumen, which is the region that we want to reconstruct, and a different constant value to the remaining pixels outside of the vessel. This reduces the problem to determining which pixels are inside of the lumen. The homogeneous mixing assumption is usually good for the reconstruction of arteries, because the proportion of blood and contrast agent during injection is never very disproportionate due to the small size of arteries (but less so for the reconstruction of the heart ventricles). The binary constraint is not exact for those pixels corresponding to the borderline of the vessel, which are usually partially filled only.

2. A cross-sectional cut along any unstenosed portion of an artery has a cylindrical shape. This assumption is based on the fact that a flexible vessel filled with a fluid which circulates under pressure will tend to keep a cylindrical shape. While this is probably true for peripheral vessels, for the coronary arteries this assumption may be valid only near end-diastole.

3. The region of reconstruction can never be outside of a Reconstruction Domain (RD) which has a circular shape and diameter equal to the diameter of the unstenosed portion of the artery. This assumption holds when the artery main axis is perpendicular to the plane of cross-sectional reconstruction (as in the cases of the reconstructions obtained

from X-ray shadowgraphs of the plexiglass vessel model). On the other hand, when this perpendicularity does not occur (as in typical clinical situations) the Reconstruction Domain becomes equal to the ellipse formed by the intersection of the circular vessel lumen with the plane of cross-sectional reconstruction. The dimensions of this elliptical Reconstruction Domain can be obtained from the diameter and the 3-D orientation of the vessel, which must be determined a priori.

3.5.3 Description of the cross-sectional reconstruction algorithm

The two orthogonal density profiles, $F_x(i,C)$ and $F_y(i,C)$, are the total absorptions along each of the X-direction and Y-direction back-projection paths. There are only N and M back-projection paths along the X and Y direction, respectively, which intersect the region of the lumen cross-section. Also, we define pixel (x_i, y_j) as the pixel located at the intersection of the i^{th} X-direction and the j^{th} Y-direction back-projection paths.

The flowchart of the **cross-sectional reconstruction algorithm** is shown on Figure 3.5.3-1. This algorithm is suitable for an artery whose main axis does not form a very sharp angle with the line perpendicular to the planes of reconstruction.

Each step of the algorithm is described, in detail, below:

1. Acquire biplane images:

Orthogonal sets of logarithmically amplified images acquired before and after contrast infusion are digitally subtracted. X-ray density profiles of the vessel lumen

are obtained from the two orthogonal, background-subtracted images. Although source images acquired by DSA systems are preferred, X-ray film based images can also be used.

2. Calculate Reference Value:

The Reference Value (*RV*) depends on the total X-ray absorption of the contrast substance inside of the lumenal cross-section and on the area perpendicular to the lumen axis. It is obtained at a nearby unstenosed region of the vessel. The reference lumen is assumed to be circular and to have its X-ray density profile limited by the regions, on each view, where the profile levels equal the level of the background. These points demarcate an absolute limit beyond which the algorithm does not allow any reconstruction. The Reference Value has the dimensions of Gray Levels per Pixel, and is calculated as follows:

$$RV = \frac{\overline{ABS_{total}}}{\pi r^2} \qquad (3.5.3\text{-}1)$$

Where

$\overline{ABS_{total}}$ ≡ Average total X-ray absorption of reference lumen.

$$= \frac{\sum_{i=1}^{N} F_{xa}(i,C) + \sum_{j=1}^{M} F_{ya}(j,C)}{2}$$

$\{F_{xr}(i,C)\}$, $i=1,\ldots,N$; $\{F_{yr}(j,C)\}$, $j=1,\ldots M$ ≡ X-ray density profiles of the reference lumen cut.

and

r ≡ Half the width (radius) of the reference region in pixel units, as calculated by the diameter finding method of Barba et al.[86,87].

3. Choose reconstruction plane and find orthogonal profiles:

Once the plane of the slice to be reconstructed is chosen, the two corresponding orthogonal density profiles on each view have to be determined using the Positional Reconstruction Algorithm (see Section 3.6).

4. Define reconstruction domain:

This is a geometric constraint which forces the cross-sectional reconstruction to only take place inside of a Reconstruction Domain (RD) of circular shape with diameter and center position determined by interpolating the centers and diameters of proximal and distal unstenosed nearby reference lumena. These centers and diameters are determined by the method of Barba et al.[86,87]. The Reconstruction Domain diameter is set one pixel smaller than the interpolated one in order to force the reconstruction of the centrally positioned pixels during the first iteration. Since most errors tend to result on the periphery of the lumen, by filling first the central pixels, the algorithm will run out of pixels to fill before it starts making many errors. Further, the diameter of the reconstruction domain is increased slightly on successive iterations (0.5 pixel

per iteration) to permit the reconstruction of the lumen borders.

5. Find number of pixels to be filled:

The number of pixels to be filled along each back-projection in this iteration, NFx_i and NFy_j, is obtained by dividing the total absorption along each path by the Reference Value (RV) derived in Step 2, as follows:

$$NFx_i = \frac{F_{xR}(i,C)}{RV} \qquad i = 1,\ldots,N \tag{3.5.3-2}$$

$$NFy_j = \frac{F_{yR}(j,C)}{RV} \qquad j = 1,\ldots,M \tag{3.5.3-3}$$

In essence, what this step does is to scale each X-ray density profile to cross-section pixel units.

6. Find candidate pixels:

For each back-projection path, make the unfilled pixels inside the reconstruction domain the only possible candidates for reconstruction during this iteration.

7. Calculate probability indicators:

Probability indicators for this iteration are assigned to each X and Y back-projection that intersects the Reconstruction Domain (RD), determined in Step 4, as follows:

i. The probability indicator, PIx_i, for the i^{th} back-projection is calculated as the number of pixels to be filled along the i^{th} path, NFx_i, divided by the number of candidate pixels for that path.

ii. The probability indicator, PIy_j, for the j^{th} back-projection is calculated as the number of pixels to be filled along the j^{th} path, NFy_j, divided by the number of candidate pixels for that path.

8. Fill lumen pixels:

In order to fill empty lumen pixels within the Reconstruction Domain, X and Y back-projection paths are examined independently. All the pixels selected according to Rule I (examining rows), explained below, are included in a set denoted $XSCP$, and all the pixels selected according to Rule II (examining columns), explained below, are included in a set denoted $YSCP$. Rules I and II are as follows:

I. For each row having a number of pixels to be filled equal to NFx_i, include in the $XSCP$ set the NFx_i pixels of that row with the highest column probability indicator PIy_j.

II. For each column having a number pixels to be filled equal to NFy_j, include in the $YSCP$ set the NFy_j pixels of that column with the highest row probability indicator PIx_i.

The number of pixels from any row or column that are included in these sets cannot be larger than the number of pixels to be filled, NFx_i or NFy_j, of the same path. In cases when there are a number of pixels with equal probability indicators which is larger than the one allowed for filling by Step 5, the ambiguity is resolved by decreasing the number of pixels to be filled of that row/column. This guarantees that these ambiguous pixels are not included in any set during this iteration.

Finally, fill all pixels which belong to the subset, denoted *CPS*, formed by the intersection of the two previously determined sets *XSCP* and *YSCP*, or equivalently

$$\{\text{Cross-section pixels}\} = CPS = XSCP \cap YSCP$$

9. Adjust isolated areas:

Pixels from small unfilled regions bordered by filled pixels are also included in the *CPS* subset, and single filled pixels, surrounded on all sides by unfilled pixels, are taken out of the *CPS* subset. The goal of this step is to eliminate the discontinuities that may occur because of random noise or ambiguities in the reconstruction. This procedure may yield a number of filled pixels larger than the one allowed by Step 5.

10. Update scaled projections:

The X and Y scaled projections are updated to reflect the parts of the cross-section that have been reconstructed. This is accomplished by subtracting from the NFx_i's and NFy_j's values, obtained in Step 5, the number of pixels filled along each row and column during this iteration.

11. Adjust domain:

The radius of the Reconstruction Domain is increased by 0.5 pixel to expand the area where reconstruction is permitted and allow the filling of border pixels.

12. This process is repeated iteratively until either no more pixels meet the conditions for filling or one of the two updated scaled projections less than or equal to zero.

3.6 Three-dimensional Positional Reconstruction Algorithm

The function of the three-dimensional positional algorithm is to automatically generate the arterial center line for each view and its position in 3-D space from the coordinates of the projected center line onto the two orthogonal views. The development of this algorithm was necessary for two reasons: first, to be able to correctly position each reconstructed slice in its original 3-D "patient space" and obtain the three-dimensional display of the artery; and, secondly, to determine on each projection the orientation of the artery, so that the appropriate elliptical Reconstruction Domain (*RD*) can be generated when the artery main axis is not perpendicular to the plane of reconstruction. We have developed two forms of this algorithm which we will refer to as the 3-D positional reconstruction algorithm I and the 3-D positional reconstruction algorithm II. The first one can reconstruct arterial center lines whose orthogonal projections are described by single-valued functions only. The second form, on the other hand, generalizes the 3-D positioning method to include cases where the center line orthogonal projections are described by multi-valued functions.

3.6.1 General overview

This algorithm was developed for a biplane X-ray system whose main components are geometrically arranged as on Figure 3.2-1. The system is composed of two perpendicular views, denoted by View 1 and View 2, each having an X-ray generator and an image intensifier. Points $S1$ and $S2$ represent the focal points of the X-ray tubes, and imaging planes $V1$ and $V2$ represent the output screens of the image intensifiers of View 1 and View 2, respectively. The perpendicular line to the imaging plane which goes through the focal

point of the corresponding X-ray tube is called the main axis of that view. The point of intersection of the two main axes, called the isocenter, is used as the reference origin of the "patient's" three-dimensional space. This is the space where the arterial center line to be reconstructed exists. Any point $P_i(x_i, y_i, z_i)$ on this center line, when imaged by this system, generates a projected image point onto the screen of each image intensifier, which belongs to the arterial center line of each shadowgraph. These projected image points are denoted as $P_i'(-B1, y_i', z_i')$ and $P_i''(x_i'', -B2, z_i'')$ on center lines of View 1 and View 2 respectively. Finally, the distances from the isocenter to the X-ray sources $S1$ and $S2$, and to the imaging planes $V1$ and $V2$, which are called the system dimensions, are variable and can be read from the system during the patient examination; therefore, they are assumed to be known. Errors in these readings and their propagation to the final results of our calculations have been investigated and found to be very small. For details of our error propagation analysis see Appendix I.

The input data for this part of the process are the coordinates of the center points of the arterial projections on each view. These midpoints are calculated by the iterative cross-correlation technique developed by Barba et al.[86,87], which assumes that the lumen of an unstenosed artery can be approximated by a cylinder. There is no need for any correspondence between the midpoints from View 1 and View 2. If a stenosis is present in the arterial segment under reconstruction, the algorithm uses the input center points proximal and distal to the stenosed region in each view to interpolate, also with cubic splines, the center line along this part of the artery.

As already stated earlier, two forms of the 3-D positional reconstruction algorithm have been developed. For the 3-D arterial center line finding algorithm I, we have assumed

that in each of the two orthogonal DSA images a single-valued function representing the projected vessel center line can be obtained using one of the two coordinate variables as the independent variable and the other as the dependent variable. This assumption, which is valid for most center lines of coronary arterial segments, is necessary because this algorithm uses cubic splines for interpolating the projected arterial center lines. Cubic spline interpolation requires that the independent variable of the interpolated data must be in a strictly increasing order. This means that only samples approximating single-valued curves can be interpolated with this technique. This condition, unfortunately, creates a problem since it is possible to find cases where the single-valued assumption is not valid. For example, when the lumen axis is perpendicular to the image plane, at least one of the projected vessel center lines does not approximate a single-valued curve. However, in this kind of cases, the center lines can still be interpolated with cubic splines if the data is first parametrized with respect to the vessel center line arc length (AL). Therefore, we decided to use that approach to develop a method that can reconstruct arterial center lines with multi-valued projections while still using cubic splines for the interpolation process. This second, more general form of the center line positioning method is called the 3-D positional reconstruction algorithm II.

3.6.1.1 Use of cubic spline interpolation

The use of cubic spline polynomials to represent the arterial center lines on each view is one of the most important contributions of this algorithm. It permits the representation of arterial center lines as piecewise mathematical functions. This allows automatic identification of corresponding points in both views since the intersection between each auxiliary line (or curve in the case of algorithm II) with the center line of View 1 can be conveniently

determined by computer with a mathematical equation. Our new approach eliminates the manual identification process present in prior methods using the auxiliary line technique, which was an impractical operation since it was slow, tedious, and subject to human errors.

The choice of using cubic splines for the interpolation was based on:

1. The fact that cubic splines are efficiently computed, easy to integrate and differentiate, and computationally stable.

2. That they are accurate for interpolating smooth, well behaved data (as in this case).

3. Their property of minimizing the propagation of interpolation errors caused by bad input data or difficult regions.

For an explanation of the basic concepts of cubic spline interpolation see Appendix II.

3.6.2 Reconstruction of the 3-D position of the center line

The equations for the 3-D coordinates of a point in terms of the coordinates of its two orthogonal projections onto two orthogonal planes and the system dimensions are derived below. We use Figure 3.2-1 and assume a point-source geometry.

First, let us adopt the convention of using prime symbols ($'$) for all the variables associated with View 1 and double prime symbols ($''$) for all those associated with View 2.

It follows that $S1 = S'$, $S2 = S''$, $A1 = A'$, $B1 = B'$, $A2 = A''$ and $B2 = B''$.

If we now let L_1 be equal to the straight line that goes through source S' and projected point $P_i'(-B', y', z')$, and L_2 equal to the straight line that goes through source S'' and projected point $P_i''(x_i'', -B'', z_i'')$, then, the equations of the original three-dimensional coordinates, relative to the isocenter, of a point $P_i(x_i, y_i, z_i)$ imaged with this biplane system can be immediately obtained by finding the intersection of lines L_1 and L_2.

In general, the equation of a straight line L in 3-D space, going through the points $P_1(x_1, y_1, z_1)$ and $P_2(x_2, y_2, z_2)$, can be represented in the two-point form as:

$$\frac{x - x_1}{x_2 - x_1} = \frac{y - y_1}{y_2 - y_1} = \frac{z - z_1}{z_2 - z_1} \tag{3.6.2-1}$$

Letting $S' = (A', 0, 0) = P_1(x_1, y_1, z_1)$, $P_i'(-B', y', z') = P_2(x_2, y_2, z_2)$, and using Equation (3.6.2-1), the equation for line L_1 can be written as

$$\frac{x - A'}{-B' - A'} = \frac{y}{y'} = \frac{z}{z'} \tag{3.6.2-2}$$

Similarly, after letting

$S'' = (0, A'', 0) = P_1(x_1, y_1, z_1)$ and $P_i''(x'', -B'', z'') = P_2(x_2, y_2, z_2)$

and also using Equation (3.6.2-1), the equation for line L_2 can be obtained as

$$\frac{x}{x''} = \frac{y - A''}{-B'' - A''} = \frac{z}{z''} \tag{3.6.2-3}$$

Now, making L_1 equal to some variable u_1 yields the equation

$$u_1 = \frac{x - A'}{-B' - A'} = \frac{y}{y'} = \frac{z}{z'} \tag{3.6.2-4}$$

from where we can obtain the following expressions for x, y, and z

$$x = -(A' + B')u_1 + A' \tag{3.6.2-5}$$

$$y = y'u_1 \tag{3.6.2-6}$$

$$z = z'u_1 \tag{3.6.2-7}$$

Similarly, if we make L_2 equal to some other variable u_2 we obtain

$$u_2 = \frac{x}{x''} = \frac{y - A''}{-B'' - A''} = \frac{z}{z''} \tag{3.6.2-8}$$

which allows us to write x, y and z as

$$x = x''u_2 \tag{3.6.2-9}$$

$$y = -(A'' + B'')u_2 + A'' \tag{3.6.2-10}$$

$$z = z''u_2 \tag{3.6.2-11}$$

To solve for the desired x, y and z coordinates we use the fact that at the intersection of lines L_1 and L_2 the 3-D coordinates are the same, then solve first for the two variables u_1 and u_2.

Equating the y's and the z's yields the system of equations in u_1 and u_2

$$y'u_1 = -(A'' + B'')u_2 + A'' \tag{3.6.2-12}$$

$$z'u_1 = z''u_2 \tag{3.6.2-13}$$

which can be rewritten as

$$\begin{pmatrix} A'' \\ 0 \end{pmatrix} = \begin{pmatrix} y' & A'' + B'' \\ -z' & z'' \end{pmatrix} \begin{pmatrix} u_1 \\ u_2 \end{pmatrix} \tag{3.6.2-14}$$

The above system of equations can be solved for the parameters u_1 and u_2 using Cramer's rule. This results in

$$u_1 = \frac{A''z''}{(A'' + B'')z' + y'z''} \tag{3.6.2-15}$$

$$u_2 = \frac{A''z'}{(A'' + B'')z' + y'z''} \tag{3.6.2-16}$$

Substituting the value of u_2 determined by Equation (3.6.2-16) in Equations (3.6.2-9) to (3.6.2-11), we can finally write the important equations defining the position in 3-D space of point $P_i(x_i, y_i, z_i)$ as

$$x_i = \frac{x_i''z_i'A''}{y_i'z_i'' + z_i'(A'' + B'')} \tag{3.6.2-17}$$

$$y_i = A'' - \frac{(A''+B'')z_i'A''}{y_i'z_i''+z_i'(A''+B'')} \tag{3.6.2-18}$$

$$z_i = \frac{z_i''z_i'A''}{y_i'z_i''+z_i'(A''+B'')} \tag{3.6.2-19}$$

In addition, the condition under which lines L_1 and L_2 intersect is

$$A''[z_i''(A'+B')+z_i'x_i''] - A'[z_i'(A''+B'')+y_i'z_i''] = 0 \tag{3.6.2-20}$$

For the details on the derivation of this expression see Appendix III.

3.6.3 Determination of corresponding arterial center line points on the two views

In the previous section we found the expressions for reconstructing the 3-D coordinates with our biplane system (Equations (3.6.2-17) through (3.6.2-19)) by determining the intersection of lines L_1 and L_2. There we assumed that image point $P_i'(-B', y', z')$ from View 1 and its corresponding point $P_i''(x_i'', -B'', z_i'')$ from View 2 were known. We are now going to explain below the method that this algorithm uses to find the correspondence between points on both views.

To find the correspondence between the arterial center-line points of View 1 and View 2 we use an **auxiliary line technique**. This approach is similar to the one used by Mackay et al. (see Section 2.2.3.1) in the sense that it also produces a straight line on View 1, used to identify a corresponding projected point on this view (strictly speaking we use an auxiliary

line in algorithm I; in algorithm II, due to the parametrization process, the auxiliary line is transformed into an auxiliary curve), but it is also very different in the way it generates the auxiliary line and determines the corresponding solution in View 1. Whereas the first method uses perspective transformations and homogeneous coordinates (previously found by a rather impractical procedure) to determine the auxiliary line (see Section 2.2.2.1), ours uses the a priori knowledge of the system geometry and dimensions to generate this line and does not introduce any impractical requirement. To obtain each corresponding point MacKay et al. used the assistance of an operator to visually determine the intersection of the auxiliary line with the branch of interest. Our approach, however, determines corresponding points automatically, thereby eliminating the intervention of an operator and the typical problems associated with manual processing. Automatic identification is possible with our approach by taking advantage of the representation of the center line in View 1 provided by the cubic spline interpolation. Because this interpolation provides a mathematical, piecewise, functional representation of the center line, the intersection of the auxiliary and center lines can be found by a straightforward algebraic mean since the equation of the auxiliary line is also known.

We find that the perspective transformations approach is elegant and powerful, specially in a research environment, but impractical to be used in the everyday clinical context. It first requires the imaging of a calibration plexiglass cube containing a minimum of six radio opaque pellets, whose position is known, to obtain the data from which the homogeneous transformations can be obtained. Then, after this step and without moving the position of any of the components of the system, the patient can be examined. This is a very difficult condition to meet since during any typical catheterization study of a patient, the position and separation of the X-ray tube and image intensifier are repeatedly changed

to try to get the best angle or position for the images. In addition, sometimes the components enclose the patient so much that in order to take him/her out of the examination table it is necessary to move these components away first. Therefore, the condition of not moving the position/distance of the X-ray tube and image intensifier after the initial imaging of the plexiglass cube is very difficult to meet during the routine procedures performed at every catheterization lab. This serious practical problem is the main drawback of the perspective transformation method.

3.6.3.1 Approaches of other researchers

Other methods for finding the corresponding points in the two views have also been reported in the scientific literature with different degrees of success.

Kim et al.[75] presented a clever dye-edge tracking algorithm, which is based on the fact that the edge of the moving contrast material has identical moving patterns in each of the two views. They used this property to identify corresponding points coinciding with this edge for different frames of the cycle. However, this method requires the intervention of a skilled operator and presents problems when it is used with vessels of less than 2 mm in diameter. In addition, the accuracy of this method seems to depend on the concentration of the radiopaque dye at the moving edge, and it has not been shown how contrast agent edge profiles of increasing diffusion affect the error in the estimation of the location of corresponding points in the two views.

Another more successful view matching technique utilizing the high spatial correlation existing between a pair of stereoscopic views (in which the angle between the two views is

much less than 90^0) have been used to obtain the 3-D representations of blood vessels.[77,78] In these studies the density profile of each center point in the first view was compared in some way with a set of profiles, centered along the stereoscopic image shift, from the second view. The center point of the profile from the second view giving the smallest root-mean-squared (RMS) difference or the maximum cross-correlation value (depending on the specific approach) was chosen as the corresponding point in the second view.

The use of stereoscopic images brings the following major advantages:

1. Lower costs because only one image acquisition system and one stereo X-ray tube are required.

2. The stereo-tube shift and the imaging distance, which are the only system dimensions required to obtain the 3-D positions, are accurately known.

3. The identification of corresponding points on both views is facilitated by the high spatial correlation existing between the two stereoscopic images.

Yet, this approach also makes it more difficult to solve other very important problems of medical imaging. These are the problem of accurately determining the shape of the lumen cross-section, and the problem of automatically tracking the blood vessels.

The drawback when trying to reconstruct the lumen shape is due to the fact that typically the angle between stereoscopic views is less than 90^0, and hence the cross-sectional information present in this type of image is even smaller than for the orthogonal case. Consequently, one should expect the cross-sectional reconstruction error to be much larger when using this type of data. Therefore, we think that it is always better to use orthogonal

than stereoscopic images if accurate cross-sectional reconstructions are important.

In the case of automatically tracking the blood vessels the disadvantage is due to similar reasons. Hoffman et al.[78] have developed a tracking algorithm which operates on stereoscopic images; others have worked with monoplane images. However, we believe that it would be easier to solve this problem using biplane images because they offer much more directional information about the blood vessels than stereoscopic images. Automatic tracking of the blood vessels is a very difficult image processing problem because of the geometric complexity of their tree-like structure and because of the noise, artifacts, and overlaying projected vessels present in X-ray images of the human vasculature. A tracking algorithm using biplane images, therefore, should also be more accurate than one using stereoscopic image data, because it has more information available to it for resolving the ambiguities which typically lead to the identification of false branches during the tracking process.

3.6.3.2 Finding corresponding points with our auxiliary line

For any chosen arterial center-line point in View 2, an auxiliary line (or an auxiliary curve in the case of algorithm II) can be generated in View 1. The corresponding point in View 1 can be found exactly at the intersection of this auxiliary line/curve with the arterial center line of this view.

The procedure for finding the auxiliary line and, with it, the correspondence between points from View 1 and View 2 can quickly be determined after observing that:

a) Lines L_1 and L_2 form a plane on which the important points $P_i(x_i, y_i, z_i)$, $P_i'(-B', y', z')$, $P_i''(x_i'', -B'', z_i'')$, S', and S'' all lie.

b) The auxiliary line on View 1 is determined by the intersection of the plane just above mentioned with the plane of View 1.

c) The positions of $P_i(x_i, y_i, z_i)$, $P_i'(-B', y', z')$, $P_i''(x_i'', -B'', z_i'')$, S', and S'' are all known (This is precisely one of the most important advantages of using a biplane system with a priori known calibration as described in Section 3.6.1).

Algorithm for the generation of our auxiliary line

The steps of our algorithm for generating in View 1 the auxiliary line of a point $P_i''(x_i'', -B'', z_i'')$ in View 2 are the following:

1. Find the intersection point $P_1(y'_1, z'_1)$ between the line that goes through X-ray focal points S' and S'' and the plane determined by View 1.

2. Find the intersection point $P_2(y'_2, z'_2)$ between the line that goes through X-ray focal point S' and selected point $P_i''(x_i'', -B'', z_i'')$ in View 2 and the plane determined by View 1.

3. With the points found in Steps 1 and 2, find the equation of the auxiliary line using the general expression of a 2-D straight line given immediately below.

$$\frac{y'-y'_1}{y'_2-y'_1} = \frac{z'-z'_1}{z'_2-z'_1} \qquad (3.6.3.2\text{-}1)$$

It is important to notice that since what we are doing to find corresponding points in the two views is to pick a point from View 2, and then determine which point from arterial center line of View 1 lies in the same plane with the X-ray focal points and $P_i''(x_i'', -B'', z_i'')$, this guarantees that lines L_1 and L_2 will almost always intersect; the only exceptions being when the corresponding points in View 1 fall around points of maxima or minima of an arterial center-line region with a very sharp curvature. In these cases, the auxiliary line may fail to intersect the center line if the interpolation of the center line does not adequately reproduce the region of sharp curvature. Fortunately, this is never the case with the main branches of the coronary arteries which have rather smooth curvatures. Besides, even in those cases of non-intersection it is always possible to approximate an acceptable solution, since usually the auxiliary and the center lines do not touch by a very small distance. Therefore, because save in few exceptions, the intersection of lines L_1 and L_2 will always occur, a routine step using Equation (3.6.2-20) to check the possible intersection of these lines is not necessary.

3.6.4 Description of the 3-D Positional Reconstruction Algorithm I

The only assumption made by the 3-D positional reconstruction algorithm I is that in each of the two orthogonal DSA images a single-valued function representing the projected vessel center line can be obtained using one of the two coordinate variables as the independent variable and the other as the dependent variable.

After the 3-D arterial center line reconstruction algorithm I inputs the coordinates of the vessel midpoints, previously determined by the vessel center-estimator algorithm, it proceeds to:

a) Do a cubic spline interpolation of the projected arterial center line, including through any stenosed segment if present.

b) Automatically identify corresponding points in both views.

c) Reconstruct the 3-D coordinates of the arterial center line using the coordinates of its projections and Equations (3.6.2-17) through (3.6.2-19).

The flowchart of the **3-D positional reconstruction algorithm I** is shown in Figure 3.6.4-1. An outline of this algorithm is given below.

Algorithm I outline

1. A total of N estimated points of the lumen center line proximal and distal to stenosed area are inputted from each view. The points from one view have no need for any correspondence with the points from the other view.

2. One orthogonal image is designated View 1 and the other is designated View 2.

3. A cubic spline interpolated curve is fit to the N arterial centers of View 1 and View 2.

4. The interpolated curve in each view is uniformly resampled to generate a minimum of $2N$ samples and a new cubic spline interpolated curve is generated for center line in View 1 using the new arterial centers.

5. The algorithm finds two consecutive samples (seed points) in View 2 whose auxiliary lines in View 1 intersect the interpolated curve once and only once each. The initial projected arterial length in View 1 is calculated from the Euclidean Distance (D) between the two intersection (seed) points.

6. For each point along the interpolated curve starting from the seed points in View 2 and progressing along the uniformly sampled curve in one direction, the associated auxiliary line in View 1 is calculated. The intersection point within $1.5D$ of the previous solution is selected as the corresponding projection in View 1 and D is updated. If more than one solution is found, the one closest to the previous one is picked. If no solution is found, the value of D is doubled and the algorithm proceeds with next point.

7. The three-dimensional coordinates of the original point which produced the corresponding two projections determined in Step 6 are computed.

8. Beginning with the seed points in View 1 and the initial value for D, Step 7 is repeated for the samples, if any, on the other side of the seed points.

3.6.5 Description of the 3-D Positional Reconstruction Algorithm II

In the previous section we presented the 3-D positional reconstruction algorithm I. This algorithm can automatically generate the arterial center line when the two orthogonal projections of this line are expressed as single-valued functions. In this section we will explain algorithm II which generalizes the 3-D positional reconstruction method to include cases where the projected center lines are described by multi-valued functions.

As for the first case, the input data for the second form of this algorithm are again the coordinates of the center points of the arterial segment in each view.

The main tasks performed by this other form of the positional reconstruction method are:

a) Interpolation across the stenosed region, if any.

b) Parametrization of the projected center lines with respect to the arterial arc length.

c) Determination, in the parametrized space, of corresponding center points on both views.

d) Computation of the 3-D coordinates of the vessel center line using Equations (3.6.2-17) through (3.6.2-19).

In contrast with algorithm I, algorithm II performs first local cubic spline interpolations in the projection space over consecutive four sample windows to obtain a local functional description of the center line within each window. This representation is required for subsequent parametrization with respect to the arc length. The local interpolation step assumes that over a four sample window the center line can be represented by a single-valued function. Since most arteries have a slowly varying curvature over short intervals this assumption is generally valid.

If a stenosis is present, a local interpolation is initially performed over that region using the two samples preceding and following it. Once center lines are interpolated through the projected stenosed region in both views, they are uniformly resampled. The spacing between samples is made approximately equal to the separation of the input data samples.

The concatenation of all the local functional representations are used to obtain the arc length along the center line. The arc length AL along the cubic spline interpolated polynomial $F(x)$ between x_0 and x_1 is given by:

$$AL = \int_{x_0}^{x_1} \sqrt{1+\left(\frac{dF(x)}{dx}\right)^2}\,dx \qquad (3.6.5\text{-}1)$$

Where $F(x)$ is given by Equation (A.II-1).

For each view, this permits obtaining a parametrized set of coordinates relating projected arterial center line position and its arc length which can then be globally interpolated using cubic splines.

To find corresponding points on the parametrized curves in each view, the auxiliary line method is again employed (see Section 3.6.3). The auxiliary line must also be parametrized with respect to the arterial arc length transforming it into an auxiliary curve. The intersection of the globally interpolated auxiliary curve and the parametrized center line of View 1 determines corresponding points. Once corresponding projected center points are determined, the algorithm computes the 3-D arterial center line coordinates using the formulas for x, y, and z that we derived in Section 3.6.2.

The flowchart of the **3-D positional reconstruction algorithm II** is shown in Figure 3.6.5-1. An outline of this algorithm is given below.

Algorithm II outline

1. For each view, input the coordinates of N center points along the arterial segment of interest.

2. If there is a stenosis segment present, do a local CSI over a four sample window. Resample the interpolated center line for the stenosis region.

3. Parametrize both center lines with respect to the arterial arc length.

4. Obtain the global CSI representation of the parametrized curves.

5. Find two consecutive samples (seed points) in View 2 whose auxiliary curves in the View 1 parametrized space intersect the interpolated curve only once each. The initial distance D between the seed points corresponding projections in the View 1 parametrized space is calculated.

6. For each sample in View 2, starting after the last seed point and working progressively along the arc length, generate its auxiliary curve in the View 1 parametrized space, find intersection(s) between auxiliary and projected center line parametrized curves, select corresponding projected point in the View 1 parametrized space as intersection within $2D$ of previous solution, update D and compute 3-D coordinates.

7. If the seed points were not the first and second samples in View 2, beginning at first seed point, repeat Step 6 with the initial value of D for the samples on the other side of the seed points.

4 RESULTS

4.1 Cross-sectional Reconstructions

The cross-sectional reconstruction algorithm described in Section 3.5.3 was applied both to computer-simulated orthogonal density profiles and to actual X-ray digitally subtracted orthogonal density profiles obtained using models of cylindrical stenosed vessels with crescent-shaped lumena and different cross-sectional area narrowing values. These experiments were conducted in order to investigate:

1. The accuracy of the reconstruction algorithm with noise free, ideal, computer generated density profiles of cross-sections with different Percent Stenosis.

2. The influence of additive Gaussian noise of increasing magnitude on the accuracy of the reconstruction algorithm.

3. The effect of Median Filtering on reconstruction accuracy of cross-sections with density profiles corrupted by noise.

4. The effect of Reference Domain (*RD*) diameter and Reference Value (*RV*) errors on reconstruction accuracy.

5. The accuracy of the algorithm when applied to actual X-ray orthogonal density profiles.

For the present study both the computer-simulated and the plexiglass vessel model were aligned to be approximately orthogonal to the two main axes of the biplane views. We

decided to use the crescent-shaped cross-section for all the experiments because this was the most difficult lumen shape that we could simulate with both the computer and the plexiglass vessel model.

The accuracy of the cross-sectional reconstruction algorithm was evaluated using a parameter similar to the one used by Reiber et al.[48]. This parameter is called the mean cross-sectional reconstruction error $\overline{R}$ and is defined as:

$$\overline{R} \equiv \frac{\sum_{\text{all } j} e_j}{\sum_{\text{all } i} o_i} \times 100 \qquad (4.1\text{-}1)$$

Where

e_j ≡ The erroneously filled cross-section pixels.

o_i ≡ The originally filled cross-section pixels.

Since we always used the partially filled pixel option of the cross-sectional data generation program, many of the original cross-section pixels were neither completely filled nor completely empty. These lumen border pixels were handled by adopting the following rule:

Pixels originally at least 75% filled with contrast which were not filled by the algorithm were considered in error. Conversely, pixels originally no more than 25% filled with contrast which were filled by the algorithm were also considered in error.

4.1.1 Reconstructions With Computer-simulated Noise-Free Data

The program explained in Section 3.1, which simulates a stenosed vessel segment, was used to generate data to test the accuracy of the cross-sectional reconstruction program described in Section 3.5. Ideal, noise free, orthogonal density profiles with partial pixel projections of the cross-section shown in Figure 3.1-2c (crescent shape II) were generated. Cross-sections with a 25%, 51%, and 73% percent stenosis were simulated by letting R1=7 and R3=3.5, R1=7 and R3=5, and R1=7 and R3=6 pixels respectively. A sensitivity of 3.8 gray levels per pixel was used.

Typical reconstructions of the crescent-shaped cross-sections with 25%, 51%, and 73% stenosis are shown on Figures 4.1-1a, b, and c respectively. Shaded areas were filled and reconstruction errors are marked with an E. Using Equation 4.1-1, the calculated mean cross-sectional reconstruction error $\overline{R}$ for the 25%, 51%, and 73% stenosed cross-sections was 1.7% (2 errors in 115 pixels), 6.7% (5 errors in 75 pixels), and 7.3% (3 errors in 41 pixels) respectively. The basic shape of the lumen was retained with most of the errors tending to occur near the tips of the crescent shape.

4.1.2 Reconstructions With Computer-simulated Noisy Data

Gaussian noise with a mean m_n equal to 0 and a variance σ_n^2 of 1, 2, 4, and 8 pixels^2 was added to the ideal orthogonal density profiles of the crescent-shaped cross-section with 25% stenosis described in Section 4.1.1. A different Gaussian noise set with the same statistics was independently added to each of the two orthogonal profiles associated with

each cross-section. For each value of the variance, ten cross-sectional reconstructions were performed using different Gaussian noise set pairs for each reconstruction. The mean reconstruction error $\overline{R}$ was calculated for each reconstruction and the average $\overline{R}$ was computed for each noise level.

The calculated average $\overline{R}$ is shown in Figure 4.1.2-1 as a function of the σ_n^2 of the noise added to the density profiles. As the variance σ_n^2 of the Gaussian noise added to the density profiles varied from 1 to 8 pixels^2, the $\overline{R}$ increased significantly from 5.7 to 21%. Noise with a variance of less than 1 pixel^2 resulted in reconstructions with a $\overline{R}$ of less than 6%.

4.1.3 Reconstructions With Median Filtered Computer-simulated Noisy Data

In order to investigate if median filtering can increase the reconstruction accuracy, a 3×3 median filter was applied, prior to reconstruction, to the same noisy computer-simulated X-ray images of the 25% stenosed artery used in Section 4.1.2. Again, for each noise variance level, ten reconstructions were performed using a different Gaussian noise set pair for each one. The average mean cross-sectional reconstruction error $\overline{R}$ was calculated for each of the noise variance levels used in Section 4.1.2 and it is plotted in Figure 4.1.3-1 for comparison purposes.

Application of the 3×3 median filter resulted in a decrease in the $\overline{R}$ at all noise levels. The decrease in $\overline{R}$ was statistically significant for noise with a variance σ_n^2 of 4 and 8 pixels^2. While the $\overline{R}$ still rose significantly as noise increased, the reconstruction error was decreased as much as one half at severe noise levels.

4.1.4 Reconstructions With Reference Domain (RD) Diameter Variation

Incorrect determination of the diameter of the circular Reference Domain *RD* used as a geometric constraint is possible when utilizing any diameter finding algorithm (we use Barba et al.'s[86,87]). Since an incorrect Reference Domain diameter could produce reconstruction errors, we investigated the effect of Reference Domain diameter error on the mean reconstruction error $\overline{R}$. This was done by performing reconstructions of the crescent-shaped cross-sections with 25% stenosis while intentionally letting the *RD* diameter be smaller and larger than its correct value.

The mean reconstruction error $\overline{R}$ resulting from these reconstructions are plotted in Figure 4.1.4-1 as a function of the % error in Reference Domain diameter. The mean cross-sectional reconstruction error increased as the *RD* diameter error increased. However, $\overline{R}$ remained small until a relatively large *RD* error was reached. Note that the $\overline{R}$ decreased as the *RD* diameter approached the optimum diameter from a smaller value.

4.1.5 Reconstructions With Reference Value (RV) Variation

Since incorrect background subtraction and idealization of the lumen shape of the Reference Domain *RD* can cause variations in the calculated reference value *RV*, we have investigated the effect of an incorrect reference value on reconstruction accuracy by performing reconstructions with both low and high reference values. We found that for errors of ±5% in the determination of the reference value, the mean cross-sectional reconstruction error $\overline{R}$ remained unchanged or slightly decreased. $\overline{R}$ increased to 6% and 7.5% when the reference value error was -11% and +11% respectively.

4.1.6 Reconstructions With X-ray Data

The plexiglass model described in Section 3.3 was used to generate digitally subtracted non-simultaneous orthogonal X-ray images of cylindrically simulated vessels having crescent-shaped cross-sections with 44 and 11% stenosis. The 44 and 11% crescent-shaped stenosis were simulated by 2 and 1 mm diameter plexiglass rods glued to the wall of the 3 mm diameter duct representing the unstenosed part of the vessel. The model was filled with a 5% sucrose solution and with a 75% Renographin 78 in 5% sucrose solution during the acquisitions of the mask and the contrast images respectively.

These X-ray images were acquired at the Catheterization Laboratory of the Department of Cardiology of The New York Hospital-Cornell Medical Center. The output of a 12 cm image intensifier was captured on a 512×512 matrix by an ECLAT 700 DSA system manufactured by Elscint Ltd. The focal spot was 0.3 mm nominal, the magnification factor was approximately 1.5 for both orthogonal views, and the pixel size equal to 0.167 mm.

The measured noise level on the subtracted logarithmic image was approximately 1 gray level. No compensation was made for the MTF of the imaging system or for the radial path of the X-rays. Radiation was at low cine levels as is costumary at New York Hospital Division of Cardiology. The X-ray voltage was unavailable. Finally, no noise reduction technique was applied to these images.

Using the diameter-finding algorithm developed by Barba et al.[86,87], the diameter of the unstenosed part of the simulated vessel was found to be equal to 18.2 pixels.

The cross-sectional reconstruction algorithm was applied to the X-ray orthogonal density profiles of the crescent-shaped cross-sections with 44 and 11% stenosis. Typical reconstructions of the 44 and 11% stenosed cross-sections are shown in Figures 4.1.6-1 and 4.1.6-2 respectively. The small shaded squares represent the pixels that were filled in the reconstruction, i.e., those which belong to the reconstructed lumen. The solid line represents only the approximate shape of the original cross-sections since we were unable to exactly determine how much of the lumen area inside the plexiglass model (specially at the crescent tips) was filled by the glue holding the small inner rod.

Using a DEC VAX 11/750 minicomputer, the reconstruction time of one cross-section was approximately 1 minute.

Taking into consideration the glue filling the tips of the crescent formed by the stenosed lumen cross-section of the plexiglass model, we have approximately calculated the mean cross-sectional reconstruction error for the slices reconstructed from X-ray data. We estimated the reconstruction error $\overline{R}$ for the crescent-shaped cross-sections with 44% and 11% stenosis to be approximately equal to 17% (24 errors in 141 pixels) and 6.2% (14 errors in

226 pixels) respectively.

As with the simulated ideal density profile data, the cross-sectional reconstruction algorithm tended to underfill the tips of the crescent-shaped cross-sections. It should be noted that the algorithm in its current form tends to underfill cross-section pixels. Nevertheless, the crescent shape of the cross-section is clearly revealed by the reconstruction.

4.2 Three-dimensional Positional Reconstructions

The 3-D positional reconstruction algorithms I and II explained in Sections 3.6.4 and 3.6.5 respectively were tested with data generated by the computer model of arterial center line program described in Section 3.2. This program was used to generate projections of a sampled three-dimensional curve onto two orthogonal planes as shown in Figure 3.2-1. These points were used to represent the output of the center-finding algorithm of Barba et al.[86,87] which can determine in each view the center points of typical-size arteries with an error no larger than 0.2 pixel. These experiments were conducted in order to investigate:

1. The accuracy of the 3-D positional reconstruction algorithms in the determination of arterial center lines with different geometrical complexities.

2. The effect of input data errors of increasing magnitude on the accuracy of these algorithms.

3. The ability of algorithms I and II to estimate different center line shapes through a stenosed region of variable length and position.

4. The influence of a stenosed region of increasing length on the overall accuracy of above algorithms.

The mean 3-D positional reconstruction error ($\overline{PRE}$), defined below, is the parameter that we used to asses the accuracy of algorithms I and II. It measures the average 3-D Euclidean distance between the samples of the original data curve and the samples of the reconstructed one.

$$\text{MEAN 3-D PRE} \equiv \overline{PRE} \equiv \frac{1}{N}\sum_{i=1}^{N}\sqrt{(x_{oi}-x_{ri})^2+(y_{oi}-y_{ri})^2+(z_{oi}-z_{ri})^2} \qquad (4.2\text{-}1)$$

Where

N ≡ Total number of arterial center-line samples.

$\{x_{oi}, y_{oi}, z_{oi}\}$ ≡ Set containing coordinates of original center-line samples.

$\{x_{ri}, y_{ri}, z_{ri}\}$ ≡ Set containing coordinates of reconstructed center-line samples.

The values of the system dimensions used for all the simulations were $A1 = 1166$, $B1 = 333, A2 = 1033$, and $B2 = 883$ pixels. For a standard 9'' (228.6 mm) image intensifier and a magnification equal to one, the pixel size is approximately equal to 0.5 mm.

To simulate the presence of stenosed region in the vessel, over which the center-finding algorithm would generally yield incorrect results, a segment of the projected sampled curve, of variable position and length, was removed in each view (see Figures 4.2-1, 2, and 3). The size of the truncated input data segment, SL, was varied over the typical range of stenosis

lengths found in patients with coronary atherosclerosis[91] ($SL \approx 1 - 15$mm). This permits to study the accuracy of both 3-D positional reconstruction algorithms when reconstructing the stenosed region center line as the amount of missing data increases.

The accuracy of the three-dimensional positional reconstruction depends directly on the accuracy of the input data provided by the center-finding algorithm. Therefore, to simulate the errors which are normally introduced by the latter algorithm, Gaussian noise with zero mean and different standard deviations σ_n was independently added to the coordinates of each projected center-line sample. Mean centering errors (MCE) of 0.1, 0.5, and 1.0 pixel were simulated in the data used to test algorithm I by adding noise with those same standard deviation values. Similarly, mean centering errors of 0.1, 0.2, 0.3, and 0.4 pixels were simulated in the data used to test algorithm II. These last MCE values are slightly smaller than those used for testing algorithm I, but more in the range of errors produced by the centering algorithm described by Barba et al.[86,87].

To test the accuracy of 3-D positional reconstruction algorithm I, two different computer-simulated vessel center lines were generated. The first was a vessel center line with a three-dimensional parabolic shape, and the second a vessel center line with a three-dimensional helical shape. Each curve was uniformly sampled 25 times along its length and these samples were projected, using the point-source geometry system shown in Figure 3.2-1, onto two orthogonal planes producing single-valued center line projections.

The 3-D parabolic curve simulates a center line with a slowly varying curvature similar to that found on many human arterial segments. It is given by

$$z = 0.004(x+y)^2 \qquad (4.2\text{-}2)$$

$$x = y \tag{4.2-3}$$

With

$0.0 \leq x \leq 120.0$ pixels

$0.0 \leq y \leq 120.0$ pixels

The 3-D helix curve approximates a type of arterial center line with a shape which is more complex than those typically found on human arterial segments. We have used this more complicated center line shape because we also wanted to test our positional reconstruction methods with a very difficult case. The 3-D helical curve used for generating data is given by the parametric equations

$$x = 10\cos u \tag{4.2-4}$$

$$y = 10\sin u \tag{4.2-5}$$

$$z = 5u \tag{4.2-6}$$

With

$0.0 \leq u \leq 9.4$ pixels

The accuracy of the positional reconstruction algorithm II was also tested with the computer-simulated parabolic and helical center line shapes described by Equations (4.2-2) through (4.2-3) and Equations (4.2-4) through (4.2-6) respectively. For this second form of the positional reconstruction algorithm, the 3-D parabolic curve was uniformly sampled,

within the specified range, 25 times along its arc length. The 3-D helical center line, on the other hand, was uniformly sampled 50 times always. The computer generated single-valued projections of the parabolic and helical center lines of stenosed vessels are shown in Figures 4.2-1 and 2 respectively. In addition, the same helix was rotated by 80° about both the Y and Z axes to produce the multi-valued orthogonal projections shown in Figure 4.2-3.

4.2.1 Results of 3-D Positional Reconstruction Algorithm I

The mean 3-D positional reconstruction error ($\overline{PRE}$) of the parabolic center-line shape without a stenosed region and in the presence of input data with varying Gaussian distributed mean centering errors (MCE) is presented in Figure 4.2.1-1.

Figures 4.2.1-2 and 4.2.1-3 show the mean 3-D positional reconstruction error ($\overline{PRE}$) through the stenosed region for the parabolic and helical center lines respectively. The error is plotted for different lengths of the stenosed segment and various Gaussian distributed mean centering error (MCE) values.

In the case of the unstenosed parabolic center line, the $\overline{PRE}$ increased as the MCE increased. For the stenosed center lines, on the other hand, the mean 3-D positional reconstruction error was smaller for the parabolic center line than for the helical one with larger values of MCE and stenosis length. At lower MCE values, the $\overline{PRE}$ appears to be independent of the stenosis length, over the range of stenosis lengths studied, for both curves. Note that the $\overline{PRE}$ is given only for the stenosed segment (where input data is missing) since the error along the rest of the vessel remained very small.

4.2.2 Results of 3-D Positional Reconstruction Algorithm II

The 3-D positional reconstruction algorithm II was applied to the computer generated biplane images of Figures 4.2-1, 2, and 3. The resulting overall mean 3-D positional reconstruction error ($\overline{PRE}$), for different MCEs and stenosis lengths, is shown in Figures 4.2.2-1, 2, and 3 respectively.

For a fixed value of MCE, the $\overline{PRE}$ remained fairly constant for stenosis lengths shorter than 18 pixels. At longer stenosis lengths, the positional reconstruction error increased slightly. In all cases, the $\overline{PRE}$ remained below 0.43 pixels over the range of simulated MCEs and stenosis lengths.

In general, the parabolic center line had the lowest $\overline{PRE}$ and the helical center line with multi-valued projections the highest one.

5 DISCUSSION AND CONCLUSION

We have developed a method for the three-dimensional reconstruction of the arterial lumen from two orthogonal digitally subtracted angiograms. By dividing the artery into a stack of parallel cross-sections, this method subdivides the original problem into the two smaller basic problems of: one, determining the cross-sectional shape of each slice, and two, finding the three-dimensional position of each slice.

To find the cross-sectional shape of each slice, an iterative binary reconstruction algorithm which incorporates a region with high probability of containing the lumen cross-section as an initial boundary constraint was investigated. The boundary constraint, which was assumed to be circular, was progressively increased with each iteration. Computer-simulated ideal density profiles were used to determine this method's reconstruction accuracy and the influence of additive Gaussian noise on the reconstruction accuracy. The accuracy of crescentic cross-section reconstructions from actual non-simultaneous biplane X-ray images of lumen models was also calculated.

In addition, two algorithms for automatically reconstructing the arterial center line for each view and its position in three-dimensional space using two orthogonal projections were also developed. Both algorithms were satisfactorily tested using computer-simulated data. In general, the first of the two algorithms is suitable for projected arterial center lines that can be expressed as single-valued functions. The second one, on the other hand, can work with both single and multi-valued projected center lines. Both algorithms use cubic spline interpolation techniques to obtain piece-wise functional representations of the projected center lines. In addition, if a stenosis is present, the positional reconstruction algorithms

can interpolate the center line through that region by using the midpoints that precede and follow the lesion. The 3-D positional accuracy of these algorithms for various projected center line shapes in the presence of simulated stenosis length and input data error of increasing magnitude was also investigated.

The mean cross-sectional reconstruction error $\overline{R}$ was low and concentrated at the tips for the simulated crescentic lumenal cross-sections. The addition of Gaussian noise to the computer-simulated cross-sectional density profiles considerably increased the $\overline{R}$ (the typical noise variance of our system was 1 pixel^2). By applying a 3×3 median filter to the noisy density profiles before reconstruction the mean cross-sectional reconstruction error was reduced.

In addition, the $\overline{R}$ was found to be relatively insensitive to both *RD* diameter and *RV* variations. The reconstruction accuracy was considerably higher when the Reference Domain diameter was underestimated than when it was overestimated. Although not studied, we believe this observed dependency of $\overline{R}$ on the *RD* diameter error to be somewhat related to the complexity of the shape to be reconstructed. For shapes which are simpler than the crescentic one, the dependence on the *RD* diameter error should be expected to decrease.

The reconstruction of cross-sectional shapes from X-ray image density profiles led to slightly larger errors than the above simulations. These errors may have resulted, among other things, from subtle misalignment of the two density profiles. Pincushion distortion did not markedly influence the accuracy of the reconstruction since we only used the region of the imaging field where this distortion is minimal (the center part of the image intensifier

screen). The effect of the finite X-ray focal spot size may have also increased the reconstruction error. While not strictly comparable, the $\overline{R}$ of our algorithm appears to be lower than the reported $\overline{R}$ for both the Slump and the BASE binary reconstruction algorithms.[48]

The three-dimensional positional reconstruction of arterial center lines from two orthogonal views with both algorithm I and algorithm II resulted in small errors when there was no lumen stenosis and no error in the vessel center estimation. Over the range of input data errors studied, the mean 3-D positional reconstruction error ($\overline{PRE}$) was generally smaller than the simulated MCE value. When a section of the simulated vessel center line was removed, as in a stenosis, the $\overline{PRE}$ increased. Additionally, the mean 3-D Euclidean distance error ($\overline{PRE}$) resulting from a given input data error was greater for the more complex helical center line than for the parabolic one. This was expected since the less geometrically complex shape of the parabolic center line should be easier to reconstruct.

The $\overline{PRE}$ (through the stenosed segment) of algorithm I for the more complex helical center line was always less than 3.3 pixels for stenosis lengths under 20 pixels and MCEs of ±1.0 pixels. For the more typical parabolic center line shape, the $\overline{PRE}$ (overall) was always less than 1 pixel, over the range of input data error examined, with no stenosis present.

For a given MCE, the overall $\overline{PRE}$ of algorithm II remained fairly constant over the simulated stenosis lengths for all of the three projected curve shapes tested. This PRE was approximately of the same magnitude as the MCE.

The 3-D positional reconstruction errors of algorithm II were lower for the single-valued curve than for the multi-valued one. This was expected since multi-valued curves

usually have a greater curvature, resulting in larger interpolation errors. In general, the $\overline{PRE}$ was due primarily to the interpolation errors, which in turn depended on the shape of the center line and stenosis. In order to maintain acceptable PREs, the sampling of the projected center line should be made denser about points of large curvature. For comparison purposes, the MCE=0.0 curve corresponding to the 3-D reconstruction with zero centering error was presented. This PRE resulted from the cubic spline interpolation errors only. In general, for the three projected curve shapes studied, the PRE always remained under 0.5 pixels (0.25 mm). Finally, when reconstructing the same center line shape both algorithms produced similar positioning error values.

While only a relatively limited study of the 3-D positional reconstruction algorithms was performed, it appears that, except for very large and uncommon MCE values, the methods allow the 3-D reconstruction of arterial segment position. When combined with the reconstruction of serial cross-sectional shapes of vessel lumena, this technique may provide an accurate 3-D representation of arterial lumen segments in vivo.

6 FUTURE RESEARCH

This research was devoted to the development of the basic ideas and algorithms for the reconstruction of both the exact arterial lumen cross-sectional shape and the 3-D positioning of vessel center line segments in the arterial tree (this ultimately permits an accurate 3-D display of the coronary arterial lumen).

Future research in this area should be aimed at turning these basic ideas and algorithms into a fully formed methodology that can be applicable to patient angiograms in the regular clinical environment. In addition, future work should also encompass further refinement and verification of the above mentioned techniques using X-ray data of more sophisticated physical three-dimensional models.

The research completed to this point shows that the developed reconstruction algorithms yield good results for the limited cases studied. The proven utility of these methods should now be expanded by performing the following additional work:

1. Modification of the cross-sectional reconstruction algorithm so that it can handle cases where the arteries are not parallel to the image planes. Since this algorithm was developed for arteries that are perpendicular to or, at most, form small angles with the plane of reconstruction, it must be now changed to take into account the possible varying orientation of real arteries. This will require a modification of the Reconstruction Domain (*RD*) since this geometric constraint, used for restricting the number of cross-section solutions, will no longer be circular, but instead elliptical. The new elliptical *RD* could be quickly generated using information provided by the center finding and the 3-D positioning algo-

rithms.

2. Application of the cross-sectional reconstruction algorithm to shapes other than the crescentic ones (e.g., double lumen and semi-circular shapes). The crescentic shape was chosen for this research because we considered it to be a difficult shape to reconstruct. We felt that further work would not be justified unless the algorithm could pass this difficult test. It should be expected that changes and adjustments will have to be made to the algorithm as the class of solutions is expanded.

3. Investigation of the reconstruction accuracy for smaller lumen sizes. Although our major interest was in moderate stenoses, that is, those for which the prognosis and treatment might depend on the shape of the lumen, the entire range of possible stenosis values will have to be tested if this method is to be finally accepted. At this point, new methods for finding the Reconstruction Domain (*RD*) will probably have to be developed based not only on the extent of the unstenosed vessel, but also based on the extent of the stenosed region on each view.

4. Study of the sensitivity of the algorithms to typical problems encountered with clinical systems such as non-orthogonality of the biplane system, measurement errors of the image intensifier to X-ray source distances, and misalignment of the isocenter.

5. Incorporation of methods to correct for pincushion distortion and the system modulation transfer function (MTF). Pincushion distortion introduces non-linear degradations of the image, and the system MTF causes edge blurring of the vessel edges (a major problem with very small vessels).

6. Integration of all different algorithms in order to have a single continuous process from the input of raw X-ray data to the 3-D display of the reconstructed artery.

7. Design and accurate construction of appropriate physical models to verify with X-ray data the simulation results of the 3-D positional reconstruction algorithms.

8. Introduction of techniques to further automate the 3-D reconstruction method. At present, this method requires the manual selection of a number of points along each projection of the arterial segment to be reconstructed. We think that, with the proper modifications, the number of points that need to be manually selected at the beginning of the process can be reduced to just two.

7 FIGURES

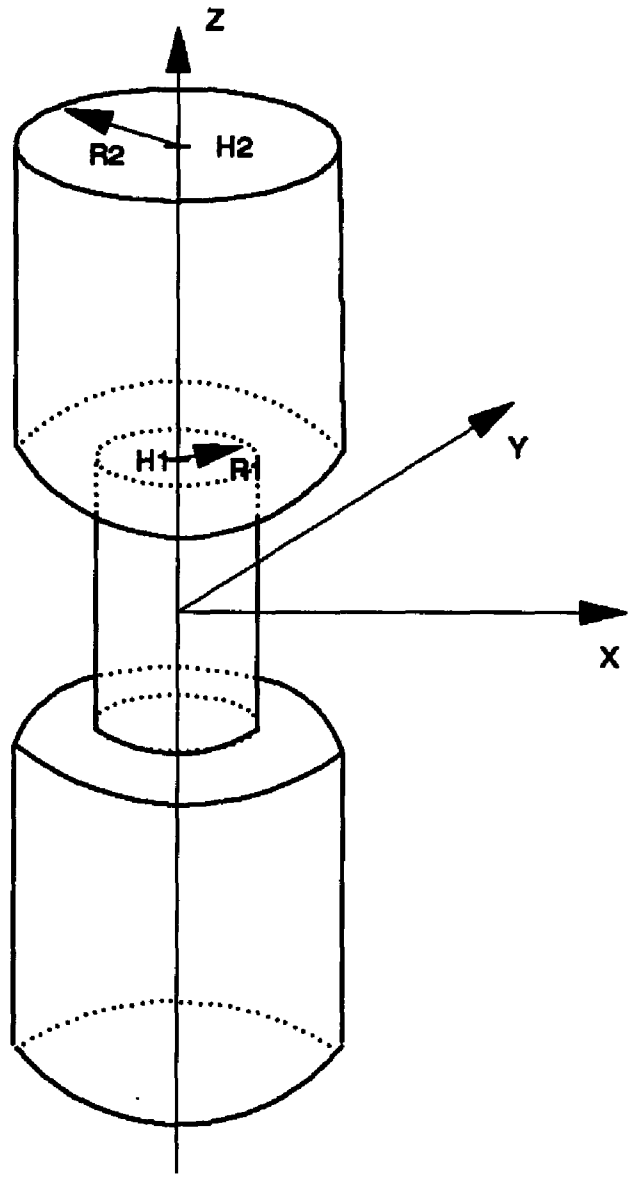

Figure 3.1-1. Diagram of computer simulated stenosed vessel segment.

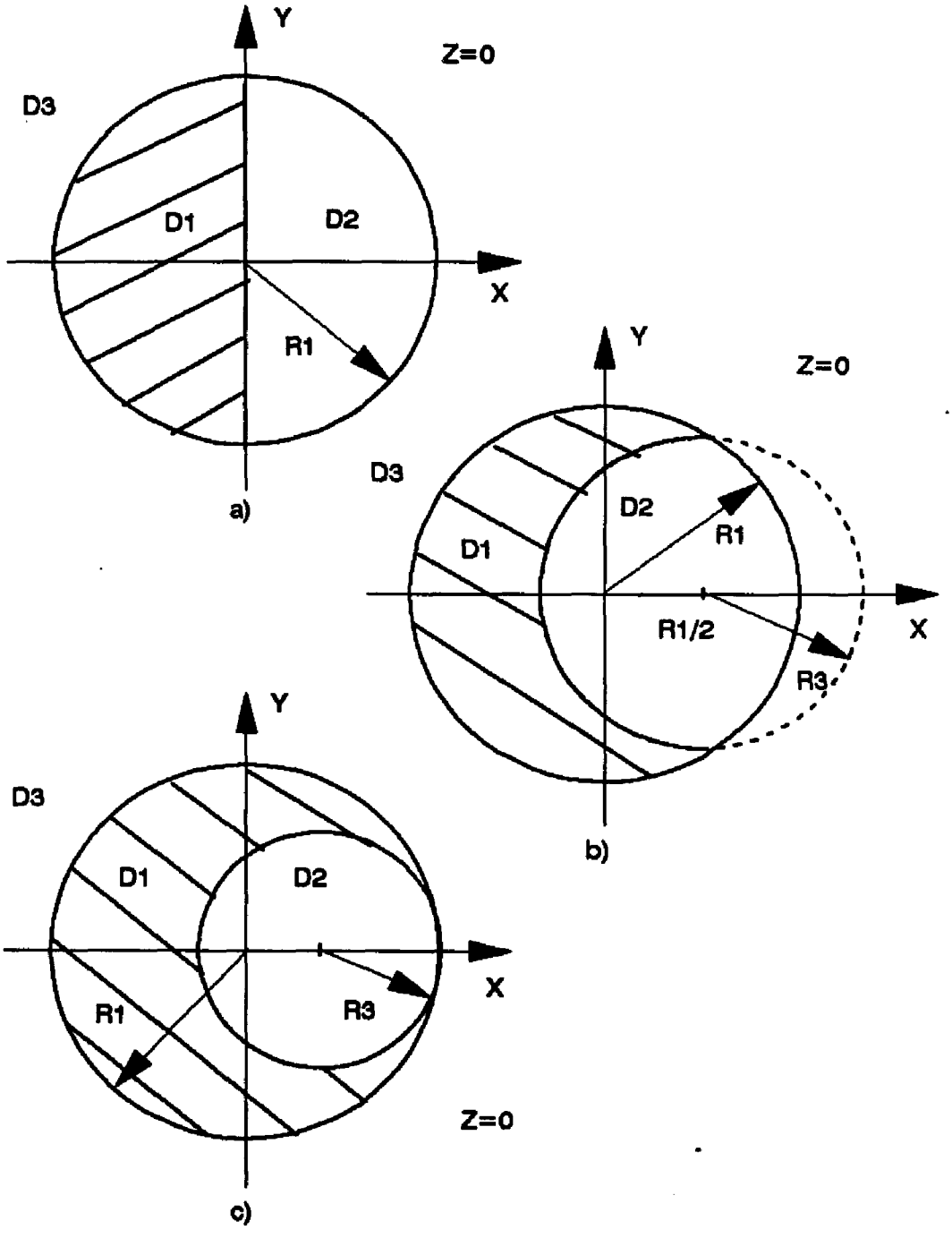

Figure 3.1-2. Lumenal cross-sectional shapes for stenosed region of computer simulated vessel. (a) Half-circle shape. (b) Crescent shape I. (c) Crescent shape II.

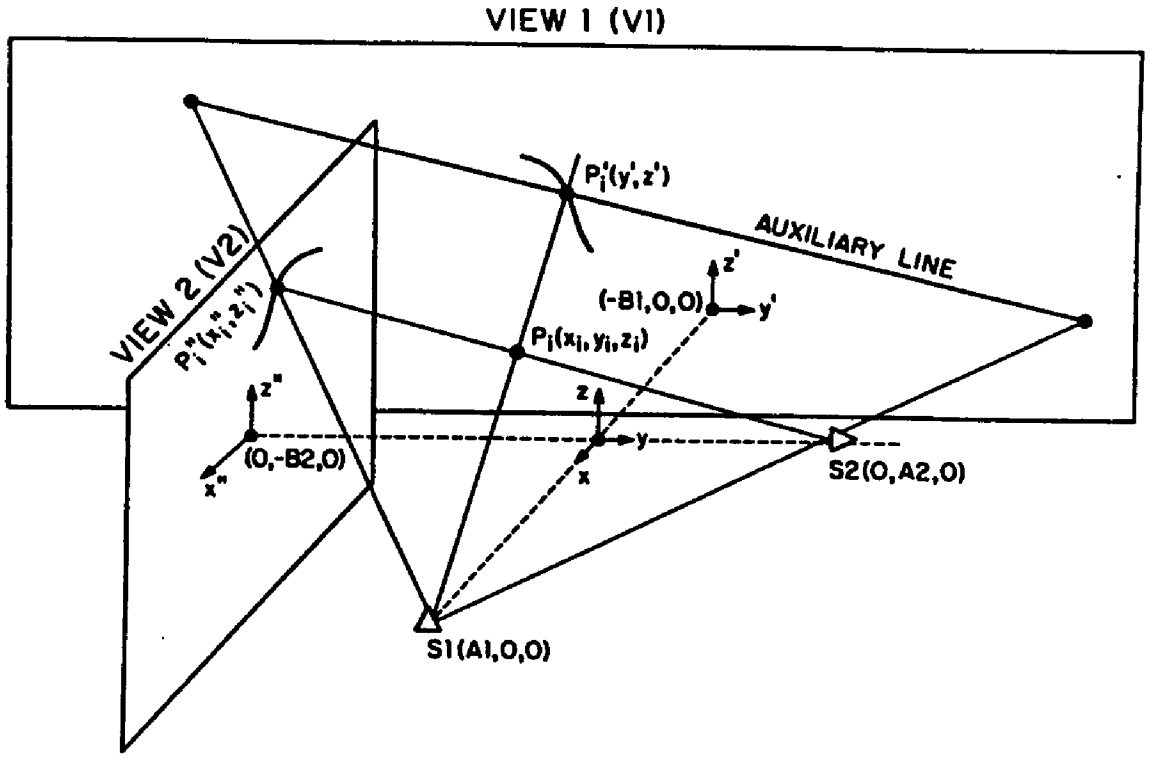

Figure 3.2-1. Geometry of the biplane X-ray system.

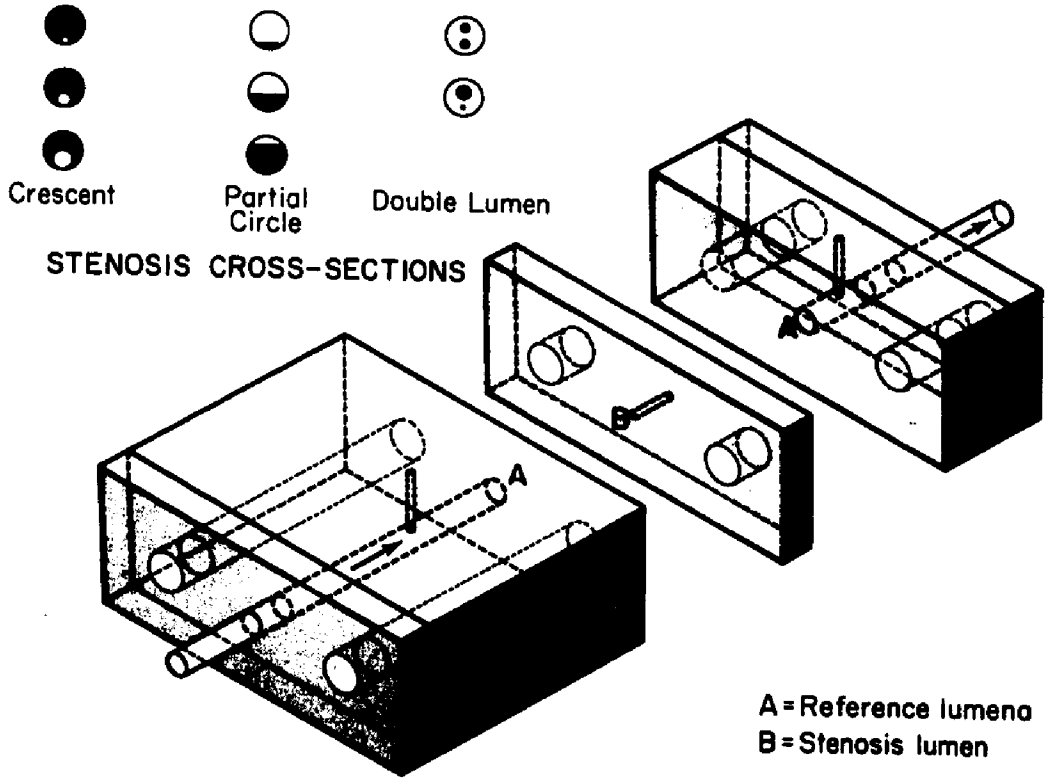

Figure 3.3-1. The plexiglass model of stenosed arterial segment.

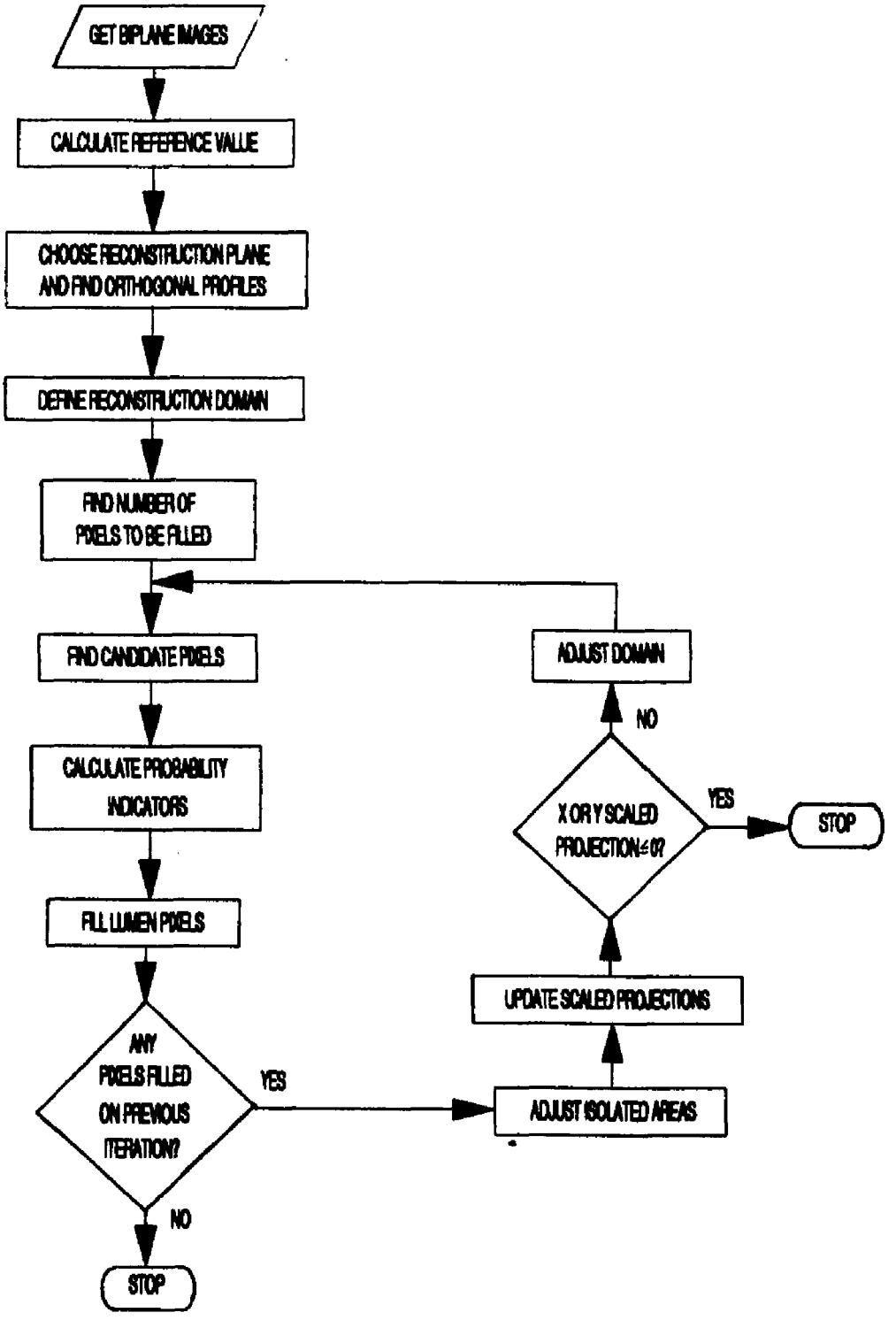

Figure 3.5.3-1. Cross-sectional reconstruction algorithm flowchart.

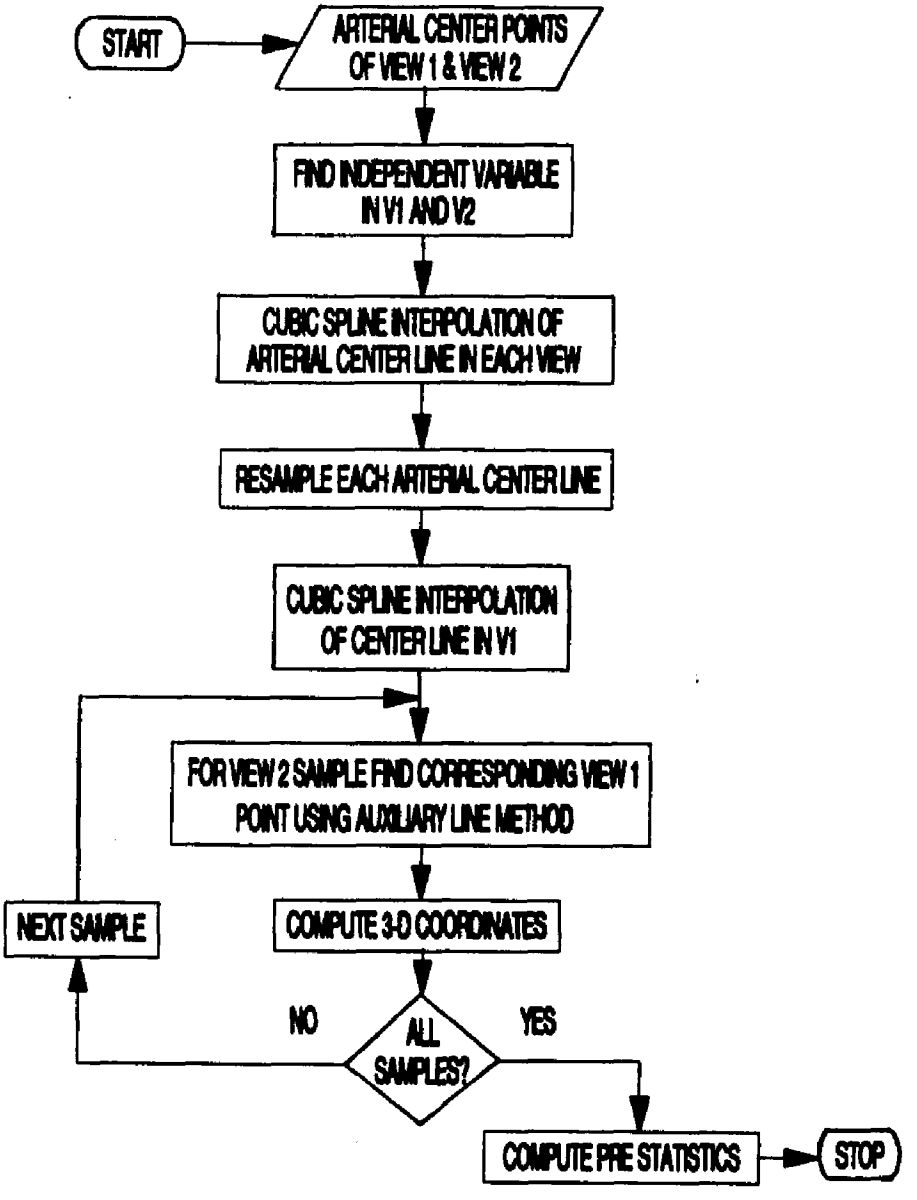

Figure 3.6.4-1. 3-D positional reconstruction algorithm I flowchart.

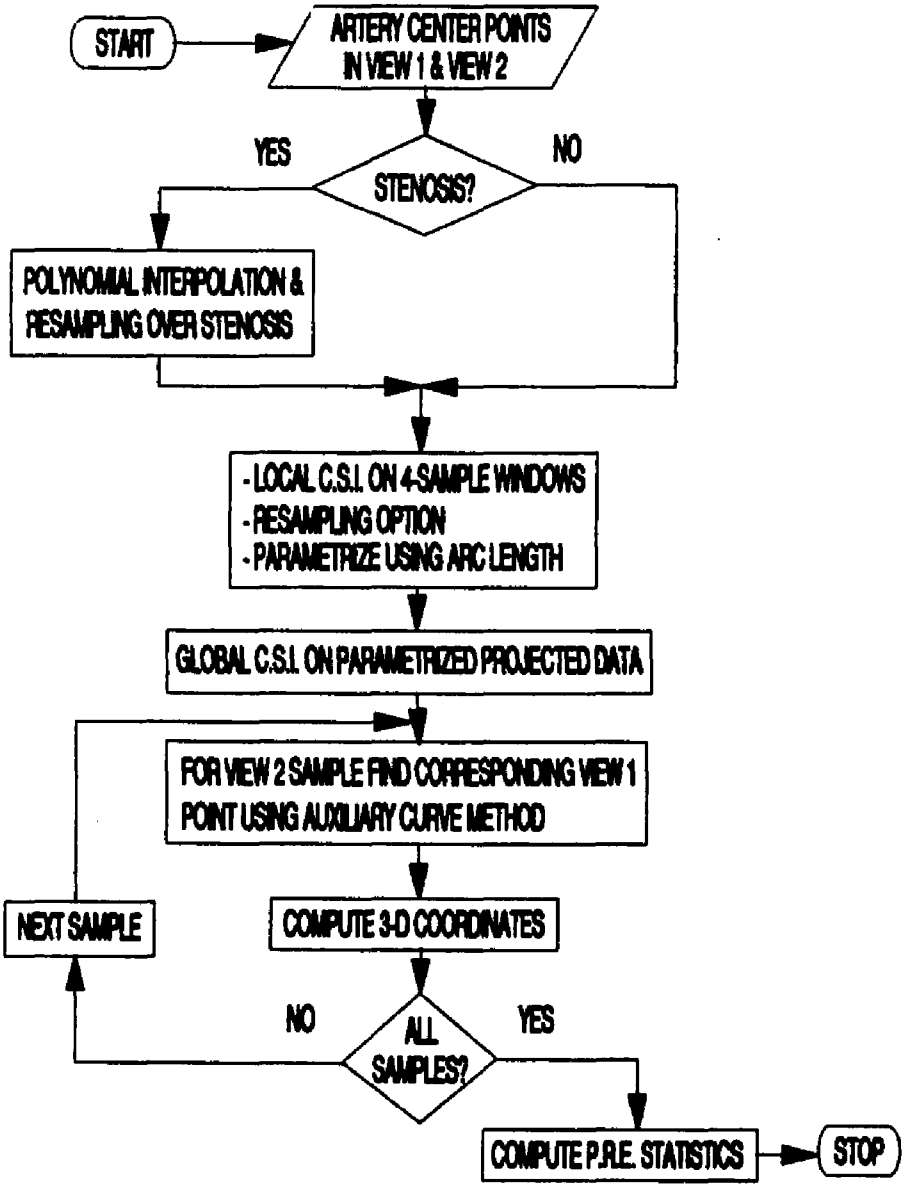

Figure 3.6.5-1. 3-D positional reconstruction algorithm II flowchart.

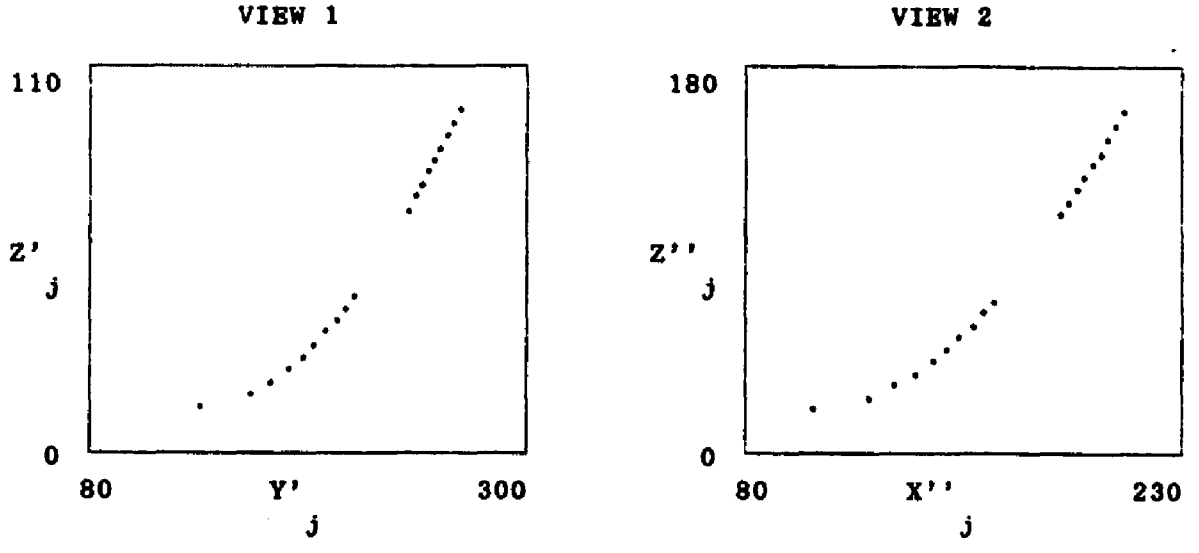

Figure 4.2-1. Single-valued biplane projections of 3-D parabolic center line (in pixels).

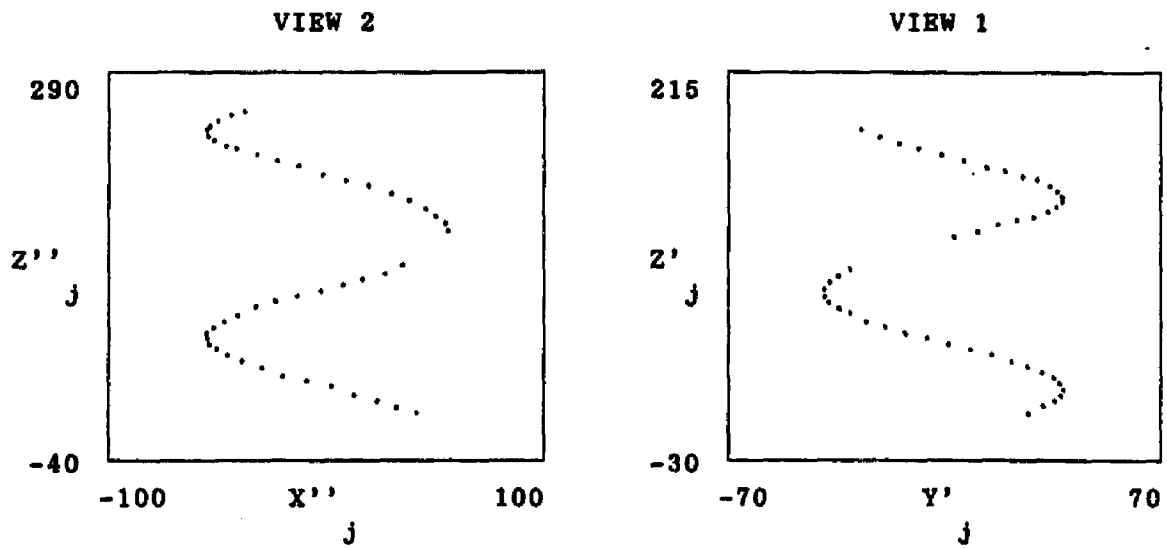

Figure 4.2-2. Single-valued biplane projections of 3-D helical center line (in pixels).

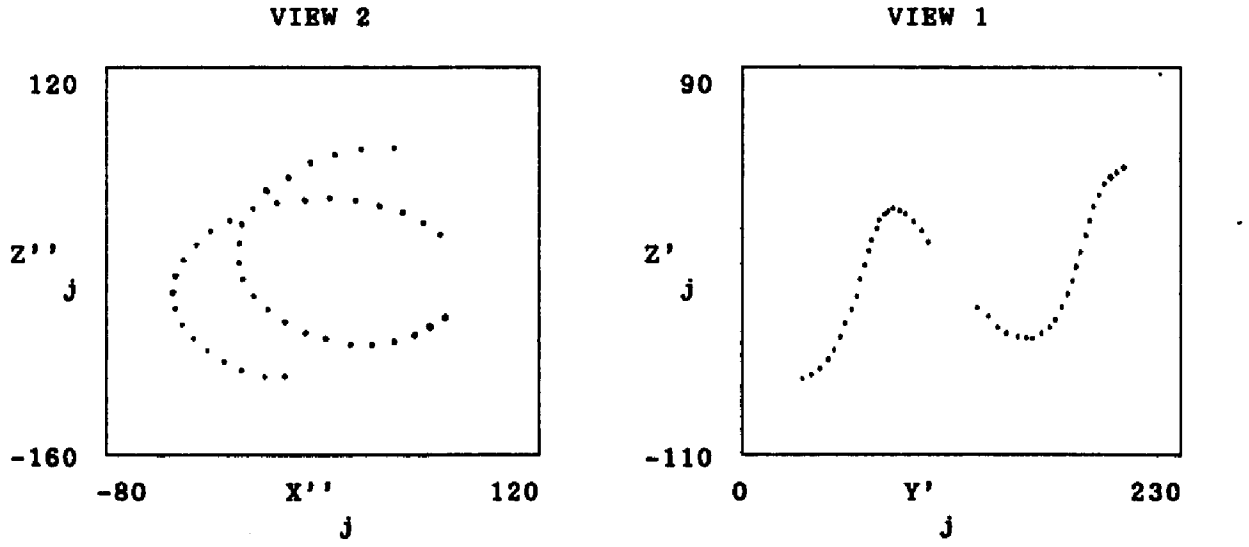

Figure 4.2-3. Multi-valued biplane projections of 3-D helical center line (in pixels).

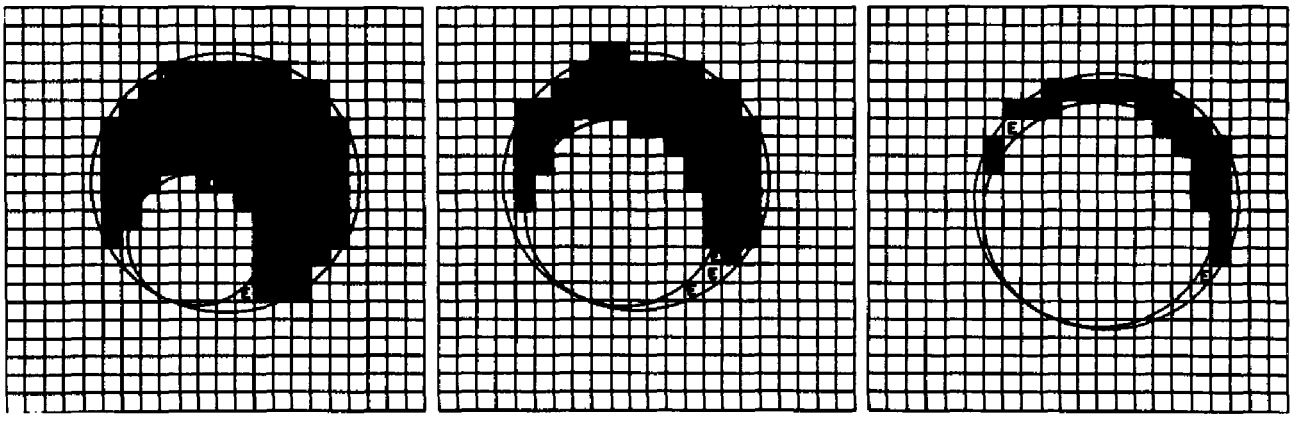

(a) (b) (c)

Figure 4.1.1-1. Reconstruction of computer simulated, noise free, crescent-shaped arterial cross-sections with partial pixel projections. Shaded areas were filled. Reconstruction errors are marked with an E. (a) R1=7, R3=3.5, 25% stenosis, 2 errors, $\overline{R}$=1.7%. (b) R1=7, R3=5, 51% stenosis, 5 errors, $\overline{R}$=6.7%. (c) R1=7, R3=6, 73% stenosis, 3 errors, $\overline{R}$=7.3%.

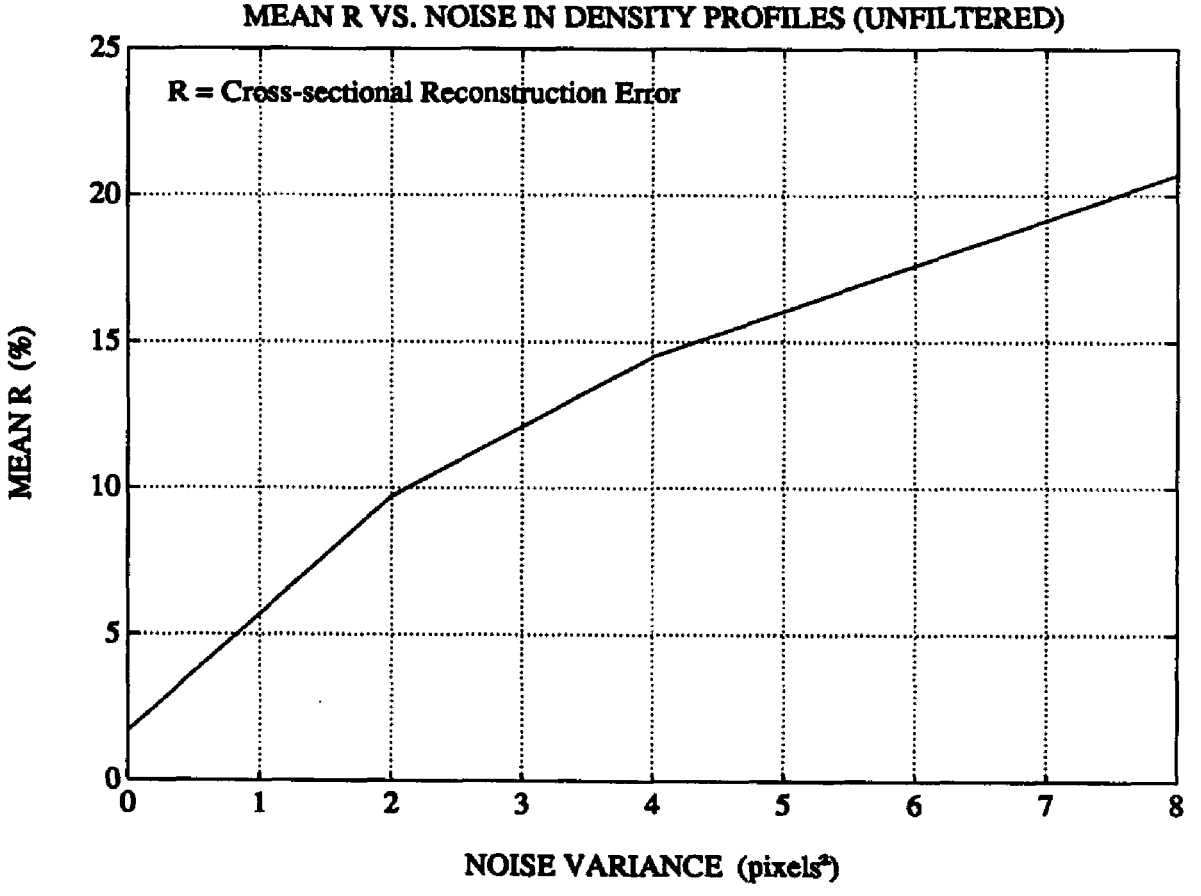

Figure 4.1.2-1. Mean reconstruction error $\overline{R}$ as a function of the noise level in the computer simulated data. No noise reduction. Computer simulated 25% stenosed crescent-shaped cross-section.

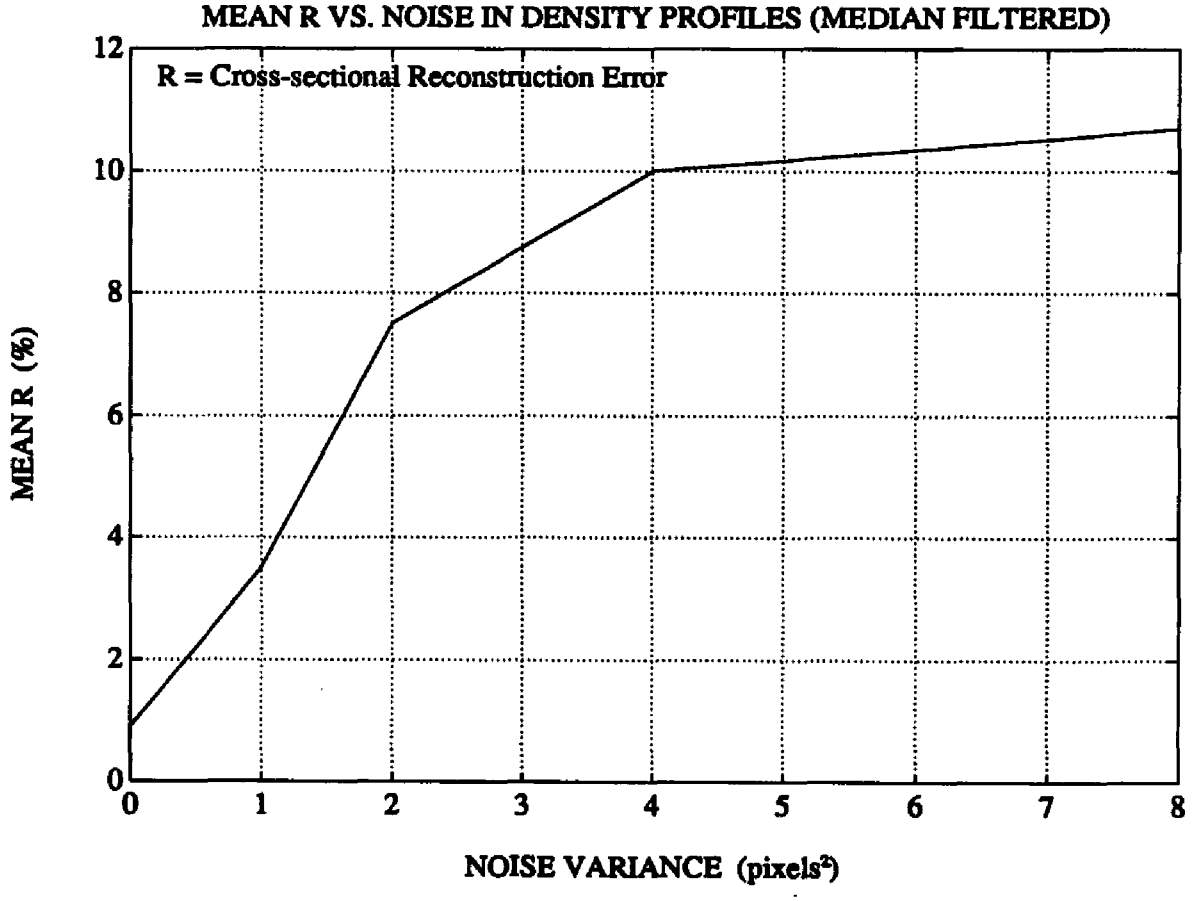

Figure 4.1.3-1. Mean reconstruction error $\overline{R}$ as a function of the noise level in the computer simulated data after noise reduction (3×3 median filtering). Computer simulated 25% stenosed crescent-shaped cross-section.

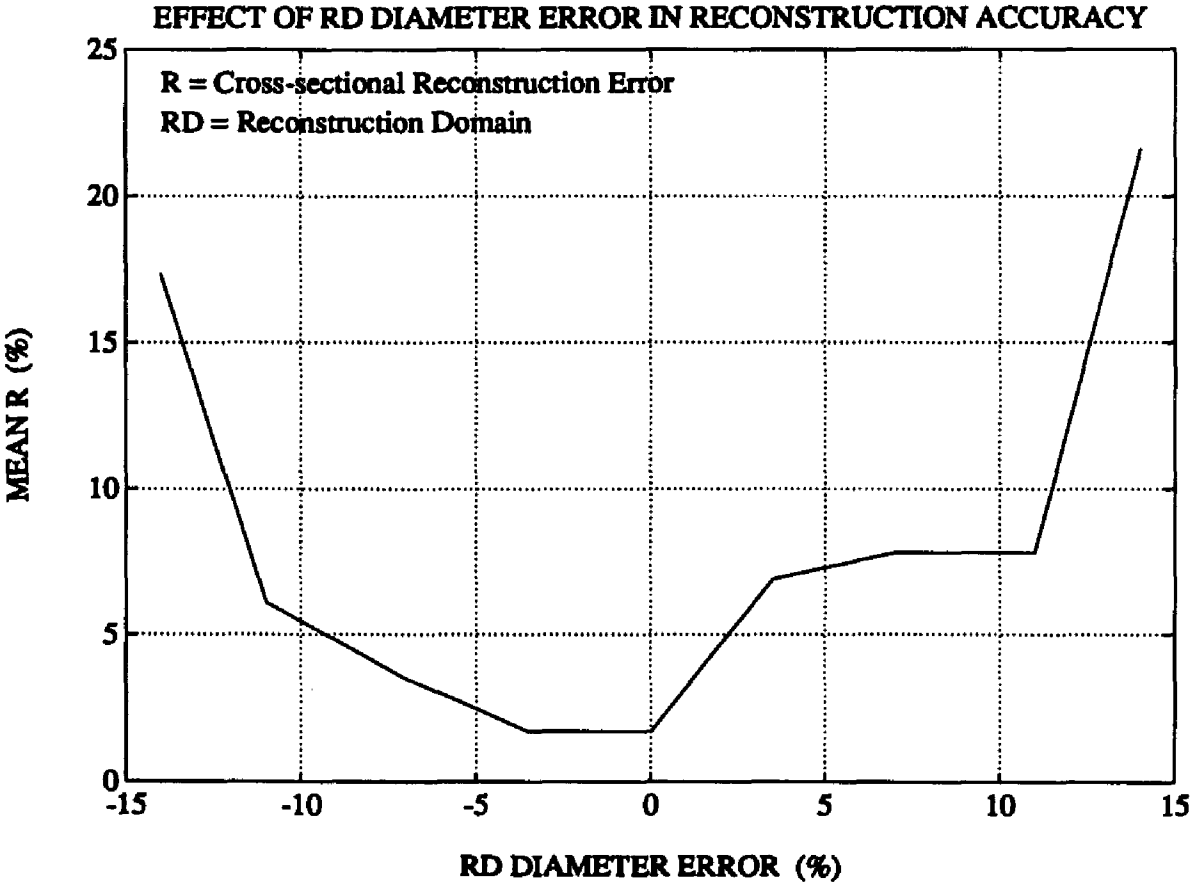

Figure 4.1.4-1. Mean reconstruction error $\overline{R}$ as a function of reference domain (*RD*) diameter error. Computer simulated 25% stenosed crescent-shaped cross-section.

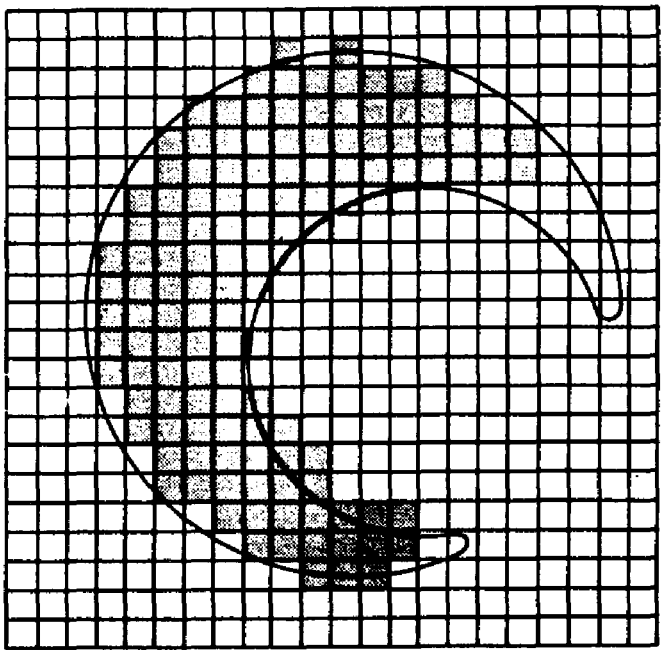

Figure 4.1.6-1. Reconstruction from biplane X-ray shadowgraphs of the 44% stenosed crescent-shaped cross-section. No noise reduction. R1=1.5mm (9 pixels on reconstructed image), R3=1mm (6 pixels on reconstructed image), 1 pixel=0.167mm, 24 errors, $\overline{R} \approx 17\%$.

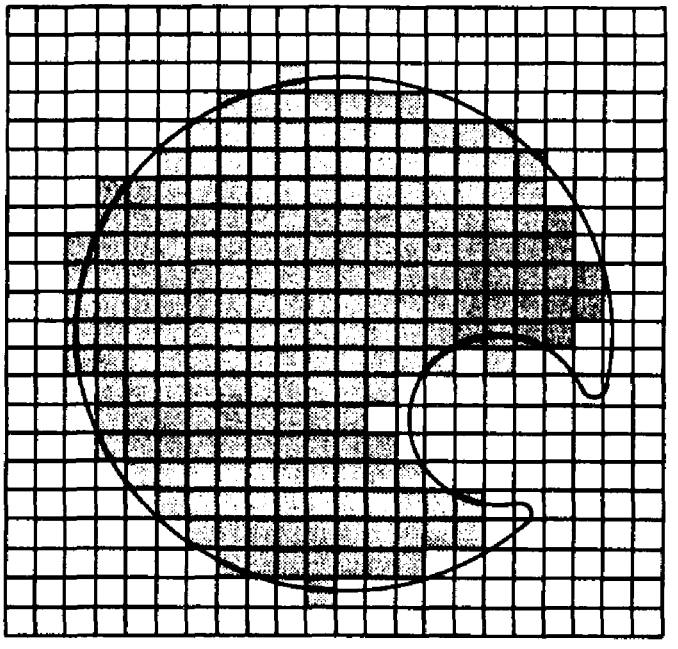

Figure 4.1.6-2. Reconstruction from biplane X-ray shadowgraphs of the 11% stenosed crescent-shaped cross-section. No noise reduction. R1=1.5mm (9 pixels on reconstructed image), R3=0.5mm (3 pixels on reconstructed image), 1 pixel=0.167mm, 14 errors, $\overline{R} \approx 6.2\%$.

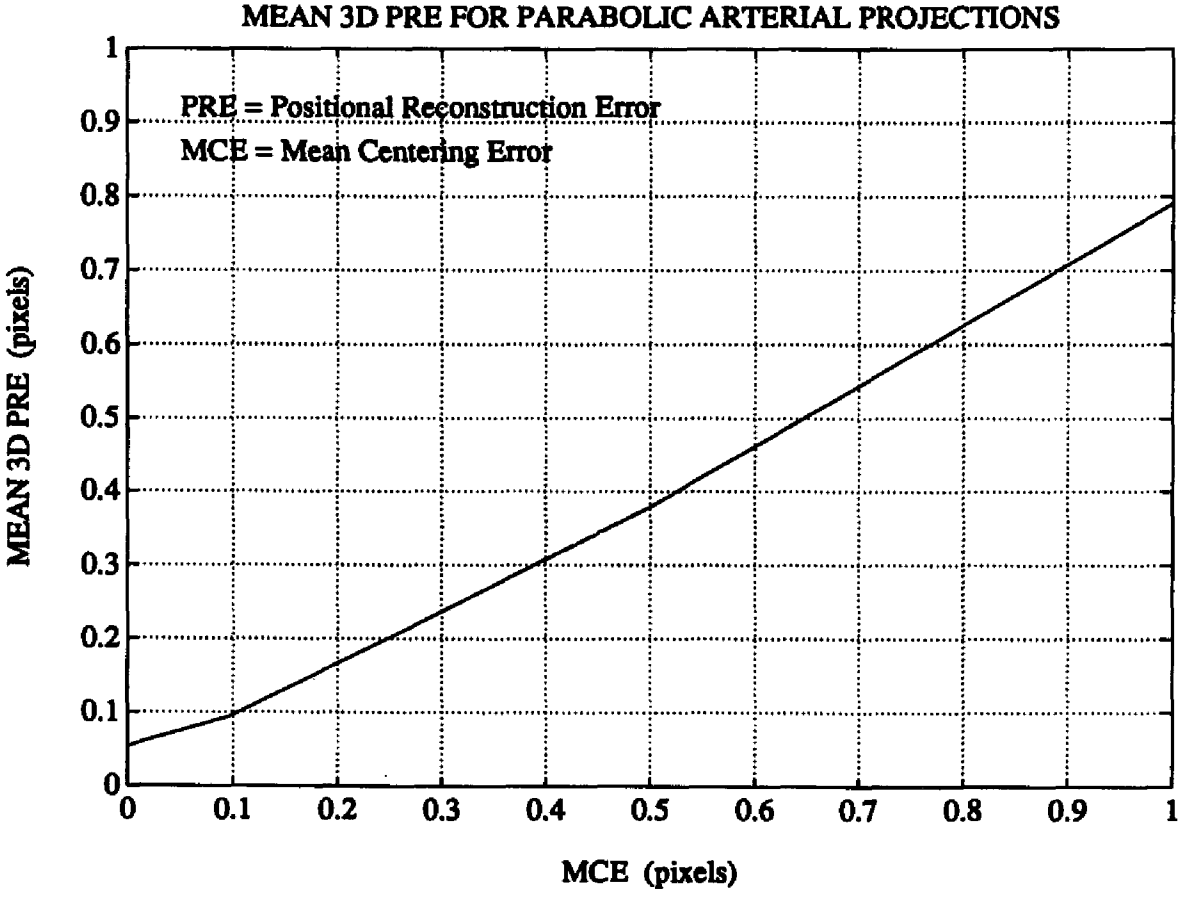

Figure 4.2.1-1. Mean 3-D positional reconstruction error ($\overline{PRE}$) of algorithm I in the reconstruction of a non-stenosed parabolic center line for input data with various values of the mean centering error (MCE).

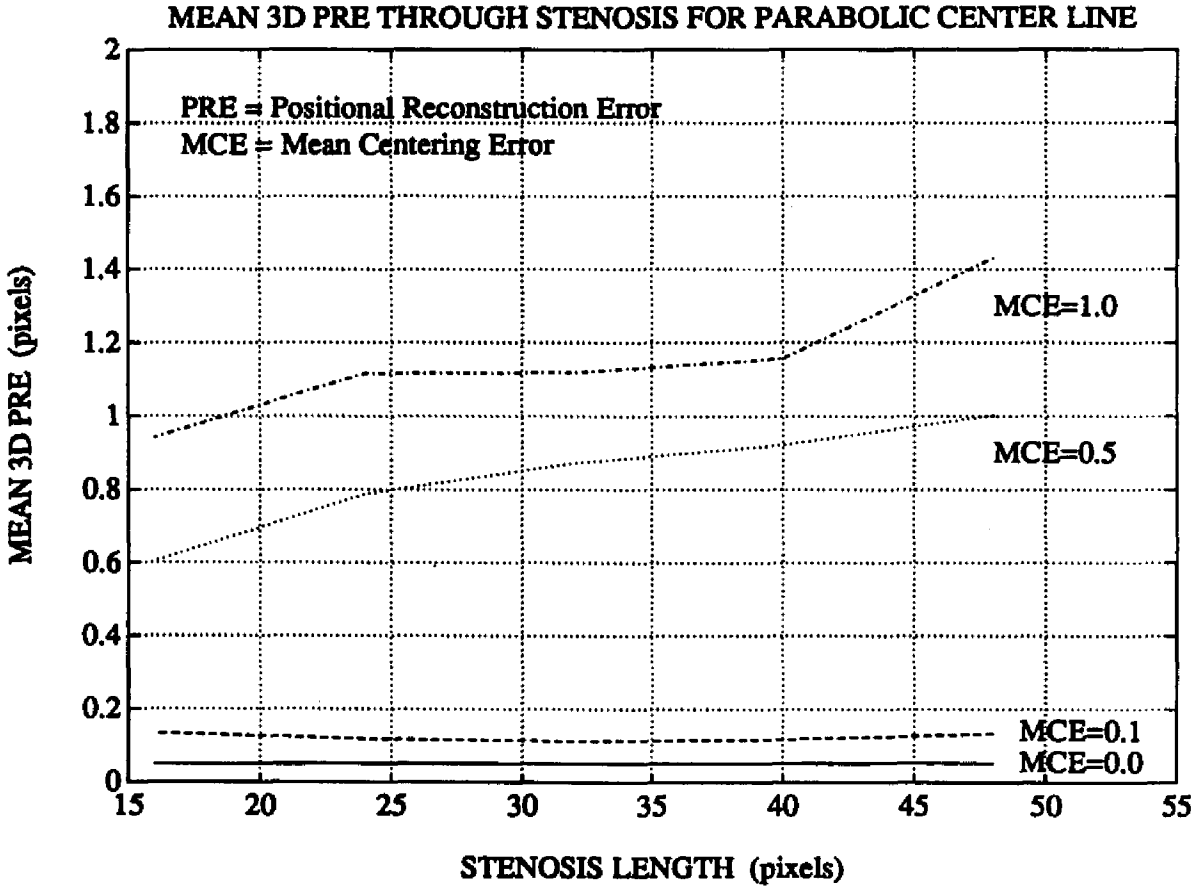

Figure 4.2.1-2. Mean 3-D positional reconstruction error ($\overline{PRE}$) of algorithm I in the reconstruction of the parabolic center line through stenosed region for various values of the stenosed segment length and mean centering error (MCE).

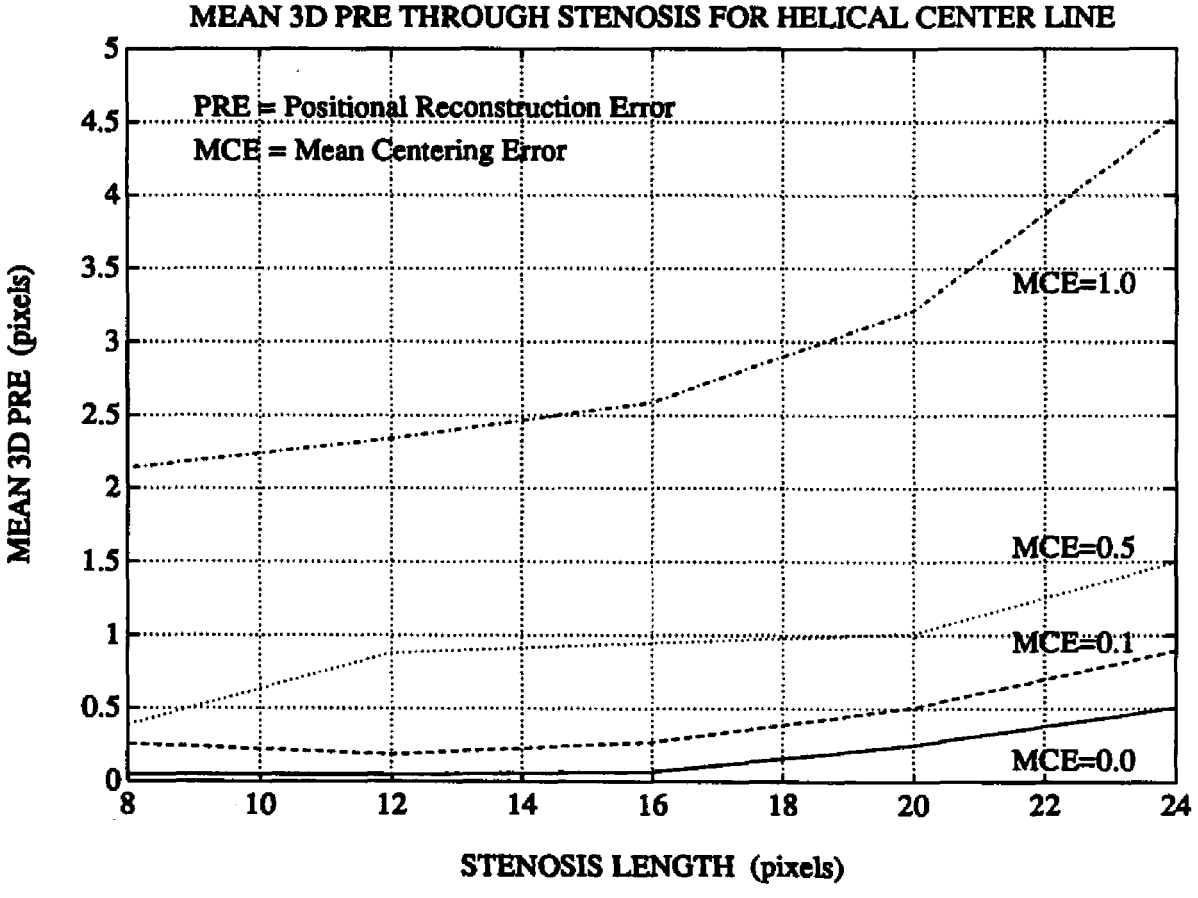

Figure 4.2.1-3. Mean 3-D positional reconstruction error ($\overline{PRE}$) of algorithm I in the reconstruction of the helical center line through stenosed region for various values of the stenosed segment length and mean centering error (MCE).

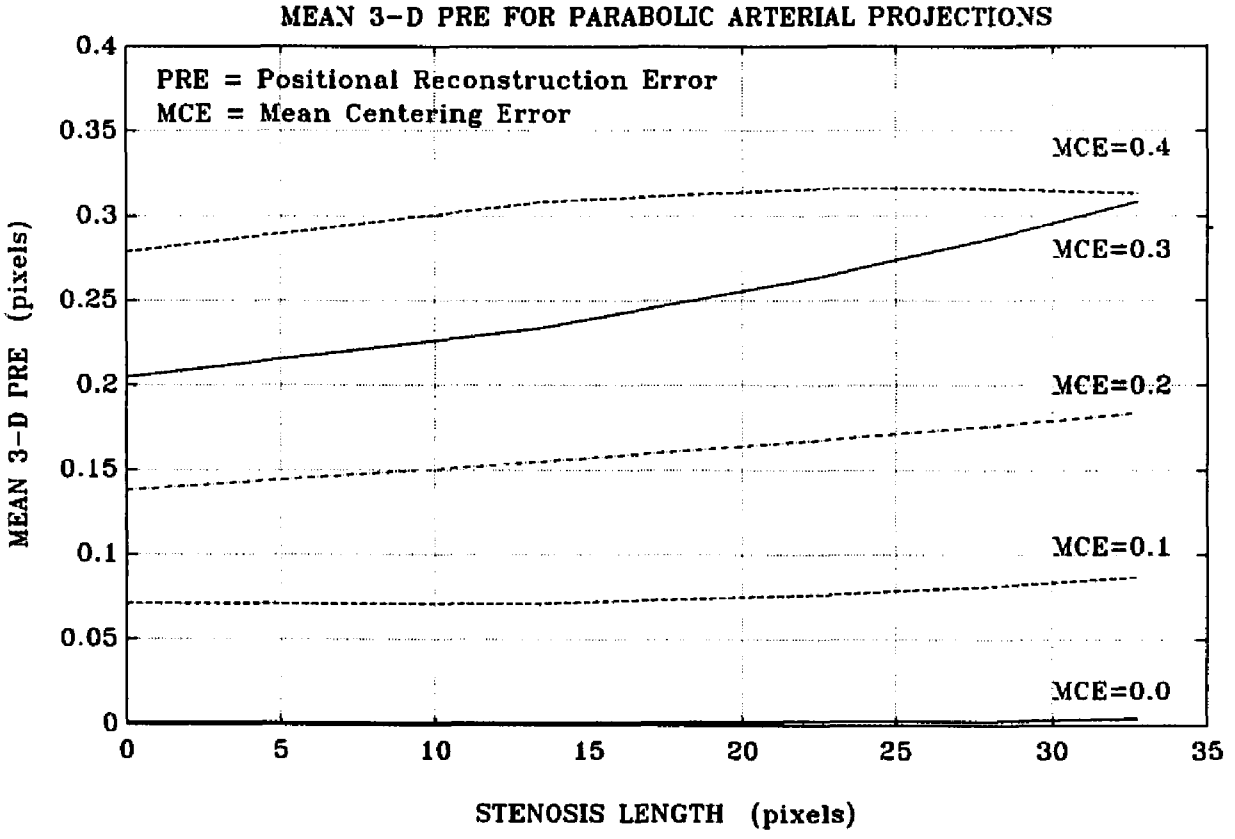

Figure 4.2.2-1. Mean 3-D positional reconstruction error ($\overline{PRE}$) of algorithm II in the reconstruction of the parabolic center line with single-valued projections for various values of the stenosed segment length and mean centering error (MCE).

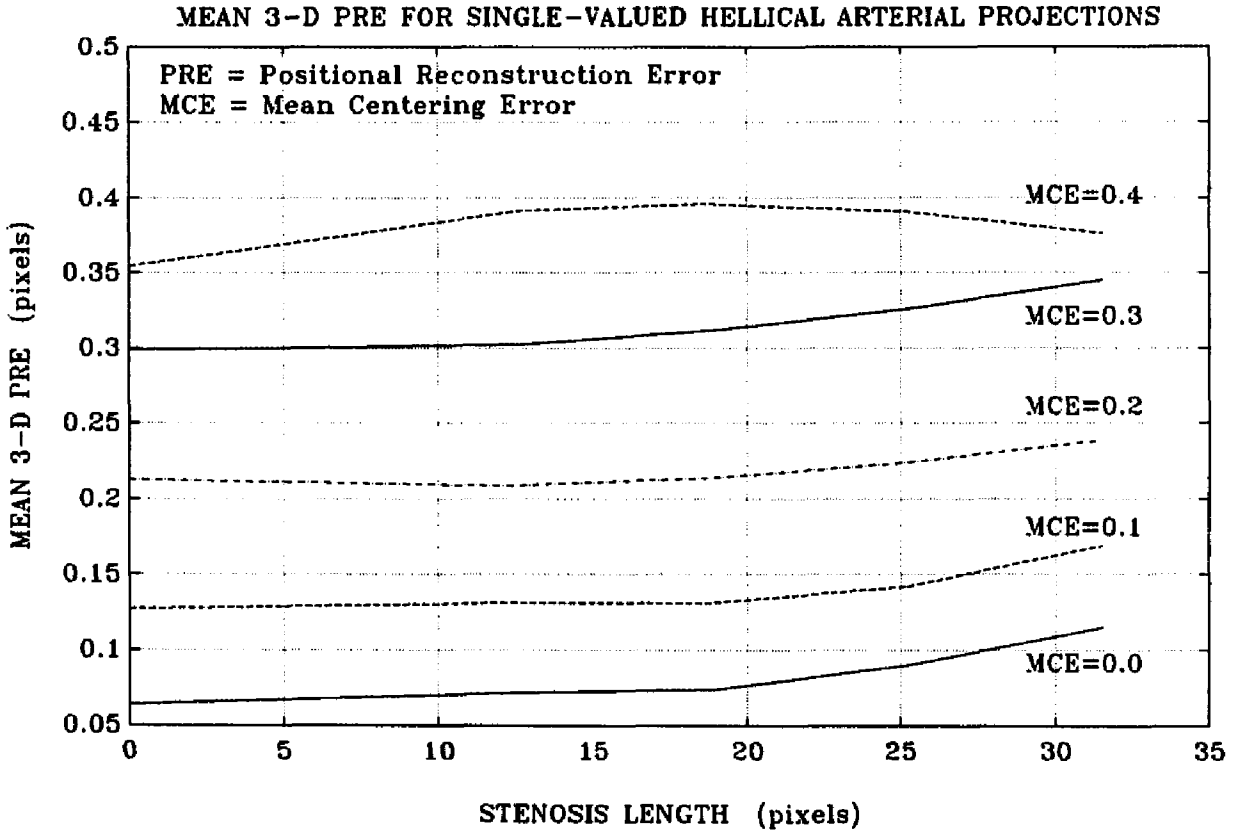

Figure 4.2.2-2. Mean 3-D positional reconstruction error ($\overline{PRE}$) of algorithm II in the reconstruction of the helical center line with single-valued projections for various values of the stenosed segment length and mean centering error (MCE).

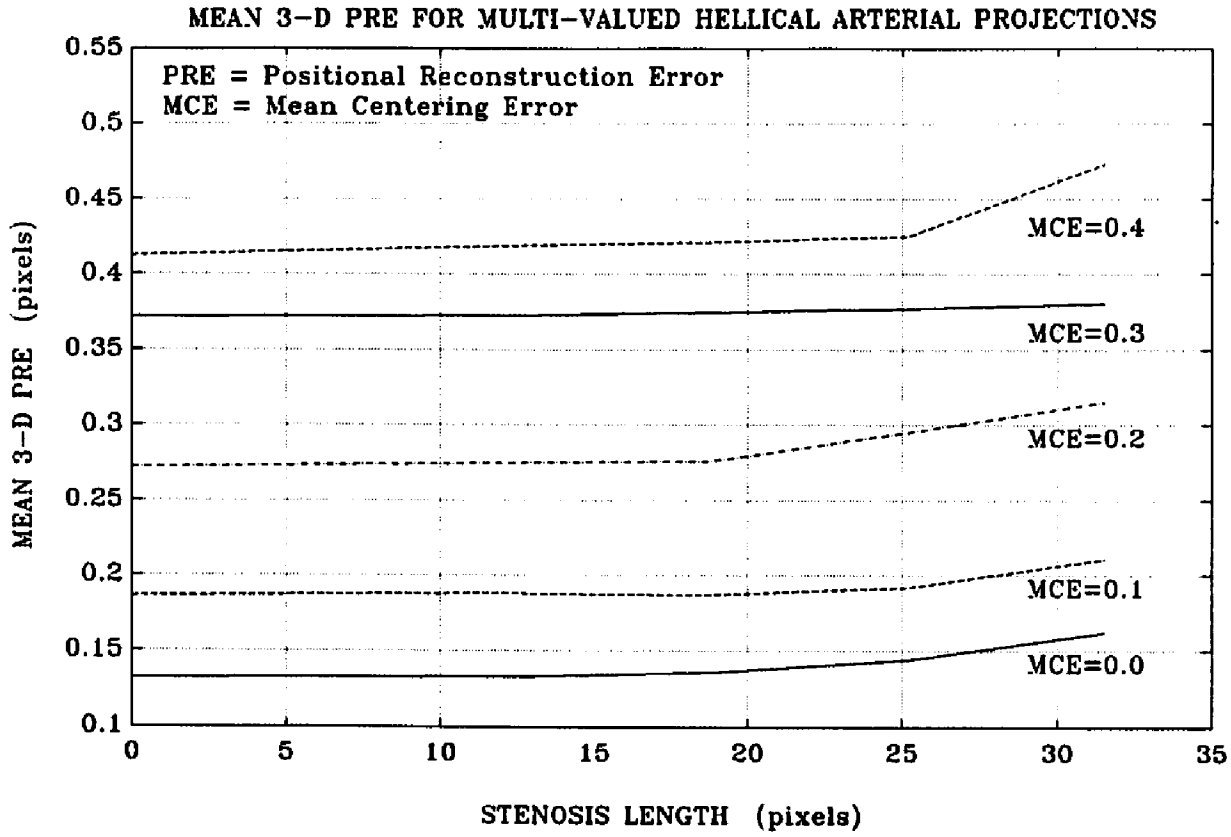

Figure 4.2.2-3. Mean 3-D positional reconstruction error ($\overline{PRE}$) of algorithm II in the reconstruction of the helical center line with multi-valued projections for various values of the stenosed segment length and mean centering error (MCE).

8 APPENDIXES

Appendix I

Error propagation analysis of biplane X-ray systems

One of the main goals of this research was to develop medical imaging algorithms which yield accurate results.

The 3-D Positional Reconstruction Algorithm, which is among the above mentioned algorithms, was developed to obtain the three-dimensional coordinates of arterial center line points in space from the two-dimensional coordinates of their projections onto two orthogonal X-ray images (see Section 3.6). These reconstructed 3-D coordinates, however, are exact only under the ideal conditions assumed for the derivation of Equations (3.6.2-17) to (3.6.2-19). In real physical systems many of these conditions (such as the perpendicularity between the two views) do not hold exactly.

It is important, therefore, to investigate which are the factors that affect the accuracy of our results and to estimate the amount of error that they introduce. This kind of information would also permit specification of the accuracy required in the calibration of the biplane X-ray system in order to obtain accurate results with the methods presented here.

Initially, we contacted a representative of BC Medical Manufacturing Co. Ltd., a Canadian company which manufactures medical X-ray systems including a biplane, ring-type system called ROTAX II, whose elements are arranged with a geometry identical to

the one assumed in this research. From this inquiry, we found out that the calibration errors in this type of system are of approximately 3 mm. This data was later used for a preliminary error propagation analysis.

We have identified the factors present in the type of X-ray systems and methods used in this research which can introduce errors in the calculated three-dimensional coordinates. These are summarized below:

1. Pincushion distortion caused by the curvature of the image intensifiers. The degrading effects of this type of distortion varies from system to system, but it can be corrected, for example, by using a "rubber-sheeting" transform.[72]

2. Non perpendicularity between the two angiographic views.

3. Non crossing of the principal axes of the two angiographic views.

4. Errors in the measurements of the distances between the image intensifier and the X-ray focal point of each view.

5. Non perpendicularity between the image intensifier and the principal axis in each view.

6. Very small errors introduced by the center-finding algorithm[86,87] which provides the input data.

7. Interpolation errors introduced by the three-dimensional positional reconstruction algorithm.

Formulas were developed, using the notation of Figure 3.2-1, to calculate the maximum propagated error in the calculated 3-D coordinates due to the X-ray system and to the

measurements made on the biplane images. These formulas were derived for each of the coordinates using a Taylor expansion up to first order, assuming that these errors are small, independent, and that they obey the law of chance.[92,93] It was also assumed that the images were first processed for pincushion distortion correction.

Letting $A1 = A'$, $B1 = B'$, $A2 = A''$ and $B2 = B''$, the expressions derived for computing the absolute value of the maximum propagated error were the following:

a. For the x coordinate component:

$$E_x = \Delta x = \sum_{\text{all } Vx_n} \left| \frac{\partial x}{\partial Vx_n} \right| \Delta Vx_n \tag{A.I-1}$$

$$= \left| \frac{\partial x}{\partial x''} \right| \Delta x'' + \left| \frac{\partial x}{\partial z'} \right| \Delta z' + \left| \frac{\partial x}{\partial A''} \right| \Delta A'' + \left| \frac{\partial x}{\partial y'} \right| \Delta y' + \left| \frac{\partial x}{\partial z''} \right| \Delta z'' + \left| \frac{\partial x}{\partial B''} \right| \Delta B'' \tag{A.I-2}$$

Where

$E_x \equiv \Delta x \equiv$ Absolute value of the maximum propagated error in the x coordinate.

$\Delta Vx_n \equiv$ Maximum error of Vx_n.

$\{Vx_n\} = \{x'', z', A'', y', z'', B''\}$, the variables present in the expression for determining the x coordinate.

and x as defined by Equation (3.6.2-17).

b. For the y coordinate component:

$$E_y = \Delta y = \sum_{\text{all } Vy_n} \left| \frac{\partial y}{\partial Vy_n} \right| \Delta Vy_n \tag{A.I-3}$$

$$= \left| \frac{\partial y}{\partial A''} \right| \Delta A'' + \left| \frac{\partial y}{\partial B''} \right| \Delta B'' + \left| \frac{\partial y}{\partial z'} \right| \Delta z' + \left| \frac{\partial y}{\partial y'} \right| \Delta y' + \left| \frac{\partial y}{\partial z''} \right| \Delta z'' \tag{A.I-4}$$

Where

$E_y \equiv \Delta y \equiv$ Absolute value of the maximum propagated error in the y coordinate.

$\Delta Vy_n \equiv$ Maximum error of Vy_n.

$\{Vy_n\} = \{A'', B'', z', y', z''\}$, the variables present in the expression for determining the y coordinate.

and y as defined by Equation (3.6.2-18).

c. For the z coordinate component:

$$E_z = \Delta z = \sum_{\text{all } Vz_n} \left| \frac{\partial z}{\partial Vz_n} \right| \Delta Vz_n \tag{A.I-5}$$

$$= \left| \frac{\partial z}{\partial z''} \right| \Delta z'' + \left| \frac{\partial z}{\partial z'} \right| \Delta z' + \left| \frac{\partial z}{\partial A''} \right| \Delta A'' + \left| \frac{\partial z}{\partial y'} \right| \Delta y' + \left| \frac{\partial z}{\partial B''} \right| \Delta B'' \tag{A.I-6}$$

Where

$E_z \equiv \Delta z \equiv$ Absolute value of the maximum propagated error in the z coordinate.

$\Delta Vz_n \equiv$ Maximum error of Vz_n.

$\{Vz_n\} = \{z'', z', A'', y', B''\}$, the variables present in the expression for determining the z coordinate.

and z as defined by Equation (3.6.2-19).

Finally, the total maximum root mean square (RMS) error is given by

$$(E_T)_{RMS} = \sqrt{E_x^2 + E_y^2 + E_z^2} \tag{A.I-7}$$

On the average, the actual error will be much smaller since the above expression represents the worst case propagated error. This maximum error will only occur when all the individual error components simultaneously contribute to reinforce the total error; in practice, there is only a small probability that this will happen, and typically actual errors will be much smaller. Besides, these errors could be reduced considerably if the construction of present biplane X-ray systems were improved to increase the accuracy to which they can be calibrated. At present, there is no demand from the medical community for biplane X-ray systems, suitable for objective measurements on clinical images, which can be calibrated very accurately and provide high precision readings of the position of their main elements.

As a consequence, manufacturers currently don't put too much attention to these aspects in the design of their X-ray systems. This seems to indicate that more accurate biplane X-ray systems would not be difficult to build if the need and the demand for them should ever arise.

Using the above formulas and assuming a pixel size of 0.5 mm, typical values of X-ray system dimensions and projected coordinates, and a very high average error of 2 pixels in the estimation of each of the coordinates of the projections on the two views, it was calculated that the total maximum root-mean-squared (RMS) error due to an error of 3 mm in the measurement of A', B', A'', and B'' would be around 1.9 pixels. The above results indicate that the propagated errors due to typical measurement errors of the distances between the image intensifiers and the X-ray sources will not affect the accuracy of the results significantly.

From the above calculations and the results published by Smith and Starmer[94], who performed a similar and very thorough similar analysis, we conclude that our methods can yield accurate results with present biplane X-ray systems such as the ROTAX II, provided that the equipment is carefully calibrated during the installation process.

Appendix II

Basic concepts of cubic spline interpolation and their application to our problem

Spline interpolating functions are a mathematical adaptation of the idea behind a flexible drafting instrument called spline which is used for drawing a smooth curve through a set of plotted dots. Spline interpolation is often used when the points to be connected do not come from experimental data, but are rather representative points of a physical structure such as the body of an automobile. In this research we used cubic spline interpolation techniques to obtain a functional representation of arterial center lines. This type of representation plays an enormously important role in our 3-D positional reconstruction algorithm since it permits:

1. The automatic identification of corresponding profiles.

2. The easy calculation of the orientation of the artery at any point.

3. The correct positioning of the reconstructed cross-sections to obtain an accurate 3-D reconstruction of the arterial lumen.

Although spline functions of different orders can be formulated, cubic splines are the most widely used in engineering applications. On the other hand, high-order polynomial interpolation can also be used to fit a curve through a plotted set of points, however this approach suffers of two major problems:

1. Large deviations from a smooth curve (wiggles in between data points).

2. Increasing complexity as the number of interpolated points increases. To fit $n+1$ points, an n^{th}- order polynomial is required.

The cubic spline equations

Let a set of n data points $x(1) < x(2) < \ldots < x(n)$, which we will call knots, define a partition of the $[x(1), x(n)]$ interval. Then, a cubic spline function $F(x)$ is a function defined on that interval consisting of set of connected continuous third-order polynomials $f_i(x)$, one per each $[x(i), x(i+1)]$ subinterval, $i = 1, \ldots, n-1$, having the property that adjacent polynomials join smoothly with continuous first and second derivatives. Hence, a functional representation that is amenable to extensive mathematical manipulation is obtained.

The equation representing the cubic polynomial $f_i(x)$ at the i^{th} interval is:

$$f_i(x) \equiv c_{3i}[x - x(i)]^3 + c_{2i}[x - x(i)]^2 + c_{1i}[x - x(i)] + y(i) \qquad \text{(A.II-1)}$$

Where

c_{ij} : an element of the $(n-1)\times 3$ matrix **C** containing the coefficients of the interpolated cubic polynomials uniquely defining the cubic spline function $F(x)$.

$$y(i) = F(x_i) = f_i(x_i)$$

and

$$x(i) \le x < x(i+1)$$

To find the value of the interpolated function $f_i(x)$ at a point $x = p$ with Equation (A.II-1), it is necessary then to determine the pertinent subinterval $[x(i), x(i+1)]$ containing this point p, and the corresponding cubic polynomial coefficients c_{1i}, c_{2i} and c_{3i}.

Cubic spline functions can be represented in different ways. This is the representation adopted by the well-known IMSL mathematical software library, which we have used for the implementation of the algorithms developed for this dissertation.

One general condition for using cubic spline interpolation is that the independent variable of the data points to be interpolated must be in increasing order, i.e., $x(1) < x(2) < \ldots < x(n)$. However, in our case of interest, namely arterial center line points, this condition cannot be generally met because sometimes the center line can only be approximated by multiple-valued functions. Due to this problem, we have developed two versions of the 3-D positional reconstruction algorithm which incorporates this interpolating technique. The first version assumes that the data points meet the increasing order condition. The second version, on the other hand, is a general one, and is based on a more complex

algorithm which imposes no ordering condition on the input data. The elimination of this restriction for the input data was achieved in the second version by doing a parametrization with respect to the arc length before performing the cubic spline interpolation.

Further information on cubic spline interpolation can be found in any book about Numerical Methods. Hamming's *Numerical Methods for Scientists and Engineers*[95] contains a concise but good introduction to this topic. For a thorough treatment of spline interpolation refer to de Boor's book.[96]

Appendix III

Condition for the intersection of two straight lines in 3-D space

The condition for the intersection of straight lines L_1 and L_2 described in Section 3.6.2 is of interest because it is precisely that intersection point what determines the position in 3-D space which we want to reconstruct.

If the coordinates of projected points $P_i'(-B', y', z')$ and $P_i''(x_i'', -B'', z_i'')$, which belong to the arterial center lines of View 1 and View 2 respectively, could always be determined correctly, the straight lines L_1 and L_2 determined by these points and their corresponding X-ray focal points S' and S'' would always intersect. However, since the coordinates of some of these projected arterial center line points could contain a significant amount of error due to inaccuracies introduced by the interpolation of the center line or the center-finding algorithm, one could expect cases in which the generated straight lines do not intersect. In light of this, the condition for the intersection of the two lines becomes valuable since it can be a convenient way to check for problems in finding the 3-D coordinates due to errors in the estimation of the position of the projections.

To determine the condition for the intersection of lines L_1 and L_2, we find the minimum distance between them, make it equal to zero, and then solve the equation obtained.

In general, if $P_1(x_1, y_1, z_1)$ and $P_2(x_2, y_2, z_2)$ are any two points on a line L, then the vector **v** joining these two points will have the same direction as this line. This vector can be written as

$$\mathbf{v} = (x_2 - x_1)\mathbf{i} + (y_2 - y_1)\mathbf{j} + (z_2 - z_1)\mathbf{k} \tag{A.III-1}$$

with **i**, **j** and **k** representing the unit vectors in the direction of increasing x, y and z respectively.

Using Equation (A.III-1), the direction vectors $\mathbf{v}_1$ and $\mathbf{v}_2$ of lines L_1 and L_2 respectively are

$$\mathbf{v}_1 = -(A' + B')\mathbf{i} + y'\mathbf{j} + z'\mathbf{k} \tag{A.III-2}$$

$$\mathbf{v}_2 = x''\mathbf{i} - (A'' + B'')\mathbf{j} + z''\mathbf{k} \tag{A.III-3}$$

Let us define a vector **p** as

$$\mathbf{p} \equiv \mathbf{v}_1 \times \mathbf{v}_2 = \begin{vmatrix} \mathbf{i} & \mathbf{j} & \mathbf{k} \\ -(A' + B') & y' & z' \\ x'' & -(A'' + B'') & z'' \end{vmatrix} \tag{A.III-4}$$

$$\mathbf{p} = [y'z'' + z'(A'' + B'')]\mathbf{i} + [z''(A' + B') + z'x'']\mathbf{j} + [(A' + B')(A'' + B'') - y'x'']\mathbf{k} \tag{A.III-5}$$

Then, $\mathbf{p}$ is a vector perpendicular to both L_1 and L_2. Hence there are two parallel planes, one containing line L_1 and the other containing line L_2, which are both perpendicular to $\mathbf{p}$.

If we form a line segment by joining one point on L_1 with one point on L_2, and project this segment onto the common perpendicular, then we can obtain the distance d between the two parallel planes, which is also the minimum distance between lines L_1 and L_2.

Letting the two points mentioned above be S' and S'', and $\mathbf{v}_3$ be the direction vector of the line segment which they determine, we obtain

$$\mathbf{v}_3 = -A'\mathbf{i}+A''\mathbf{j} \tag{A.III-6}$$

If in addition, we let $\mathbf{n}$ be a unit vector

$$\mathbf{n} = \frac{\mathbf{p}}{|\mathbf{p}|} \tag{A.III-7}$$

then, the minimum distance d between the two lines is

$$d = \left|\frac{\mathbf{p}\cdot\mathbf{v}_3}{|\mathbf{p}|}\right| \tag{A.III-8}$$

$$d = \frac{1}{|\mathbf{p}|}\{-A'[y'z''+z'(A''+B'')]+A''[z''(A'+B')+z'x'']\} \tag{A.III-9}$$

The lines will intersect when $d = 0$ in Equation (A.III-9), or equivalently when

$$-A'[y'z''+z'(A''+B'')]+A''[z''(A'+B')+z'x''] = 0 \tag{A.III-10}$$

which can finally be expressed, after rearranging, as

$$A''[z''(A'+B')+z'x'']-A'[z'(A''+B'')+y'z''] \quad = \quad 0 \qquad \text{(A.III-11)}$$

Equation (A.III-11) above gives the condition for the intersection of lines L_1 and L_2. This condition was useful for detecting and solving unexpected problems causing large coordinate errors which arised during the developmental phase of our 3-D positional reconstruction algorithms.

9 REFERENCES

1. Council for Agricultural Science and Technology (CAST), "Diet and Coronary Disease," *Nutrition Today*, pp. 26-33, Mar./Apr. 1986.

2. Special Report, "The search for the large pore," *Kaleidoscope*, vol. III, no. 1, The City College of New York/CUNY, Fall 1986.

3. B.M. Moores, "Radiological techniques in cardiology: An overview," *Physical Techniques in Cardiological Imaging*, pp. 143-152, Session F, Southampton, Jul. 1982.

4. A. Macovski, *Medical Imaging*, Prentice-Hall, N.J., 1983.

5. *The Current State of Digital Fluorography*, Elscint Ltd., Israel, 1985.

6. *Diagnostic Radiology--An Anglo-American Textbook of Imaging*, R.G. Grainger and D.J. Allison (eds.), vol. 3, Section 11, chapter 94, Churchill Livingstone, New York, 1986.

7. S. Seldinger, "Catheter replacement of the needle in percutaneous arteriography," *Acta Radiol.* (Stockh.), vol. 39, pp. 368-376, 1953.

8. B.G. Brown, L.L. Bolson, H.T. Dodge, "Arteriographic assessment of coronary atherosclerosis", *Arteriosclerosis*, vol. 2, pp.2-15, Jan./Feb. 1982.

9. W. Bulawa and S.N. Meyers, "Computerized cardiovascular imaging," *Progress in Cardiovascular Disease*, vol. 25, no. 6, pp. 487-512, May/Jun. 1983.

10. P. Jaques, F. Dibianca, S. Pizer, F. Kohout, L. Lifshitz and D. Delany, "Quantitative digital fluorography. Computer vs. human estimation of vascular stenoses," *Investigative Radiology*, vol. 20, no. 1, pp. 45-52, Jan.-Feb. 1985.

11. B.G. Brown, E.L. Bolson and H.T. Dodge, "Quantitative computer techniques for analyzing coronary arteriograms," *Progress in Cardiovascular Diseases*, vol. 28, no. 6, pp. 403-418, May/Jun. 1986.

12. S.J. Riederer, "Digital Radiography in cardiac imaging," *Physical Techniques in Cardiological Imaging*, pp. 199-204, Session G, Southampton, Jul. 1982.

13. Z. Vlodaver, R. Frech, R.A. Van Tassel and J.E. Edward, "Correlation of antemortem coronary angiograms and the postmortem specimen," *Circulation*, vol. 47, pp. 162-169, Jan. 1973.

14. C.M. Grondin, I. Dyrda, A. Pasternac, L. Campeau, M.G. Bourassa and J. Lesperance, "Discrepancies between cineangiographic and postmortem findings in patients with recent myocardial revascularization," *Circulation*, vol. XLIX, pp. 703-708, Apr. 1974.

15. K.M. Detre, E. Wright, M.L. Murphy and T. Takaro, "Observer agreement in evaluating coronary angiograms," *Circulation*, vol. 52, pp. 979-986, Dec. 1975.

16. L.M. Zir, S.W. Miller, R.E. Dinsmore, J.P. Gilbert, and J.W. Harthorne, "Interobserver variability in coronary angiography," *Circulation*, vol. 53, no. 4, pp. 627-632, Feb. 1976.

17. T.A. DeRouen, J.A. Murray and W. Owen, "Variability in the analysis of coronary arteriograms," *Circulation*, vol. 55, no. 2, pp. 324-328, Feb. 1977.

18. P.E. Lange, D. Onnasch, F.L. Farr and P.H. Heintzen, "Angiocardiographic left ventricular volume determination. Accuracy, as determined from human casts, and clinical application" *European Journal of Cardiology*, 8/4-5, pp. 449-476, 1978.

19. M.E. Sanmarco, S.H. Brooks and D.H. Blankenhorn, "Reproducibility of a concensus panel in the interpretation of coronary angiograms," *American Heart Journal*, vol. 96, no. 4, pp. 430-437, Oct. 1978.

20. A. Cameron, et al., "Left main coronary artery stenosis: angiographic determination," *Circulation*, vol. 68, no. 3, pp. 484-489, Sep. 1983.

21. L. Kaufman, D. Shosa, L. Crooks and J. Ewins, "Technology needs in Medical Imaging," *IEEE Transactions on Medical Imaging*, vol. MI-1, no. 1, pp. 11-16, Jul. 1982.

22. A.R. Potvin, W.G. Crosier, E. Fromm, J.C. Lin, M.R. Neuman, T.C. Pilkington, C.J. Robinson, L.W. Schneider, J.W. Strohbehn, P. Szolovits and W.J. Tompkins, "Report of an IEEE task force--An IEEE opinion on research needs for biomedical engineering systems," *IEEE Transactions on Biomedical Engineering*, vol. BME-33, no. 1, pp. 48-59, Jan. 1986.

23. J.H. Kinsey, C.R. Hansen, R.W. Roessler, M.H. Rhyner and E.L. Ritman, "Technical characteristics of the X-ray-video imaging chain of the DSR system," *Digital Imaging in Cardiovascular Radiology*, P.H. Heintzen and R. Brennecke (eds.), pp. 151-163, Thieme-Stratton Inc., New York, 1983.

24. A.J. Feiring, J.A. Rumberger, S.J. Reiter, D.J. Skorton, S.M. Collins, M.J. Lipton, C.B. Higgins, S. Ell and M.L. Marcus, "Determination of left ventricular mass in dogs with rapid-acquisition cardiac computed tomographic scanning," *Circulation*, vol. 72, no. 6, pp. 1355, 1985.

25. R.A. Kruger et al., "Rapid circular tomographic system suitable for cardiac imaging," *Proc. SPIE*, vol. 535: Application of Optical Instrumentation in Medicine XIII, 1985.

26. E. Herrold, H. Goldberg, N. Lippman, A. Diamond, J. Carter, R. McClellan, J. Hill and J. Borer, "Accuracy of stenosis measurements using digital videodensitometry in static and dynamic coronary models," *Circulation*, vol. 72 (Supp 3), no. 3, pp. 453.

27. S.E. Logan, "On the fluid mechanics of human coronary artery stenosis," *IEEE Transactions on Biomedical Engineering*, vol. BME-22, no. 4, pp. 327-334, Jul. 1975.

28. D.F. Young and F.Y. Tsai, "Flow characteristics in models of arterial stenoses -I-steady flow," *Journal of Biomechanics*, vol. 6, pp. 395-410, 1973.

29. D.F. Young and F.Y. Tsai, "Flow characteristics in models of arterial stenoses -II-unsteady flow," *Journal of Biomechanics*, vol. 6, pp. 547-559, 1973.

30. R.L. Feldman, W.W. Nicols, C.J. Pepine and C.R. Conti, "Hemodynamic significance of the length of a coronary arterial narrowing," *American Journal of Cardiology*, vol.41, pp.865-871, 1973.

31. E.L. Yellin, "Laminar-turbulent transition process in pulsatile flow," *Circulation Research*, vol. 19, pp. 791-904, 1966.

32. L.C. Cheng, M.E. Clark and J.M. Robertson, "Numerical calculations of oscillating flow in the vecinity of square wall obstacles in plane conduits," *Journal of Biomechanics*, vol. 5, pp. 467-484, 1972.

33. L.C. Cheng, J.M. Robertson and M.R. Clark, "Numerical calculations of plane oscillatory non-uniform flow-II: parametric study of pressure gradient and frequency with square wall obstacles," *Journal of Biomechanics*, vol. 6, pp. 521-538, 1973.

34. R. Pearce and J. Kornfeld, "Digital coronary angiography," *Cardio*, pp. 36-40, Mar. 1986.

35. H.J. Ryser, "Combinatorial properties of matrices of zeros and ones," *Canad. J. Math.*, vol. 9, pp. 371-379, 1957.

36. H.J. Ryser, *Combinatorial Mathematics*, Wiley, New York, 1963.

37. Y.R. Wang, "Characterization of binary patterns and their projections," *IEEE Transactions on Computers*, pp. 1032-1035, Oct. 1975.

38. S.K. Chang and C.K. Chow, "The reconstruction of three-dimensional objects from two orthogonal projections and its applications to cardiac cineangiography," *IEEE Transactions on Computers*, vol. C-22, no. 1, pp. 18-28, Jan. 1973.

39. S.K. Chang and Y.R. Wang "Three-dimensional object reconstruction from orthogonal projections," *Pattern Recognition*, vol. 7, pp. 167-176, Pergamon Press, 1975.

40. D.G.W. Onnasch and P.H. Heintzen, "A new approach for the reconstruction of the right or left ventricular form from biplane angiocardiographic recordings," *Computers in Cardiology 1976*, pp. 67-73, IEEE Computer Society, 1976.

41. D.G.W. Onnasch, "A concept for the approximate reconstruction of the form of the right or left ventricle from biplane angiocardiograms," *Roentgen-Video-Techniques for Dynamic Studies of Structure and Function of the Heart and Circulation*, P.H. Heintzen and J.H. Bürsch (eds.), pp. 235-242, Thieme, Stuttgart, 1978.

42. D.G.W. Onnasch, W. Schmitz and P.H. Heintzen, "Problems of the binary reconstruction of the left and right ventricle from biplane angiocardiograms," *Digital Imaging in Cardiovascular Radiology*, P.H. Heintzen and R. Brennecke (eds.), pp. 141-151, Thieme-Stratton Inc., New York, 1983.

43. S. Alliney and F. Sgallari, "A new algorithm for 3D ventricular reconstruction from orthogonal projections," pp. 517-520, 1982.

44. J.R. Spears, T. Sandor, R. Kruger, W. Hanlon, S. Paulin and G. Minerbo, "Computer reconstruction of luminal cross-sectional shape from multiple cineangiographic views," *IEEE Transactions on Medical Imaging*, vol. MI-2, no. 1, pp. 49-54, Mar. 1983.

45. G. Minerbo, "MENT: A maximum entropy algorithm for reconstructing a source from projection data," *Computer Graphics and Image Processing*, vol. 10, pp. 48-68, 1979.

46. G.N. Minerbo and J.G. Sanderson, "Reconstruction of a source from a few (2 or 3) projections," Informal Report LA-6747-MS, Los Alamos Scientific Laboratory, Los Alamos, N.M., 1977.

47. G.J. Daniell and S.F. Gull, "Maximum entropy algorithm applied to image enhancement," *IEE Proc.*, vol. 127, pt. E, no. 5, pp. 170-172, Sep. 1980.

48. J.H.C. Reiber, J.J. Gerbrands, G.J. Troost, C.J. Kooijman and C.H. Slump, "3-D reconstruction of coronary arterial segments from two projections," *Digital Imaging in Cardiovascular Radiology*, P.H. Heintzen and R. Brennecke (eds.), pp. 151-163, Thieme-Stratton Inc., New York, 1983.

49. J.H.C. Reiber, J.J. Gerbrands, F. Booman, G.J. Troost, A. den Boer, C.J. Slager, J.H.C. Schuurbiers, "Objective characterization of coronary obstructions from monoplane cineangiograms and three-dimensional reconstruction of an arterial segment from two orthogonal views," *Applications of Computers in Medicine*, M.D. Schwartz (ed.), pp. 93-100, IEEE, 1982.

50. C.H. Slump and J.J. Gerbrands, "A network flow approach to reconstruction of the left ventricle from two projections," *Computer Graphics and Image Processing*, vol. 18, pp. 18-36, 1982.

51. L.R. Ford and D.R. Fulkerson, "A simple algorithm for finding maximal network flows and an application to the Hitchcock problem," *Canad. J. Math.*, vol. 9, pp. 210-218, 1957.

52. J.G. Sanderson, "Reconstruction of fuel pin bundles by a maximum entropy method," *IEEE Transactions on Nuclear Science*, vol NS-26, No. 2, pp. 2685-2686, Apr. 1979.

53. S.K. Chang, "The reconstruction of binary patterns from their projections," *Communications of the ACM*, vol. 14, no. 1, pp. 21-25, Jan. 1971.

54. S.K. Chang and G.L. Shelton, "Two algorithms for multiple-view binary pattern reconstruction," *IEEE Transactions on Systems, Man, and Cybernetics*, vol. SMC-1, pp.90-94, Jan. 1971.

55. G.T. Herman, "Reconstruction of binary patterns from a few projections," *International Computing Symposium 1973*, A. Gunther et al. (eds.), North-Holland Publ. Co., 1974.

56. C.K. Wong and P.C. Yue, "Reconstruction of patterns by block-projection," *Information Sciences*, vol. 4, pp. 357-366, 1972.

57. A. Kuba, "The reconstruction of two-directionally connected binary patterns from their two orthogonal projections," *Computer Vision, Graphics, and Image Processing*, vol. 27, pp. 249-265, 1984.

58. H.T. Dodge, H. Sandler, D.W. Ballew and J.D. Lord, "The use of biplane angiocardiography for the measurement of left ventricular volume in man," *American Heart Journal*, vol. 60, no. 5, pp. 762-776, Nov. 1960.

59. C.N. Nelson and E.O. Lipchik, "A computer method for calculation of left ventricular volume from biplane angiocardiograms," *Investigative Radiology*, vol. 1, no. 2, pp. 139-149, Mar.-Apr. 1966.

60. R.P.V. Wijk Van Brievingh, A. Richtering Blenken, "A new geometric model for determination of left ventricular shape," pp. 263-265.

61. J.M. Hughes, F.G. Hoppin and A.G. Wilson, "Use of stereoscopic X-ray pairs for measurements of airway length and diameter *in situ*", *The British Journal of Radiology*, vol. 45, no. 535, pp. 477-485, Jul. 1972.

62. L.P. Adams, "X-ray stereo photogrammetry locating the precise, three-dimensional position of image points," *Medical & Biological Engineering & Computing*, vol. 19, pp. 569-578, Sep. 1981.

63. I.E. Sutherland, "Three-dimensional data input by tablet," *Proceedings of the IEEE*, vol. 62, no. 4, pp. 453-461, Apr. 1974.

64. S.A. MacKay, M.J. Potel and J.M. Rubin, "Graphics methods for tracking three-dimensional heart wall motion," *Computers and Biomedical Research*, vol. 15, pp. 455-473, 1982.

65. M.J. Potel, J.M. Rubin, S.A. MacKay, A.M. Aisen, J. Al-Sadir and R.E. Sayre, "Methods for evaluating cardiac wall motion in three dimensions using bifurcations points of the coronary arterial tree," *Investigative Radiology*, vol. 18, no. 1, pp. 47-57, Jan.-Feb. 1983.

66. M.J. Potel, S.A. MacKay, J.M. Rubin, A.M. Aisen and R.E. Sayre, "Three-dimensional left ventricular wall motion in man. Coordinate systems for representing wall movement direction," *Investigative Radiology*, vol. 19, no. 6, pp. 499-509, Nov.-Dec. 1984.

67. K.J. Liu, J.M. Rubin, M.J. Potel, A. Aisen, S.A. MacKay, R.E. Sayre and C.E. Anagnostopoulos, "Left ventricular wall motion: its dynamic transmural characteristics," *Journal of Surgical Research*, vol. 36, no. 1, pp. 25-34, Jan. 1984.

68. L.D.R. Smith, G.P. Robinson, D.J. Stevenson, H. Sanghera and P. Quarendon, "A semi automatic computerised system for the production of quantitative moving three dimensional images of the heart and coronary arteries," *Image Processing and Its Applications*, IEE conference publication 265, 1986.

69. W.K. Pratt, *Digital Image Processing*, Wiley-Interscience, New York, 1978.

70. W.M. Smith and C.F. Starmer, "Computer representation of coronary arterial trees," *Computers and Biomedical Research*, vol. 9, pp. 187-201, 1976.

71. R.E. Sayre, J.M. Rubin, E.E. Duda and N.J. Patronas, "Quantitative three-dimensional angiograms: Applications, including augmentation of computed tomograms," *Proc. IEEE Conf. Comput. Appl. Radiol.*, pp. 95-102, 1979.

72. C.R. Mol, "3D reconstruction from biplane angiography," IBM Research Report UKSC 124, Sep. 1984.

73. C.R. Mol, J.M. Burridge and A.J. Morffew, "Three-dimensional graphics display of X-ray angiography data," *Computers and Biomedical Research*, vol. 19, pp. 47-55, 1986.

74. C.R. Mol, A.C.F. Colchester and D.J. Hawkes, "Three dimensional reconstruction of vascular configurations from bi-plane X-ray angiography," Pre-publication copy submitted to *British Journal of Radiology*.

75. H.C. Kim, B.G. Min, T.S. Lee, C.H. Lee, J.H. Park and M.C. Han, "Three-dimensional digital subtraction angiography," *IEEE Transactions on Medical Imaging*, vol. MI-1, no. 2, pp. 152-158, Oct. 1982.

76. P. Suetens, A. Haegemans, A. Oosterlinck and J. Gybels, "An attempt to reconstruct the cerebral bloodvessels from a lateral and a frontal angiogram," *Pattern Recognition*, vol. 16, no. 5, pp. 517-524, 1983.

77. P. Suetens, P. Jansen, A. Haegemans, A. Oosterlinck and J. Gybels, "3D reconstruction of the blood vessels of the brain from a stereoscopic pair of subtraction angiograms," vol. 1, no. 1, pp. 43-51, Feb. 1983.

78. K.R. Hoffmann, K. Doi, H. Chan and K. Chua, "Computer reproduction of the vasculature using an automated tracking method," *Proc. SPIE*, vol. 767 Medical Imaging, pp. 449-453, 1987.

79. K.R. Hoffmann, K. Doi, H. Chan, L. Fencil, H. Fujita and A. Muraki, "Automated tracking of the vascular tree in DSA images using a double-square-box region-of-search algorithm," *Proc. SPIE*, vol. 626, pp. 326-333, 1986.

80. D.L. Parker, D.L. Pope, R.V. Bree and H.W. Marshall, "Three-dimensional reconstruction of moving arterial beds from digital subtraction angiography," *Computers and Biomedical Research*, vol. 20, pp. 166-185, 1987.

81. T.V. Nguyen and J. Sklansky, "Computing the skeleton of coronary arteries in cineangiograms," *Computers and Biomedical Research*, vol. 19, pp. 428-444, 1986.

82. S.A. Stansfield, "ANGY: A rule-based expert system for automatic segmentation of coronary vessels from digital subtracted angiograms," *IEEE Transactions on Pattern Analysis and Machine intelligence*, vol. PAMI-8, no. 2, pp. 188-199, Mar. 1986.

83. P. Suetens, J.V. Cleynenbreugel, F. Fierens, C. Smets and A. Oosterlinck, "An expert system for blood vessel segmentation on subtraction angiograms," *Proc. SPIE*, vol. 767 Medical Imaging, pp. 454-459, 1897.

84. Y. Sun and E. Bergerson, "Automated 3D reconstruction of tree-like structures from two orthogonal views," *Proc. IEEE ICASSP 88*, vol. II, pp. 1296-1299, 1988.

85. G. Harauz and F.P. Ottensmeyer, "Interpolation in computing forward projections in direct three-dimensional reconstruction," *Phys. Med. Biol.*, vol. 28, no. 12, pp. 1419-1427, 1983.

86. J. Barba, P. Fenster, M. Suardíaz, K.K. Wong, E.M. Herrold, R.O. Kenet and J.S. Borer, "3D arterial traces from biplane projections," *Proc. SPIE*, vol. 767, no. 2, pp. 445-448, 1987.

87. P. Fenster, J. Barba and R. Wong, "Algorithm for the determination of vessel center and diameter from X-ray shadowgraphs", *Proc. SPIE's 32nd Annual International Technical Symposium on Optical & Optoelectronic Applied Science & Engineering*, 1988.

88. J.H. Lambert, *Photometria sive de mensura et gradibus luminus colorum et umbrae*, Augsburg, Germany, 1760.

89. A. Beer, "Bestimmung der absorption des roten lichts in farbigen hussin keiten," *Ann. Phys.* (Leipzig), vol. 86, p. 78, 1882.

90. E.E. Christensen, T.S. Curry and J.E. Dowdey, *An Introduction to the Physics of Radiology*, pp. 59-76, Lea and Febiger, Philadelphia, 1978.

91. M.M. McMahon, B.G. Brown, R. Cukingnan, E.L. Rolett, E. Bolson, M. Frimer and H.T. Dodge, "Quantitative coronary angiography: measurement of the "critical" stenosis in patients with unstable angina and single-vessel disease without collaterals," *Circulation*, vol. 60, no. 1, pp. 106-113, 1979.

92. A.J. Lyon, *Dealing with Data*, Section 13.3, Pergamon Press, 1970.

93. B. Hallert, *X-ray Photogrammetry*, Elsevier Publishing Company, Amsterdam, 1970.

94. W. M. Smith and C. F. Starmer, "Error propagation in quantitative biplane cineroentgenography," *Phys. Med. Biol.*, vol. 23, no. 4, pp. 677-685, 1978.

95. R.W. Hamming, *Numerical Methods for Scientists and Engineers*, Second Edition, Chapter II, Dover Publications, Inc., New York, 1973.

96. C. de Boor, *A Practical Guide to Splines*, Applied Mathematical Sciences, vol. 27, Springer Verlag, New York, 1978.